DELFT UNIVERSITY OF TECHNOLOGY

SECTION OF ENVIRONMENTAL FLUID MECHANICS

Issues in Numerical Modelling and Assessing the Flow over Weirs and Groynes

Student:
Chit Yan Toe
4580389

Graduation Committee:
Prof. dr. ir. WIM UIJTTEWAAL
Dr. ir. ERIK MOSSELMAN
Dr. ir. KEES SLOFF
Dr. ir. MARTINE RUTTEN
Dr. ir. MOHAMED YOSSEF

30 January 2018

TU Delft

Abstract

Issues in Numerical Modelling and Assessing the Flow over Weirs and Groynes

by Chit Yan Toe
4580389

In this research two problem statements are defined, namely (1) the validity of the assumption that groynes and weirs are equivalent in hydraulic models, and (2) the difficulty of modelling groynes and weirs in the 3D numerical solver package `OpenFOAM`. Using the incompressible 3D Navier-Stokes equations solver for multiphase phase flows, the so-called `interFoam` solver under `OpenFOAM` framework, two different models are set up for tackling the two problem statements.

The *interFoam evaluation model* addressed the issues of computational mesh types which affect the simulation results, and the methods for regulation of water level at the downstream boundary. The two types of the meshes which are used in the research are *structured non-orthogonal* mesh and *unstructured more-orthogonal* mesh. The benchmark test is the flow over the weir in the flume. The use of a non-orthogonal mesh could simulate the flow separation which is found downstream of the weir. However the unstructured meshes which are composed of more orthogonal parts and less non-orthogonal parts, could not reproduce the flow separation in 2D simulations correctly for high and small specific discharges. For the 3D simulations, the unstructured meshes apparently simulate the correct flow profile for low specific discharges. In this *interFoam evaluation model* the control structure or gate is used for maintaining the water level at the downstream boundary. In other words, it uses the physical method of water level boundary condition.

The *weir-groyne comparison model* is developed with different settings from the former model for the assessment of the differences between weirs and groynes in open-channel flumes. The water level is regulated by a trial-and-error discharge adjustment method making use of inlet and outlet tanks. The mesh type used is the unstructured more-orthogonal mesh in 3D simulations since the severely non-orthogonal meshes introduce numerical artifacts. A variety of weirs and groynes with different slopes are simulated for the comparison of energy losses and streamlines patterns. From the simulation results, the streamlines of the flow over the weir and the groyne are found to be different and the energy head losses also differ between these two structures.

For recommendations, to evaluate the skill of the `interFoam` solver the 3D simulations for unstructured meshes should be carried out to make sure that they can reproduce the flow separation correctly. The use of a mathematical boundary condition for defining the water level is recommended to avoid the extra computational power for the control structure. To acquire the knowledge of flow around groynes and weirs, the experimental set-ups are recommended, and well-proved non-linear $k - \epsilon$ and $k - \omega$ turbulence closure models should be applied in the numerical modellings.

Acknowledgements

First of all, I would like to sincerely thank Marjan Kreijns who took me to the TUDelft of The Netherlands, and Alwin Commandeur who introduced me the great things of hydraulic engineering. Then, I am also grateful to my teachers from my home university, Myanmar Maritime University, for allowing me to study in TUDelft under the NICHE capacity development project.

I also would like to express my sincere thanks to the graduation committee composed of Prof. Dr. ir. Wim Uijttewaal who always gives critical thoughts to me, Dr. Erik Mosselman who explained patiently the essential background knowledge, Dr. Kees Sloff who provided me very constructive suggestions, Dr. Martine Rutten who encouraged me during undertaking the thesis, and Dr. Mohamed Yossef who initiated the main theme of this thesis. Moreover, I would like to say thank you to Dr. Jeremy Bricker who helped me with `OpenFOAM` framework.

I should mention my sincere appreciation to Myanmar friends who always helped me during my stay in The Netherlands, especially Daw Thadoe for catering her delicious lunch to me.

Last but not least, I would like to acknowledge deeply my parents who always support everything what I want in my life, for their greatest love.

Contents

List of Figures

List of Tables

Chapter 1

Introduction

1.1 Motivation

The use of mathematical models and physical models has become indispensable in engineering and scientific research, especially research dealing with the development of the society. Likewise, in the fields of river engineering and hydraulic engineering, these tools play an important role in the stages of predicting, designing and optimizing engineering works, such as construction of weirs, dams, groynes, etc., in such a way that these hydraulic structures are able to work properly and minimize undesirable failures. Accordingly the reliability and validity of these numerical tools need to be ensured for the quality of their predictions. On the other hand, these models need to be employed efficiently and economically attractively.

Myanmar, a country in south-east Asia, comprises huge river systems which are required to be managed for training the waterways, protecting the riverine inhabitants against bank erosion and floods during the rainy season and controlling the water storage during the summer season for agriculture and navigation. To accommodate these purposes, different types of hydraulic structures need to be constructed for their respective tasks. Among them, the groyne is a type of hydraulic structure used for navigation and bank protection in Myanmar. The issue of how to model the groynes in numerical models arose.

There are two practices for modelling groynes in hydraulic models, which are (1) structural representation and (2) non-structural representation. In the latter representation, a sub-grid approach is used, given that the dimensions of the hydraulic structure are small compared to the computational grid size.

In the sub-grid approach, weir formulas are applied for groynes, assuming that weirs and groynes are equivalent. However, it is doubtful whether they can actually represent the same. This doubt necessitates research on the differences between groynes and weirs in terms of near-field flow characteristics.

This research is motivated by the fact that groynes need to be modelled properly and attractively in terms of reliability and limited computational resources in real-life applications. The issues of detailed numerical modelling of flow over these structures need to be identified.

1.2 Background

In nature, the environment of fluid comprises different scales of motion, length and time, leading to the different scales of energy. While one is interested in the smaller scale phenomenon such as the respiratory system of the human body, one may be fascinated by the large-scale behaviour such as the prediction of catastrophic cyclones. On the other hand, one may be in love with the research of mid-range flow problems e.g. ventilation systems for residential buildings. Fortunately sometimes these different scales can be studied separately in an uncoupled system - in other words, the flow dynamics of a swimming man in the river is negligible for the study of long-term river bed degradation and aggradation. In such uncoupled cases, the strategy for

solving the main problem of interest, e.g. solely long-term river morphology, is more straightforward. However in most cases of fluid dynamics problems, one has to deal with a coupled system. For instance, the consequences of hydraulic structures cannot be eliminated in the study of river morphology, since their interaction plays an important role. Therefore one should include the different ranges of scales in the problem formulation, but mostly it is not possible to include every single scale in the huge problem domain due to the constraints of human ability and machines. Therefore it has to be achieved by *wisely* eliminating the smaller scales which are not very important.

In numerical modelling of hydraulic engineering, there exists a challenging task of tackling the different ranges of scales *simultaneously* i.e. from the huge ocean currents of about 100 kilometers to the tiny vertical flow of approximately 1 meter around a hydraulic structure. Actually there already had been a number of numerical simulation packages to solve the *large-scale* and *small-scale* flow problems in the natural environment and man-made environment *independently*. It means that a particular model designed for solving the large-scale phenomenon usually neglects the detail or *fine* contribution of small-scale ones, but they do include the *coarse* effects on the large size problem. Therefore generally it is difficult to incorporate the small-scale effects into the large-scale problems *appropriately* i.e without overestimating or underestimating the small-scale events. The reason is because the computational cells should be small enough to capture such a tiny flow pattern whilst using these small mesh cells leads to huge consumption of computational power.

In numerical simulations, the dependence of computational time on the discretized mesh size hampers the modelling of small-scale problems in large-scale models, leading to an excessive amount of computations in a single model. This difficulty is commonly associated with the turbulence of the flow which consists of a wide range of length scales and time scales. In order to overcome this problem, most of the conventional hydraulic models have hypothesized various assumptions regarding the small length and time scales.

In river engineering practice, the effect of hydraulic structures on the hydrodynamic and morphodynamic conditions is evaluated using numerical modelling and physical modelling. In the aspect of numerical modelling, one difficulty arises in modelling the hydraulic structures in the river or canal i.e. the compromise between the computational time and the accuracy of the simulation result, because very small computational meshes are required to resolve the detailed effect of structures, but these small-sized meshes cause overloading for the large river model, leading to unnecessary computational waste.

To circumvent this notorious crisis, the *sub-grid* approach has been used in case the dimensions of the hydraulic structures are much smaller than the grid size (Deltares, 2014). In this approach, only the overall influence of the hydraulic structures is considered in the usual hydraulic models by means of inserting the energy losses term or friction term in the momentum equations. The reason why the energy loss term is used in the governing equations is that the hydraulic structures are responsible for turbulent flows and energy dissipation in the flow generally.

Nevertheless, regarding the issue discussed above some achievements have been obtained using the sub-grid approach for modelling some kind of hydraulic structures in large-scale river problems. These workable examples of structures constitute gates, weirs, current deflecting walls, floating structures, culverts and barriers. One exception is integration of the *groyne* into river models directly. Traditionally *weir* structures have been used instead of an exact groyne representation, with the help of the energy loss coefficient in the governing equations (Deltares, 2014). However there is still a lack of theoretical support for representing groynes by weirs in large-scale flow models: no literature can yet guarantee the modelling of weirs in a river can reproduce the effect of groynes realistically.

Moreover, it is primarily important to discern the differences in flow behaviour between groynes and weirs in small-scale problems. Observation of these differences can lead to better understanding of flow parameterization for groynes in large-scale models.

1.3 Problem Statements

Zagonjolli et al., (2017) reported that the discharge coefficient of groynes is lower than that of weirs. They found that the lack of a definite and suitable formula for calculating the discharge for a groyne is a bottleneck to obtain the reliable discharge coefficient. Besides, for low submergence ratios, 2D circulation occurs around the groyne, hence the lateral exchange of flow plays a role. This needs to be investigated for parameterizations. Therefore it remains unclear whether weir formulations could be used for groynes in large-scale models.

The difficulty of modelling groynes and weirs in 3D models is the huge requirement of computational power and robust turbulence models. In 3D Navier-Stokes equation solvers, the implementation of a free-surface representation is also important for the flow over weirs and groynes. It is associated with the difficulty of defining the boundary conditions in the numerical packages e.g. the `interFoam` solver. Moreover, different types of meshes can influence the simulation results.

Therefore, numerical modelling of groynes poses two problems - (1) the debated assumption that groynes and weirs are equivalent in hydraulic models, and (2) the difficulty of modelling groynes and weirs in 3D detailed hydrodynamic modelling.

1.4 Research Objectives

The two problem statements lead to the following two research objectives. The first one reads:

> To understand the differences in flow character between the flow over a groyne and flow over a weir in fine-scale numerical models.

The understanding of the different flow behaviours will shed light on a better parameterization of groynes in large-scale hydraulic models, setting aside the use of weir formulations.

Another objective of the research, which came out from the usage of the `interFoam` solver as a research tool, states:

> To assess the limitations and advantages of `interFoam` in the field of river hydraulic applications, especially the simulation of hydraulic structures in the numerical flume.

1.5 Research Questions

In order to reach the research objectives described above, the following research questions are to be answered:

1. What are the differences in 3-dimensional flow structure between the weir and the groyne?
2. How does the groyne and the weir differ in terms of energy head loss?

For the above questions, there is the hypothesis that the flow around a short groyne is different from the flow over a weir while the flow over a long groyne is a combination of the flow around a groyne structure and the flow over a weir. Hence a research question also came out:

> To which extent (for which part) does a long groyne behave as a weir?

Regarding the additional research objective on the usage of the research tool, the set of research questions is as follows:

1. Which kinds of boundary conditions are required for the `interFoam` solver to simulate the open channel flow in the numerical hydraulic flume?
2. How can the required boundary conditions be implemented in `interFoam` solver for simulation of flow over the hydraulic structures?
3. How does the computational mesh affect the numerical simulations of `interFoam` solver in the study of flow over weirs and groynes?

1.6 Research Methods

The research methods are twofold for two different research objectives - the *interFoam evaluation model* and *weir-groyne model*.

The incompressible full Navier-Stokes equations multiphase solver, `interFoam` under `OpenFOAM` framework, was used for setting up the numerical models. Two different models, called *weir-groyne comparison model* and *interFoam evaluation model*, were created for different research objectives.

1.6.1 `interFoam` Evaluation Model

The *interFoam evaluation model* is intended for gaining insight of numerical issues, especially the results dependence on the mesh type, in the simulations of flow over the weir in `interFoam`. The unstructured non-orthogonal mesh and structured more-orthogonal mesh were tested for their influences on the simulation results. The *weir-groyne comparison model* is simulated in 2D and 3D numerical settings using the high and low specific discharges. The criteria for assessing the quality of the models is if they can reproduce the flow separation in the correct position or not.

The *literature review* for this model will include the following two parts:

1. Structure of `interFoam` solver
   The historical and technical background of the `interFoam` solver is studied and some practical difficulties, especially for hydraulic engineering applications, are reviewed.
2. Examples for `interFoam` solver application in hydraulic engineering
   Three research papers were read for analyzing their methods for defining boundary conditions, especially the ways to tackle the constant water level at the downstream end.

For the analysis, the skill of the *interFoam evaluation model* will be assessed. It is necessary to evaluate how the mesh types effect the numerical results, especially the eddy formation in the flow over the weir. Besides, since maintaining the constant water level at the downstream edge of the flume is a necessity, it is required to judge how `interFoam` solver tackles it.

1.6.2 Weir-Groyne Comparison Model

The *weir-groyne comparison model* is set up for realizing the differences between the weir and the groyne. The physical and numerical settings are different from those of the *weir-groyne comparison model* in order to overcome some constraints of the latter one. A variety of flow simulations were performed using the different lengths of groyne and weir in narrow and wide flumes. The streamline patterns and energy head losses were compared between these two structures.

The literature study will consist of the following parts:

1. Flow dynamics around groynes
   This part of the literature review is intended to study how the flow behaves around a single groyne and groyne fields during submerged and emerged conditions. The scientific knowledge of flow processes will support the evaluation of numerical simulations.
   This part also addresses the different numerical methods to simulate the flow around a groyne.
2. Common practices for modelling groynes in large-scale problems
   This part is to acquire the knowledge of how the traditional simulation packages include groynes or other hydraulic structures in large-scale problems. Furthermore, it is important to recognize which assumptions are used for modelling a groyne.

3. Parameterization methods for simpler models
   The final part of the literature review describes a parameterization methods towards simpler models. However since it is far beyond the scope of the current research, detailed technical information about parameterization is omitted.

The analysis for this model is for understanding the differences between the groyne and the weir. Therefore, the flow streamlines around the groyne and over the weir need to be visualized and their patterns need to be differentiated. The energy head losses occurring to the groynes and the weirs are also calculated and compared to realize the groyne and weir differences.

Based on these research findings, the conclusions will be drawn, and then the recommendations are supported for the comprehensive considerations for the future research. Moreover, the method of representing a groyne in depth-averaged models will be presented.

1.7 Outline

Chapter 1 introduces the research motivation, objectives and methods. It is followed by two literature reviews in Chapters 2 and 3 which present the flow dynamics around the structures and the numerical methods for such kind of flow simulations. Chapter 4 describes how the models were constructed and how the sets of simulations were performed. Chapters 5 and 6 present the simulation results for the corresponding models. Chapter 7 concludes the research findings and the recommendations for future research. Appendix A presents the flow near the groyne fields, and the numerical techniques for flow simulation. Appendix B comprises the common practices for modelling the groynes in the large-scale problems. Appendix C describes the analysis of the relationship between the drag coefficient and the water level using a simple 1D momentum equation. Appendix D provides detailed findings during set-up of *weir-groyne comparison model*, and Appendix E presents the derivation of the modified Volume of Fluid equation from the literature.

Chapter 2

Literature Review: Flow near Structures

2.1 Introduction

The *groyne* is a kind of hydraulic structure projected from the bank of the river towards the channel for the purposes of the bank protection, ecological services for riverine animals, and deepening the navigable channel during the low season. The groynes are mostly constructed in series along the river to achieve the desirable purposes. Their orientation angles can be at any angle from the bank towards the river, and they can be built of using different construction materials. Sometimes the groynes can be permeable while others are intended to be impermeable, or solid and rigid structure.

The groynes can be categorized based on (1) the permeability and materials of construction, (2) the submergence stage, (3) the action on the stream flow, and (4) the appearance in planview (Yossef, 2005). The important characteristics of the group of groynes are (1) planview shape and orientation, (2) spacing between the groynes, (3) length of the groynes, (4) crest elevation and base depth, and (5) cross-section and construction materials (Yossef, 2005). The different combinations of aforementioned characteristics lead to the different results of the hydrodynamics and morphodynamics in the river. The reader is referred to the thesis of Yossef, (2005) for more details on choosing the numerical values of these parameters.

In this literature review, the flow around a single groyne will be studied during the submerged condition and the emerged condition. Following the physics of flow dynamics around the groyne, the brief story of numerical modelling used for solving this complex flow problem will be presented. In the numerical aspects of this study, the mathematical modelling techniques will be emphasized more than the physics of the flow. Moreover, some common practices for modelling the groynes in the 2D large-scale numerical models are presented, where the local flow behaviour is neglected by using the parameterized relationships. It should be noted that since this research does not deal with the sediment transport or morphology, the local scour problem will be omitted here.

2.2 Flow dynamics around the groynes

Actually there are a lot of aspects regarding the complex turbulent flow structure around the groyne, and it is not possible to study all of these aspects in this study. However since the main objective of this research is to incorporate the small-scale effects of groynes into the large-scale models, it becomes necessary to realize the physical interaction of these two processes. Therefore the study will include (1) the eddy formation around the groyne, (2) its effect on the mean flow velocity and momentum exchange between the mean flow and the flow in groyne field, and (3) the shear stress distribution. Moreover in this study, groynes on only one bank of the river will be focused, however in reality on both sides of bank, the groynes are built.

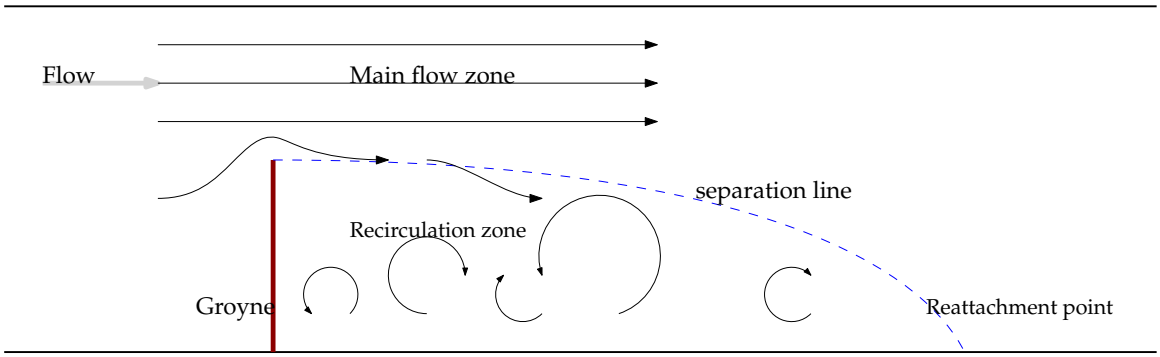

FIGURE 2.1: General flow pattern around a single emerged groyne. The different size of eddies occur in the recirculation zone due to flow separation. The streamline denotes the shear layer where a velocity gradient exists between main flow zone and recirculation zone. The same flow pattern cannot expected for the submerged groyne.

2.2.1 Experimental studies

Pattanaik, (1966) was one of the pioneers who studied the effect of groynes on the river flow using the experimental hydraulic flume. He did intensive investigation of complex flow structures i.e. vortex and eddy structures at both the surface and near the bed. Moreover he studied the effects of the structural parameters of the groyne on the recirculation zone and eddy dimensions of which the terminology will be explained later in this section. The work of Francis et al., (1968) was appreciated for outlining such a complicated study of flow structure around the groyne i.e. their study dealt with not only horizontal structures but also vertical structures.

2.2.1.1 Flow around a single emerged groyne

Generally once a hydraulic structure (e.g. bridge piers, abutments, or groynes) is confronted by the flow of water in the emerged condition, the streamlines will deflect around the structure, causing the flow separation induced by the adverse pressure gradient. This flow separation is mainly responsible for the formation of the detached shear layer (or mixing layer) at the tip of the groyne, and the wake (or eddy) flow past it, which occur in the horizontal plane. Also in the vertical plane there is an adverse pressure gradient along the surface of the groyne which leads to the downward flow of some incoming streamlines, and flow separation again. Eventually the flow separation forms the vortices at the base of the groyne, the so-called *horse-shoe vortex* system (Koken and Constantinescu, 2008). It should be noted that during the submerged condition, the different hydrodynamics may result in around the submerged groyne.

These vertical-structure and horizontal-structure vortices can move downstream from the groyne tip, of which their motions may be steady or unsteady, depending on the inflow condition (Koken and Constantinescu, 2008). It means that the fully turbulent inflow condition guarantees the unsteady vortex shedding. This so-called *vortex shedding* can be seen mostly in 2D horizontal plane of the laboratory experiments. The vortex shedding is the intermittent process which can enhance the exchange process of momentum much larger than the exchange by mixing layer only (Uijttewaal et al., 2001). The vortex shedding is triggered by a relatively energetic and steady secondary circulation cell (which is explained later) existing near the upstream corner of the groyne (Uijttewaal et al., 2001).

The streamlines are separated or deflected by the groyne causing the eddy motion behind the structure, and then after some distance (in terms of length scale), the streamline arrives back its original (imaginary) position, or reattaches a point on the side wall of the channel, the so-called *reattachment point*. Rajaratnam and Nwachukwu, (1983) denoted the shear layer as the horizontal

distance on the downstream of the groyne, ranging between the solid wall of the flume and the outer layer of the deflected flow which appeared due to the separating streamline. The shear layer is primarily due to the differences of momentum, or velocity between the undisturbed main flow, and the groyne-affected flow behind the groyne.

The knowledge of the reattachment point seems important for estimating the energy dissipation. The turbulent motions or eddy motions which are responsible for turbulent viscosity leading to energy dissipation, occur within the area between the groyne tip and the reattachment point. In this sense, the reattachment length or size of *recirculation zone* can indicate the amount of eddy zone, or turbulent viscosity. Rajaratnam and Nwachukwu, (1983) found that the reattachment length is approximately six times the maximum width of this recirculation zone, or $x \approx 12L_g$, where L_g is the length of the groyne, and x is the horizontal dimension in x-direction in case of thin groynes. For the case of semi-cylindrical shape groyne, the reattachment length was found to be $x \approx 5L_g$. Therefore the shape of the groyne implies the streamline curvature around the groyne and eddy formation behind the groyne.

The area which happens to the exchange of mass and momentum between the recirculation zone and the main channel is also called the *mixing layer* and has been paid a lot of attention by the researchers, in cases of not only groyne problems but also other shallow flow problems (Uijttewaal and Tukker, 1998; Talstra, 2011; Van Prooijen, 2004). Generally the mixing layer develops as a result of two different velocities in a single conveyed channel. In fact in the groyne case, the mixing layer is accompanied with the downstream recirculation zone, caused by the streamline separation due to the groyne. The turbulent structures appearing in the shallow mixing layer or in the recirculation zone are of large 2D character which can also interact with vertical shear and small scale turbulence (Uijttewaal and Tukker, 1998), hence called *quasi 2D coherent structures* (Q2CS) by Higham et al., (2017).

The sudden expansion in the mixing layer is originally studied by Talstra et al., (2006) with the name of *scale jump* which is due to the interaction of large primary cell and small secondary cell in the recirculation zone. In their tests, they observed these two cells of circulation pattern, and in some cases three cells in the wake zone, which is similar to the observation of Koken and Constantinescu, (2008). Talstra et al., (2006) noticed that when the mixing layer approaches the primary cell, the flow structures appear to be boosted significantly in terms of energy and spatial scale. This is positive interaction between the vorticity cores from the mixing layer and the primary cell i.e. the effect of *vortex merging*. This jump scale structure can penetrate sufficiently the main flow and the primary cell, causing a lot of exchange of materials. The initialization of the jump scale is located near the interface between the primary cell and the secondary cell (Talstra et al., 2006).

In short, the *large*-scale shed vortices or scale jump phenomenon is the inherited feature of the vortex shedding process caused by the presence of secondary recirculation zone in the upstream corner of the groyne. Therefore it became important to realize about the circulation cells for estimating the scale jump and consequently, the boosted exchange of mass and momentum. Talstra et al., (2006) claimed that these large-scale shed vortices do not emerge from the flow separation, but from the interaction of the mixing layer vortices, and the primary and secondary cells.

Although the lateral momentum transfer is dominated by the 2D structures and horizontal shear layer, the secondary flow can contribute to that as well (Talstra, 2011). The secondary flow is a consequence of centrifugal force on the vortex in the large coherent structures, a phenomenon discovered by Carmer et al., (2004) through the experiment of a cylindrical pier i.e. a von Kármán vortex system. In the region of secondary flow, the divergence and convergence zones occur due to upwelling and downwelling of water. More specifically the divergence zones exist inside the coherent structures themselves while the convergence zones lie along the eddy boundaries connecting the eddies (Carmer et al., 2004). Similarly in the experiment on lateral expansion flow by Talstra, (2011) which geometry is slightly different from the groyne in the flow, the secondary flow pattern was found to enhance the lateral transport of mass and momentum. However this effect

is obvious only in the near-field and middle-field of the groyne region whereas it degenerates in the far-field (Carmer et al., 2004; Talstra, 2011) so the secondary flow should not be neglected in the mathematical modelling of shallow turbulent flows.

Finally, in the emerged case of the groynes installed at the shallow water, the dominant process was found to be predominantly 2D horizontal exchange of mass, momentum and energy, based on the experimental results. The findings on the size of the reattachment zone are not universal or generic for every type of groynes, regarding the shape, permeability, spacing of groynes and orientation angle.

2.2.1.2 Flow around a single submerged groyne

The flow dynamics around the submerged groyne during the high water season is also interesting especially for the tropical regions where receives high rainfall intensity during the rain season, e.g. Southeast Asia countries. It is also important for the groynes to function very well during the high season, and subsequently the knowledge of the interaction between the flow and the submerged groyne becomes the crucial part. Although a lot of researches have been done on this aspect by many researchers (Uijttewaal et al., 2001; Yeo and Kang, 2009; Kadota et al., 2006; Kuhnle et al., 2008) , in this section only the study focused on a single submerged groyne will be presented.

Kadota et al., (2006) studied experimentally the flow patterns around a single groyne during both the submerged and the emerged conditions for the specific case in a river of Japan. They noticed the flow separation in the vertical plane over the submerged groyne and it accompanied with vertical velocities. Due to this effect, the high flow velocity over the groyne occurred due to the flow constriction, reduces dramatically just past the groyne. The turbulent intensities just downstream the groyne can be enhanced by the vertical flow separation. Therefore the highest turbulent intensities were seen at the tip of the groyne. This 3D flow nature does not appear in the emerged case whereas the horizontal flow separation due to the submerged groyne is apparently much smaller than the one in the emerged case where 2D horizontal eddies are larger. During the submerged condition, the velocity at the base of the groyne is higher due to the overflow effect than the velocity at other parts (Kadota et al., 2006).

Yeo and Kang, (2009) also analyzed the flow around a single submerged groyne using the laboratory and 3D numerical experiments, observing that the length of the recirculation zone was five to six times the length of the groyne. The recirculation zone length is dependent on the water depth of approach flow. The complicated flow pattern was generated by the interaction of the vertical overflow and the vortex in the recirculation zone. The intense turbulent energy was at this location and the velocity at the water surface was reduced, which might be as a similar observation as Kadota et al., (2006) did.

Kuhnle et al., (2008) used a trapezoidal shape groyne in the flume to observe the 3D flow structures, and they observed that the different reattachment lengths from the work of Rajaratnam and Nwachukwu, (1983). It is due to the overtopping flow and the groyne shape, which also proves the existence of 3D eddy as the previous researches observed. The 3D flow separation occurred downstream of the groyne while the large portion of the water crossed over the groyne. The highly 3D eddy can effect the shear stress distribution around the structure. It should be noted that there was no clear evidence for the presence of strong downward flow at the upstream face of the groyne (Kuhnle et al., 2008). It can be stated that this finding is very different from the downward flow due to the emerged groyne.

It has been already remarked that the flow behaviors around the submerged groyne and emerged groyne are very different in terms of the composition of eddy structure downstream of the groyne, and the dimensionality of the eddy. While the emerged groyne can cause essentially the downward flow at the upstream face of the structure (leading to the horse-shoe vortex system), the submerged case is not supposed to create it. During the submerged condition the extra force appeared as the overflow impact across the groyne. It was also noticed that the difference

in the recirculation zone between these two cases. In the coming sections, the discrepancies between the submerged and emerged groyne fields will be presented as well as their flow patterns and exchange process.

2.3 Parameterization methods for simpler models

The parameterization is the representation of complex physical phenomenon by use of obviously significant parameters for the sake of construction of a simpler model. The parameterization can provide the foundation steps for further analysis. The procedures for building the parameterized relationship in the environmental fluid mechanics are briefly explained in the book by Shen et al., (2002) but the explanation is found very general. In this book they focused solving the inverse problem with the statistical methods and numerical optimization methods. Since they seem to intend the usage of big data, this reference is apparently far from the present research.

However some examples about the parameterization of flow in the turbulent flow can be seen in some literatures. The parameterizations for the flow dynamics around the groyne are proposed by Yossef and Vriend, (2010) considering the fact the turbulent fluctuations relate to the mean value. Among the two sizes of fluctuations, the large-scale ones are observed significantly contributing to the total turbulent intensity by means of comparison. They estimated that the maximum large-scale velocity is the product of a constant coefficient β with the velocity difference between the time-averaged velocity of fast main channel and that of slow stream in the groyne fields i.e. $u'_{max} = \beta_1 \Delta u$ for streamwise velocity component, but for transverse component $v' = \beta_2 u'$ which is different definition from the former one. Besides, the parameterizations for the mixing layer width, flow periodicity via Strouhal number , and coherence were also presented by Yossef and Vriend, (2010) analyzing the laboratory measurements.

Another example is the parameterization of momentum exchange into the drag resistance, conducted by Kruijt, (2013). He considered the momentum exchange occurring between the main channel, the groyne fields, and the flood plain, of which these components constitute a compound channel. For the compound channel, the momentum balance can be described as the following (Van Prooijen, 2004):

$$ghi = \underbrace{\frac{g}{C_{base}^2} u^2}_{\text{bed resistance}} + \underbrace{\frac{1}{\rho}\frac{\partial h \tau_{xy}}{\partial y}}_{\text{momentum transfer}} \tag{2.1}$$

where h is the water depth, i is the bed slope, C_{base} is the bottom resistance, and τ_{xy} denotes the transverse exchange of momentum or depth-averaged transverse shear stress. This formulation has as a similar structure as that of Yossef, (2005), equation B.13, however the latter one considered the control volume excluding the mixing layer, but including only the groyne fields. Kruijt, (2013) modified the equation 2.1 by considering for the three separate channels i.e. main channel, groyne fields, and the flood plain, resulting in three velocity equations. These velocity equations are a bit lengthy, which use their corresponding friction coefficients. It should be noted that one has to model the turbulent stress from the equation appropriately 2.1.

In fact it is hard to predetermine which methods will be necessary for the parameterization without knowing the physical processes in hand.

2.4 Conclusion

The different configurations of the groynes could give rise to their corresponding flow structures, for instance the emerged groyne fields initiate the 2D-dominant eddies while the submerged ones present the 3D eddies. Moreover the transfer of momentum and mass between the groyne field and the main channel does not hold the same for both of these two different groyne settings.

The 3D effect should not be excluded in the mathematical simplification of the flow around the groyne. This is in fact the case for the large-scale 2D numerical models. The knowledge how to represent the 3D flow features wisely in the 2D models is still lacking although many different kinds of turbulence models are introduced by many researchers.

The choice of turbulence closure modelling is crucial since it plays an important role in the simulation of different rages of turbulent length scales. However the usage of advanced turbulent closure models are relatively expensive for basin-wide applications, so it is desirable to model the groyne without using any turbulence models for these applications.

To the knowledge of the author, the sub-grid approach is still being used widely in the commercial hydraulic models for the inclusion of groynes in the river or channel, except for FLOW3D software suite of Flow Science®. Under the non-structural sub-grid approach, there are two formulations for modelling the groyne: (1) weir formulation, and (2) the drag resistance approach.

When both of weir formulation approach and drag resistance approach are applied for the groyne cases, there is one ambiguity of measuring the water depth in the equations B.2 and B.11 because the water level is not uniform anymore across the width of the channel unlike the weir cases. It should be noted that this is prominent behaviour only in the near-field groyne simulations rather than in the far-field models. For the far-field calculations, it is assumed that the water surface slope in the groyne field and the main channel are the same.

Chapter 3

Literature Review: Characteristics of Numerical Models

3.1 Governing equations

Generally the fluid dynamics researches mainly rest on the Navier-Stokes equations. Since there exists a lot of different versions of Navier-Stokes equations depending on the degree of complexity, the researcher has to decide which a particular version would be used in order to realize the specific purpose.

The linear or non-linear Shallow Water Equations (SWEs) are mainly applied in the hydraulic models in which the horizontal dimension of the flow is assumed to dominate the vertical direction of motion. In other words, the vertical acceleration in the flow is negligible compared to the horizontal component of acceleration since the change in vertical velocity is extremely small in the so-called hydrostatic pressure assumption. In fact, the SWEs are one set of equations which are simplified version of the full Navier-Stokes equations by transforming the vertical momentum equation into the hydrostatic relationship 3.1.

$$\frac{\partial p}{\partial z} = -\rho g \tag{3.1}$$

Although the SWEs or simple hydraulic models possess computationally cheap advantages, it lacks to solve some hydraulic problems where the vertical acceleration is dominating e.g wave breaking, tidal bore, baroclinc flows. Henceforth the original SWEs are modified by including the additional non-hydrostatic pressure term in the horizontal momentum equations and vertical momentum equation. The aforementioned non-hydrostatic pressure arises from the decomposition of total pressure term into the hydrostatic and non-hydrostatic ones (Stelling and Zijlema, 2009). The so-called *3D-quasi hydrostatic* or *non-hydrostatic* equations are solved with the use of *fraction step* method numerically (Casulli and Stelling, 1998; Zijlema and Stelling, 2005).

The fully 3D Navier-Stokes equations can describe any kind of flow phenomenon. They do not hold any assumption except the turbulence closure modelling which is explained in the section 3.3. The numerical models which solve these equations are generally embedded in the Computational Fluid Dynamics (CFD) softwares which are suitable for the small-scale problems and complicated flow phenomenon. They solve the complete set of three dimensional equations of momentum conservation and continuity equation with a combination of appropriate turbulent modelling technique.

3.2 Representation for water surface

Regarding the simulation of the top surface of the fluid domain, there are two ways to consider that top surface in the models. The first one is the rigid-lid assumption and the second is the free surface modelling.

The rigid-lid assumption is valid only when the water surface elevation η does not change in time t (Casulli and Stelling, 1998) where generally the river flows exist in the subcritical condition. Since it neglects the movement of the water surface in time, this assumption is not applicable even for the simulation of real waves and tides. In most cases the river shows the variation of water level in time and space.

The free surface equation is essential for the simulation of realistic long and short waves. There are different levels or methods for representing the free surface condition in terms of the accuracy. Some of the well-known free surface tracking methods for their good accuracy are Marker-and-Cell (MAC), Volume-of-Fluid (VOF), and Level-set method since they can mimic the actual breaking waves near the shore, air entrainment in the flow over the hydraulic structures, and dam breaking cases (Stelling and Zijlema, 2009). However due to their requirement of expensive computational power, they are attractive for only the small-scale problems, not for the whole river and ocean.

The alternative way for capturing the free surface motion is the usage of a single-valued function. This method is more simpler and requires less grid cells, therefore less computational resource compared to the aforementioned complicated methods e.g VOF method. The near-shore processes and short waves in the deep water can be simulated with good accuracy by using the single-valued function approach of free surface representation (Stelling and Zijlema, 2009).

Froude Number

The Froude number can be used to choose precisely the appropriate free-surface representation; rigid-lid assumption or free surface tracking methods. Moreover it can determine that the flow regime is whether subcritical, critical, or supercritical. The Froude number reads:

$$Fr = \frac{U}{\sqrt{gd}} \tag{3.2}$$

wheter U is the mean velocity, and d is water depth. It is the measure of inertial forces to gravity forces (Te Chow, 1959). If the Fr is larger than unity, it is critical condition while it is subcritical flow for $Fr < 1$. Otherwise the flow is in the supercritical condition.

In the case of high Fr, the rigid-lid approximation cannot capture the flow surface correctly. Therefore the free-surface tracking method should be used for the case of $Fr \geq 0.5$ (Paik et al., 2014). It should be noted that the larger Fr value causes the large variation in the flow surface (Roulund et al., 2005).

3.3 Turbulence closure modelling

It has been researched that the set of Navier-Stokes equations can describe the details of the flow behaviour, provided enough computational resources and time. However in reality it is very restrictive to solve these equations numerically for retrieving the complete information about the turbulent flow, the so-called Direct Numerical Simulation (DNS). The turbulent flow contains the fluctuation component of the field variables in different scales ranging from the integral to micro scales. The current computational facility cannot resolve all these scales for the high Reynolds number whereas it is possible for low Reynolds numbers (Moriche et al., 2017). It means that the DNS approach cannot be used for the real world applications at which high Reynolds number occurs.

The original set of Navier-Stokes equations can be transformed to averaged versions which depict only the mean value of field variables by averaging methods. The Reynolds Averaged Navier-Stokes equation, also called RANS, is one of averaged versions manipulated by Reynolds averaging. Unfortunately the averaging step results in the new unknown terms called Reynolds

stresses which need to be closed. Therefore, the turbulence closure modelling is used to close these system of equations. There are enormous amount of turbulence closure modelling for different interests and degrees of accuracy and complexity.

In fact the turbulence modelling is a technique to approximate the statistical properties of the turbulent flow. The closure models can be categorized into (a) the algebraic (zero-equation) model, (b) the one-equation model, (c) two-equation model, and (4) second-order closure models (Wilcox et al., 1998). Among them, the two-equation model types are the popular ones in the hydraulic engineering practices which do not necessitate the empirical relationships for the length scales or other turbulent quantity (Rodi, 2017).

One of the famous turbulence closure modelling is the $k-\epsilon$ model which uses the transport equations of turbulent kinetic energy, k, and dissipation rate, ϵ. It should be noted that the $k-\epsilon$ model is restricted to the high Reynolds numbers and the application of where local isotropy prevails (Rodi, 2017).

Standard $k-\epsilon$ model

Before describing the $k-\epsilon$ model, the RANS reads without including the free surface effect (Tryggvason, 2011):

$$\frac{\partial \boldsymbol{U}}{\partial t} + \nabla \cdot (\boldsymbol{U}\boldsymbol{U}) = -\frac{1}{\rho}\nabla P + (\nu + \nu_t)\nabla^2 \boldsymbol{U} \tag{3.3}$$

where $\boldsymbol{U}$ is the averaged value of the velocity vector excluding the fluctuation components, P is average pressure, and ν_t is turbulent eddy viscosity defined by:

$$\nu_t = C_\mu \frac{k^2}{\epsilon} \tag{3.4}$$

in which C_μ is the empirical constant, and k and ϵ need to be modelled again.

The transport $k-\epsilon$ equations are written respectively as below (Tryggvason, 2011):

$$\frac{\partial k}{\partial t} + \boldsymbol{U}\cdot\nabla k = \nabla\cdot(\nu + C_2\nu_t)\nabla k - \tau_{ij}\frac{\partial U_i}{\partial x_j} - \epsilon \tag{3.5}$$

$$\frac{\partial \epsilon}{\partial t} + \boldsymbol{U}\cdot\nabla \epsilon = \nabla\cdot(\nu + C_3\nu_t)\nabla \epsilon + C_4\frac{\epsilon}{k}\tau_{ij}\frac{\partial U_i}{\partial x_j} - C_5\frac{\epsilon^2}{k} \tag{3.6}$$

where

$$\tau_{ij} = \overline{u_i' u_j'} = \frac{2}{3}k\delta_{ij} - \nu_t\left(\frac{\partial U_i}{\partial x_j} + \frac{\partial U_j}{\partial x_i}\right)$$

known as Reynolds stress. The empirical coefficients are $C_\mu = 0.09, C_2 = 1.0, C_3 = 0.769, C_4 = 1.44$ and $C_5 = 1.92$.

Reynolds number

The Reynolds number is the indicator whether the flow regime is laminar, transition, or turbulent flow. It is the ratio of the inertial force to the viscous force. If the flow is in laminar region, no turbulence modelling needs not to be used since turbulent fluctuations are not allowed in the laminar flow. The Reynold number reads:

$$Re = \frac{\rho U L}{\mu} \tag{3.7}$$

where ρ is fluid density, U is free stream velocity, L is the characteristic length, and μ is the dynamic viscosity. The flow becomes turbulent when the Re value is large and the flow will be

TABLE 3.1: List of numerical softwares and frameworks for solving the continuum partial differential equations.

	Type	Method	Equations	Free-surface	Availability	Remark
FLUENT	CFD[1]	FVM	3D NSEs	VOF	Commerical	Software
COMSOL	CFD	FEM	3D NSEs	Level-set	Commercial	Software
Delft3D	HM[2]	FDM	SWEs	single-valued	Open-source	Software
MIKE3 DHI	HM	FDM	SWEs	single-valued	Commercial	Software
SWASH	HM	FDM	SWEs	single-valued	Open-source	Software
FEniCS	-	FEM	PDEs	-	Open-source	Framework
OpenFOAM	-	FVM	PDEs	VOF	Open-soruce	Framework

[1] Computational Fluid Dynamics is a branch of fluid dynamics science, and the CFD models are capable for simulating the complicated continuum flow problems. It solves the fully 3D Navier Stokes equations with the advanced turbulence modelling.
[2] Hydraulic model designed for free-surface and morphological problems in the coastal, rivers and seas, and it uses the non-linear Shallow Water equations and/or non-hydrostatic equations.

laminar if the Re value is small. The transition flow occurs if Re is in between 500 to 2000 (Te Chow, 1959).

3.4 List of simulation softwares

The table 3.1 summarizes the numerical tools for solving the Navier-Stokes equations with their own numerical discretization schemes and different styles of meshing. Among them, the so-called hydraulic models are designed for free-surface flow problems occurring in the rivers, seas and oceans naturally. These model apply the linear and/or non-linear SWEs for prescribing the flow physics. In some special cases where the vertical acceleration is as important as horizontal motions e.g. short waves, they use the non-hydrostatic equations as the governing equations, for instance SWASH (Simulating WAves till SHore). Due to the nature of hydraulic models of which less computational power is demanded, it uses single-valued function to represent free surface movement e.g Delft3D, MIKE3.

The different one from hydraulic softwares is the CFD software which is intended primarily for industrial applications, but later it merges with the environmental flow problems. Unlike the former ones, these softwares solve the full 3D Navier-Stokes equations and implement the complex free surface tracking methods e.g Volume of Fluid (VOF), level-set methods. In general the CFD models are not used for hydraulic engineering purposes, except for the small-scale local problems, for instance the flow over the weir, and local scour around the hydraulic structure.

Both of the hydraulic models and CFD models include the turbulence closure modelling for estimating turbulent viscosity. It is important to recognize which softwares can represent the turbulent properties correctly for the particular problem, and to pick one correct choice. Although the commercial software packages provide a variety of the closure modelling choices and user-friendliness, it is impossible to implement own creation because it is closed-system environment, in addition to its expensiveness.

The different numerical discretizations affect the accuracy of the solution in terms of transport conservation, monotonicity, stability and mesh flexibility. While the finite element approximation can work on the unstructured mesh flexibly for the complicated geometry (Hans Petter Langtangen, 2016), the other two methods, Finite Volume Method (FVM) and Finite Difference Method (FDM), prefer the structured mesh to unstructured mesh. However the FVM can guarantee that the numerical recipe is aligned with the conservation property while the Finite Element Method (FEM) and FDM cannot guarantee it intrinsically.

Apart from the CFD packages, there are also the numerical solver frameworks like FEniCS, OpenFOAM as described in the table 3.1. The user has a complete freedom to modify, implement, and use the source code, so the result is totally dependent on the governing equations specified by the user. The well-known FEM and FVM open-source frameworks are FEniCS and OpenFOAM respectively. The OpenFOAM has a good reputation for VOF methods in multiphase flow for free surface tracking. Furthermore there are a lot of flow solvers for the specific governing equations and the physical problems inside the OpenFOAM environment.

3.5 OpenFOAM

OpenFOAM is an acronym of Open Source Field Operation and Manipulation that is a framework for solving the problems in the continuum mechanics. The libraries which are *solver* and *utilities* in the OpenFOAM framework are written in C++ language, which are modifiable and extendable according to the modifications in the governing equations and desired workflow, since it is open source framework (Greenshields, 2015).

The principle numerical discretization method applied by the OpenFOAM is the FVM approach. The OpenFOAM can deal with the physical problems constructed with the un-structured polygonal meshes. The OpenFOAM is also capable of tracking the complex interfaces arising from the multiphase flow problems, using the VOF free surface tracking technique. Moreover, the OpenFOAM offers the end-user a wide range of choices for the computation by supporting the built-in libraries.

The governing equations solved by the OpenFOAM are hard to say generally, but it is possible to describe for a particular solver, because there are many different solvers which are designed for their specific purposes. Accordingly their governing equations are different from each other, plus the user can develop his own mathematical models and can implement it under the OpenFOAM framework by naming the new solver. In the present research, for the fluid flow problems, the governing equations solved by the incompressible and multiphase types of solver are incompressible Navier-Stokes equations.

The OpenFOAM has implemented a variety of turbulence closure models for the incompressible/compressible RANS equations and LES equations (Greenshields, 2015). The user can choose one of the three algorithms (SIMPLE, PISO and PIMPLE) in OpenFOAM to tackle the pressure-velocity coupling that inherited from the nature of Navier-Stokes equations. Besides it is also possible to select the *linear*-solver from the OpenFOAM libraries to solve the systems of algebraic equations resulted from the numerical discretization procedures.

3.5.1 OpenFOAM in hydraulic engineering applications

The interFoam solver, a multiphase solver of the OpenFOAM, has been widely used in the coastal engineering and ocean engineering applications (Higuera et al., 2013; Higuera et al., 2014). The main concerns of interFoam solver in these applications are the accuracy of interface representation in the wave breaking processes, and the boundary conditions of the wave generation and absorption. Due to the differences in boundary conditions between the coastal modelling and river hydraulics modelling, the explanation of the interFoam in the coastal fields are omitted here. Only the applications in the river hydraulics will be presented.

Jellesma, 2013 studied the form drag of subaqueous dunes in the river channel using the modified version interFoam solver. With the interFoam solver, Ducrocq et al., 2017 also investigated the drag force around a cylinder in the environmental flow. Duguay et al., 2017 used the interFoam solver to study the pool and weir fishway and compared the results against the FLOW3D simulations. The interFoam can also be used for studying sediment transport and bed deformation in the free surface flow (Sattar et al., 2017).

Using the built-in libraries under the `OpenFOAM` framework and combining with other numerical approaches, the researchers developed their own solvers to study the specific problems. For instance, to study the sediment transport problems Cheng et al., 2017 and Sun and Xiao, 2016 created the `SedFoam` and `SediFoam` respectively. Regarding the scour holes problems in the hydraulic engineering applications, Bom, 2017 used the modified version of `pimpleFoam` solver to study the hydrodynamic processes inside them, but that research did not include the free surface variation in the model set-up.

3.5.2 `interFoam`

The essential feature of modelling the open channel flow is the existence of the free surface. Since this research deals with the flow over the weir and the groyne, it is important to consider the free surface in the model. To the best of the author's knowledge, under the `OpenFOAM` framework the `interFoam` solver is the most well-known and reliable one for modelling the free surface variations in the hydraulic engineering problems, given the good pre-processing such as mesh generation (size and quality), numerical schemes choice, and matrix solvers choice (Schulze and Thorenz, 2014).

In immiscible and incompressible two-phase modelling practices, there are two possibilities of writing the governing equations (Rusche, 2003) i.e.

1. developing two sets of conservation equations for each phase or fluid and matching them at the interface between these two fluids, and
2. using a single system of conservation equations for the whole domain in which two fluids properties are discontinuous across the interface.

The latter representation, the so-called *single-field* representation, uses the Heaviside step function H which is 1 in the one type of fluid and 0 in the rest one, to represent the two kinds of fluids. In other words, any fluid property can be defined using their constant values on each side of the interface and the step function:

$$\chi(\boldsymbol{x},t) = \chi_a H(\boldsymbol{x},t) + \chi_b(1 - H(\boldsymbol{x},t)) \tag{3.8}$$

where χ is the material quantity (density, viscosity, etc.) , $\boldsymbol{x}$ is the position vector, and the subscripts a, b denote the two phases respectively. The interface between two phases is defined by the a non-zero value of the gradient of the step function (Rusche, 2003). It should be noted that the gradient of the step function is given by the Dirac δ function (Bracewell, 1986).

The `interFoam` solver solves the incompressible Navier-Stokes equations composed of the continuity equation and momentum conservation equations (Rusche, 2003):

$$\nabla \cdot \boldsymbol{u} = 0 \tag{3.9}$$

$$\frac{\partial(\rho \boldsymbol{u})}{\partial t} + \nabla \cdot (\rho \boldsymbol{u}\boldsymbol{u}) = -\nabla p + \nabla \cdot \boldsymbol{\tau} + \rho \boldsymbol{f} + \int_{S(t)} \sigma \kappa' \boldsymbol{n}' \delta(\boldsymbol{x} - \boldsymbol{x}') dS \tag{3.10}$$

where $\boldsymbol{u}$ is the velocity vector, ρ is the density, p is the pressure, t is the time, $\boldsymbol{\tau}$ is the stress tensor, and $\boldsymbol{f}$ is the acceleration due to body forces. The primed variables represent the values at the interface of two fluids. In the `interFoam` solver, the only body force is the gravity, so $\boldsymbol{f} = \boldsymbol{g}$. The last term in the equation 3.10 denotes the momentum source term due to the surface tension. The presence of 3-dimensional δ function ($\delta(\boldsymbol{x}) = \delta(x)\delta(y)\delta(z)$) indicates this surface tension term acts only at the interface $S(t)$, i.e. $\int_{S(t)} \delta(\boldsymbol{x} - \boldsymbol{x}')dS$. For the Newtonian fluid, the stress tensor reads:

$$\boldsymbol{\tau} = \mu(\nabla \boldsymbol{u} + \nabla \boldsymbol{u}^T) \tag{3.11}$$

where μ is the kinematic viscosity. It should be noted that different turbulent modelling will introduce additional viscosity terms in the equation 3.10 (Rusche, 2003).

In order to capture the interface, three methods are available namely (1) surface tracking methods, (2) moving mesh methods, and (3) volume tracking methods. The `interFoam` solver uses the volume tracking method that does not define the interface as a sharp boundary and can use the massless particles or indicator functions to represent the different fluids. The `interFoam` applies the volume fraction as the indicator function to track the interface which is of course a transition region where the fluid is treated as the mixture of two fluids (Rusche, 2003). Defining the regions of phase a and phase b as $\Re_a$ and $\Re_b$ respectively, the indicator function or volume fraction function reads:

$$\gamma(\boldsymbol{x}) = \begin{cases} 1 & \text{for } \boldsymbol{x} \in \Re_a \\ 0 < \gamma < 1 & \text{for } \boldsymbol{x} \in (\partial\Re_a \cup \partial\Re_b) \\ 0 & \text{for } \boldsymbol{x} \in \Re_b \end{cases} \tag{3.12}$$

The volume fraction is advected with the local velocity of corresponding phase, acting as a Lagrangian invariant (Hirt and Nichols, 1981). Therefore the indicator function follows the transport equation form (Berberović et al., 2009):

$$\frac{\partial \gamma}{\partial t} + \nabla \cdot (\boldsymbol{u}\gamma) = 0 \tag{3.13}$$

which is the essential equation solved by the `interFoam` solver.

As described in the equation 3.8, the local density ρ and local viscosity μ can be expressed using the indicator function as follows:

$$\rho = \gamma\rho_a + (1-\gamma)\rho_b \tag{3.14}$$

$$\mu = \gamma\mu_a + (1-\gamma)\mu_b \tag{3.15}$$

as well as the local velocity can be described (Sattar et al., 2017):

$$\boldsymbol{u} = \gamma\boldsymbol{u}_a + (1-\gamma)\boldsymbol{u}_b \tag{3.16}$$

It should be noted that the violation of the volume fraction bounds can cause the negative values of the material properties, and it is also necessary to calculate the γ values exactly. However due to the numerical difficulty in solving the equation 3.13, there was no perfect solution to ensure the boundedness of phase fraction and its conservativeness (Damian, 2012). The discretization of equation 3.13 results in unnecessary artificial diffusion, leading to the diffusive interface.

Therefore in order to overcome this notorious numerical diffusion arising from the discretization on the equation 3.13, an additional term is introduced into this equation (Rusche, 2003), resulting in the following modified indicator equation:

$$\frac{\partial \gamma}{\partial t} + \nabla \cdot (\boldsymbol{u}\gamma) + \nabla \cdot (\boldsymbol{u}_r\gamma(1-\gamma)) = 0 \tag{3.17}$$

where $\boldsymbol{u_r}$ is called the relative velocity or compressive velocity defined by $\boldsymbol{u_r} = \boldsymbol{u}_a - \boldsymbol{u}_b$. The role of compressive velocity is to sharpen the interface by compressing the free surface, not to be confused with compressible flow (Berberović et al., 2009). The compressive velocity acts on the interface and does not work outside the interface region due to the term $\gamma(1-\gamma)$ in the equation 3.17 (Rusche, 2003). The derivation of equation 3.17 can be found in the Appendix E.

In the equation 3.10, the momentum source term due to the surface tension can be calculated using the continuum surface force (CSF) model (Brackbill et al., 1992):

$$\int_S (t)\sigma\kappa'\boldsymbol{n}'\delta(\boldsymbol{x}-\boldsymbol{x}')dS \approx \sigma\kappa\nabla\gamma \tag{3.18}$$

where κ is the curvature of the interface defined by:

$$\kappa = \nabla\cdot\left(\frac{\nabla\gamma}{|\nabla\gamma|}\right) \tag{3.19}$$

Therefore, the momentum equation 3.10 becomes:

$$\frac{\partial(\rho\boldsymbol{u})}{\partial t} + \nabla\cdot(\rho\boldsymbol{u}\boldsymbol{u}) = -\nabla p + \nabla\cdot\boldsymbol{\tau} + \rho\boldsymbol{g} + \sigma\kappa\nabla\gamma \tag{3.20}$$

The momentum equation 3.10 needs to be reformulated for the sake of convenient definition of the pressure boundary condition. For instance, at the non-slip wall the equation 3.10 reduces to the following relation:

$$\nabla p = \rho\boldsymbol{g} \tag{3.21}$$

which describes that pressure gradient and buoyancy term are in balance (Rusche, 2003). This relationship 3.21 is violated at the non-vertical wall because the pressure gradient has to be different for each fluid. In a single pressure system, it is impossible to satisfy the momentum equation.

Moreover, the hydrostatic pressure results in the steep gradient in the total pressure of the incompressible flows. Therefore it is often desirable to remove the hydrostatic pressure gradient from the total pressure term by using the following relation:

$$p^* = p - \rho\boldsymbol{g}\cdot\boldsymbol{x} \tag{3.22}$$

where p^* is called the modified pressure or dynamic pressure. It is also denoted as the variable p_{rgh} in the `interFoam` practices. The gradient of the equation 3.22 will eliminate the pressure gradient term and gravity force term from the equation 3.20. Taking the gradient on the equation 3.22 results in:

$$\nabla p^* = \nabla p - \rho\boldsymbol{g} - \boldsymbol{g}\cdot\boldsymbol{x}\nabla\rho \tag{3.23}$$

and then can be rearranged:

$$-\nabla p + \rho\boldsymbol{g} = -\nabla p^* - \boldsymbol{g}\cdot\boldsymbol{x}\nabla\rho \tag{3.24}$$

Finally the equation 3.20 becomes:

$$\frac{\partial(\rho\boldsymbol{u})}{\partial t} + \nabla\cdot(\rho\boldsymbol{u}\boldsymbol{u}) = -\nabla p^* + \nabla\cdot(\mu\nabla\boldsymbol{u}) + (\nabla\boldsymbol{u})\cdot\nabla\mu - \boldsymbol{g}\cdot\boldsymbol{x}\nabla\rho + \sigma\kappa\nabla\gamma \tag{3.25}$$

since the viscous stress tensor in the equation 3.20 can be expressed as:

$$\nabla\cdot\boldsymbol{\tau} = \nabla\cdot(\mu\nabla\boldsymbol{u}) + (\nabla\boldsymbol{u})\cdot\nabla\mu \tag{3.26}$$

It should be noted that in the equation 3.25 there is an additional term that is the density gradient $\nabla\rho$. This term leads to infinity gradient at the interface because the density jump exists there and the function is not differentiable anymore (Thorenz and Strybny, 2012). Thorenz and Strybny, 2012 remarked that the use of p_{rgh} or p^* does not work smartly in the boundary condition from the hydraulic engineering point of view. The reason is why the hydraulic models require simply the velocity or the discharge in the upstream condition while the water level at the downstream, not the complex pressure terms. Moreover initially the `interFoam` did not intend to use fixed water level boundary condition instead of the freedom of hydrostatic pressure with

free surface at the boundary .

The literature study was done below regarding how the previous researchers had used the interFoam for their studies and defined boundary conditions, especially the water level condition at the downstream. The most relevant examples for the river hydraulic engineering applications are the works done by Thorenz and Strybny, 2012, Jellesma, 2013, Teuber et al., 2013 and who required the fixed water level boundary condition.

Thorenz and Strybny, (2012)

Thorenz and Strybny, (2012) pointed out the deficiency of the usage of modified pressure term in the interFoam especially if one wants to use it in the hydraulic engineering applications. The difficulty arises when the fixed water level is required at the downstream of the river or channel. Therefore they developed a new set of boundary conditions compatible with original formulations of interFoam i.e. the governing equations are not modified. They created the boundary conditions for water level, phase function and velocity.

For fixing the water level, the approach of Thorenz and Strybny, (2012) is that the water level will be prescribed through the pressure value for each cell on the boundary:

$$p_{wt} = p_0 - \beta\rho(\boldsymbol{n}\cdot\boldsymbol{u})^2 + \begin{cases} \rho_b(\boldsymbol{g}\cdot(\boldsymbol{x}-\boldsymbol{x}_0)) & \text{if } \boldsymbol{g}\cdot(\boldsymbol{x}-\boldsymbol{x}_0) < 0 \\ \rho_a(\boldsymbol{g}\cdot(\boldsymbol{x}-\boldsymbol{x}_0)) & \text{if } \boldsymbol{g}\cdot(\boldsymbol{x}-\boldsymbol{x}_0) > 0 \end{cases} \tag{3.27}$$

with $\beta = 0$ if $\boldsymbol{n}\cdot\boldsymbol{u} > 0$, where p_{wt} is the required pressure at the boundary, p_0 is the pressure at the prescribed water surface, $\boldsymbol{x}_0$ is the position vector for the prescribed water surface, and β is the stabilization parameter.

Next the new boundary condition set for the VOF function reads:

$$\text{for } \boldsymbol{n}\cdot\boldsymbol{u} > 0 : \nabla\gamma = 0 \tag{3.28}$$

$$\text{for } \boldsymbol{n}\cdot\boldsymbol{u} < 0 : \gamma = \begin{cases} 0 & \text{if } \boldsymbol{g}\cdot(\boldsymbol{x}-\boldsymbol{x}_0) < 0 \\ 1 & \text{if } \boldsymbol{g}\cdot(\boldsymbol{x}-\boldsymbol{x}_0) > 0 \end{cases} \tag{3.29}$$

which explains that for the outgoing flows the zero gradient is specified at the boundary whereas for the ingoing flows the Dirichlet type or fixed value boundary condition is applied there.

Regarding the boundary condition of the velocity for the fixed discharge, they set up the following:

$$\text{for } Q > 0 : \boldsymbol{u} = \frac{\boldsymbol{n}Q}{\int_\Omega \gamma d\Omega} \tag{3.30}$$

$$\text{for } Q < 0 : \boldsymbol{u} = \frac{\boldsymbol{n}Q}{\int_\Omega \gamma d\Omega} + (\boldsymbol{u}_{domain} - (\boldsymbol{u}_{domain}\cdot\boldsymbol{n})\cdot\boldsymbol{n}) \tag{3.31}$$

where Ω denotes the regarded boundary. For the negative discharge case, the transversal component of the velocity has to be out of the domain, otherwise the transverse momentum would accumulate nonphysically on the boundary.

They applied their new boundary conditions for the simulation of the filling-emptying systems for locks, and found the results agree well with the laboratory tests.

Jellesma, (2013)

Jellesma, (2013) intended to use the cyclic boundary conditions in the interFoam solver, but this action is not compatible for the initial governing equations of interFoam. The cyclic boundary conditions required the horizontal driven force. The horizontal force will be driven by

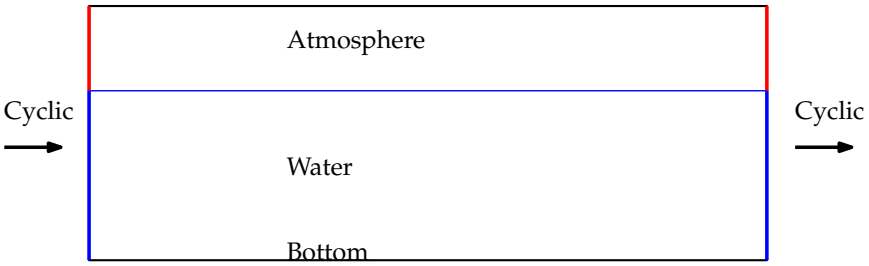

FIGURE 3.1: Model domain and boundary conditions for the `cyclic` case (Jellesma, 2013). The red line shows the inlet and outlet of air phase, and the vertical blue lines denote the water inlet and outlet. Due to the fixed nature of the boundary patch, the water level will not change any time at those boundaries.

the water weight. Therefore, Jellesma, (2013) modified the governing equations by inserting the additional body force term as follows:

$$\frac{\partial(\rho \boldsymbol{u})}{\partial t} + \nabla \cdot (\rho \boldsymbol{u}\boldsymbol{u}) = -\nabla p^* + \nabla \cdot (\mu \nabla \boldsymbol{u}) + (\nabla \boldsymbol{u}) \cdot \nabla \mu - \boldsymbol{g} \cdot \boldsymbol{x} \nabla \rho + \sigma \kappa \nabla \gamma + \rho \boldsymbol{f}_a \tag{3.32}$$

where $\boldsymbol{f}_a$ denotes the acceleration due to additional body force defined by $\boldsymbol{f}_a = ig\boldsymbol{i}$ in which i is the bed slope and $\boldsymbol{i}$ is the unit vector in x-direction.

The schematic drawing of model domain and boundary conditions applied by Jellesma, (2013) is shown in the figure 3.1: In the figure 3.1, the red lines indicate the inlet and outlet patch of the air phase while the vertical blue lines show those patches of the water phase. Since these patches are fixed geometrical boundary conditions, the water level at those locations will not change ever.

In the model, the water level and the slope of the river or channel have to be predefined that makes the bed shear stress and shear velocity constant ever even for the different scenarios. Only the velocity or the discharge will change consequently due to the physical processes inside the model area e.g. the form drag of river dunes or structures. If needed the correct discharge in the inlet, one should adjust the body force term for each case of modelling the different types of structures or dunes (Jellesma, 2013).

Teuber et al., (2013)

Differently from the former two cases, Teuber et al., (2013) did not change any mathematical terms in the solver, but they inserted a weir near the end of the model domain to fix the water level. Although this approach is simple, the difficulty is to know the correct relationship between the weir height and the water level because this relationship also depends on the computational mesh quality. This leads to the iterative simulations for obtaining the correct water level at the downstream. Moreover the weir control structure should be far enough away from the main area of model such that the reflected velocity signals will not interfere with the interested quantity.

3.5.3 Mesh types

The numerical results depend largely not only on the quality but also the type of the computational mesh because the differential equations are solved on the finite grid of the geometrical structure. Generally the meshes are categorized into two types (Maliska, 1994) as shown in the figures 3.2a and 3.2b:

1. Structured meshes

   It is the structured mesh if (1) any internal element of the mesh has the same number of neighbours, and (2) the mesh can be deduced from the coordinate system i.e. the elements can be sorted in the natural sequence. The advantages of the structured mesh are that (1) the

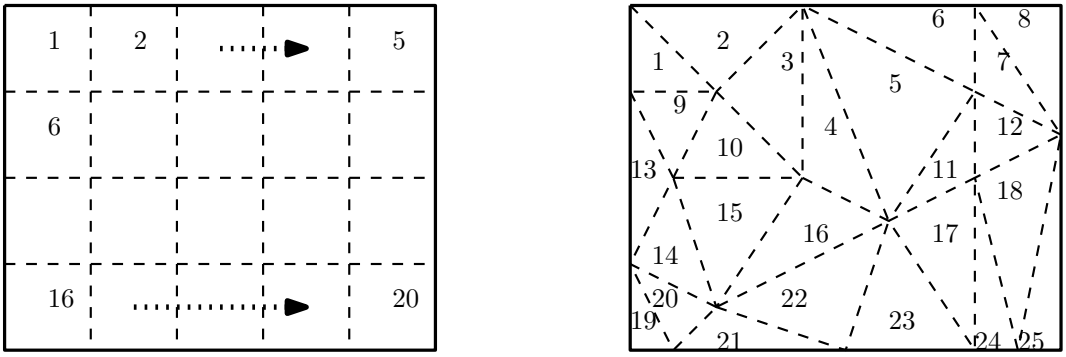

(A) Structured mesh. (B) Unstructured mesh.

FIGURE 3.2: Examples of structured mesh and unstructured mesh where the former type has the regular numbering whilst the latter one has irregular indexing (Moraes et al., 2013).

matrix of discretizations have the fixed bandwidth, (2) the variables can be indexed easily by mesh ordering, and (3) the resulting quality metric which measures the robustness of the mesh, is excellent when properly built up. However, the structured meshes do not fit well the complex geometries.

2. Unstructured meshes

   The mesh are called unstructured meshes when (1) the number of neighbours vary with the geometry type, (2) the element connectivity is of random type, and (3) the quality metric is not good as that of structured mesh. Although these type of the mesh can represent the complex geometry very well, the correction techniques are essential to make sure the numerical results are reliable because the severe distortion of the mesh orientation can introduce the numerical errors.

`blockMesh` utility

The `blockMesh` utility can be used to create the computational mesh of the geometry by splitting up the multiple hexahedral blocks of which the edges can be straight lines, arcs or splines. The `blockMesh` is suitable tool only for the meshing of the relatively simple geometries, although it provides a limited range of adjustment parameters. The reader is referred to "Openfoam User Guide" for detailed implementations.

`snappyHexMesh` utility

The `snappyHexMesh` is a meshing utility which makes the background mesh conform to the surface of the desired geometry by refining multiple times. In other words, the `snappyHexMesh` requires the background mesh and the geometry file formatted with Stereolithography (STL) or Wavefront Object (OBJ) file types. The utility will cut the geometry shape out of the background mesh. Detailed information can be accessed in the "Openfoam User Guide".

3.5.4 Mesh quality

The two indicators for measuring the quality of the mesh are (1) orthogonality and (2) skewness which are explained later in this section. Moreover the flow misalignment needs to paid attention for accurate simulation results because the orthogonal cells not aligned with the flow direction can cause the numerical mixing (Rhoads, 2014). The misalignment between the mesh and the

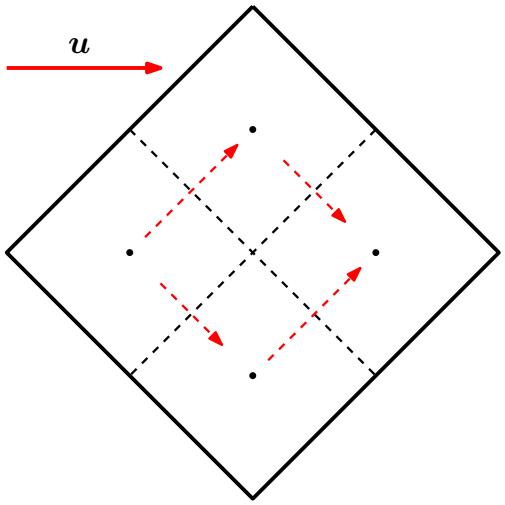

FIGURE 3.3: Flow misalignment due to the rotation of the mesh which causes the change in flow direction, velocity vector $\boldsymbol{u}$, according to the red dotted line.

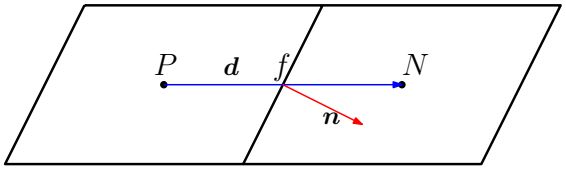

(A) Non-orthogonal mesh since $\boldsymbol{n} \neq \boldsymbol{d}$.

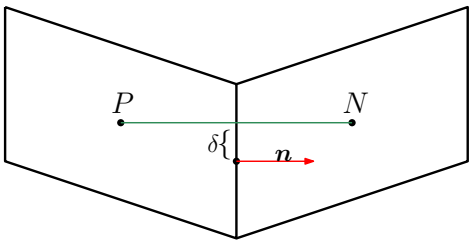

(B) Skewed mesh due to the gap between face center location and the center-to-center line location, or δ.

FIGURE 3.4: (Rhoads, 2014)

flow direction introduces the error in the imposed flow direction due to the projected area as depicted in the figure 3.3.

Orthogonality

As shown in the figure 3.4a, the mesh is called *non-orthogonal* mesh when the face normal vector $\boldsymbol{n}$ is not parallel to the vector $\boldsymbol{d}$ directing from cell centroids P and N. The non-orthogonal mesh of having the angle between these two vectors greater than 70° can contribute the significant error in numerical results, especially in the discretization of Laplacian operator (Rhoads, 2014).

In `OpenFOAM`, the correction to non-orthogonality can be accomplished by increasing the iterative count in the `nNonOrthogonalCorrectors` in `fvSolution` directory.

Skewness

When the face center point does not exist on the line connecting between the cell centers as shown in the figure 3.4b, the mesh is *skewed*. The skewness can give rise to the numerical diffusion and plays an important role in the discretization for the convective term (Rhoads, 2014).

To mitigate the skewness effect, one can use `skewCorrected` method in the interpolation schemes of the `OpenFOAM`. It should be note that applying the correction schemes can cause extra computational time.

Chapter 4

Model Set-up and Simulation sets

The very first important step to be determined is which governing equations will be used to represent the flow dynamics in the research. Since the current research is interesting in the complicated flow process around and over the groyne, the incompressible Navier-Stokes solver will be preferred to the Shallow Water solver. Regarding the representation of the water surface, the VOF free surface tracking method is more suitable than the single-valued function approach because the studied problem might include complex flow geometries and air entrainment.

When simulated the flow over the weir, Fr will become at the top of the weir:

$$Fr = \frac{U}{\sqrt{gd}} \approx \frac{1.0}{\sqrt{9.81 \cdot 0.1}} = 1.01 \tag{4.1}$$

indicating the supercritical flow there, and subsequently the water level change can occur. Therefore, the current research adopted the free surface method for simulation of the flow over the weir and the groyne.

To determine the flow characteristics, Re number was found to be:

$$Re = \frac{\rho U L}{\mu} \approx \frac{1000 \cdot 0.2 \cdot 0.5}{10^{-3}} = 10^7 \tag{4.2}$$

which shows the flow is indeed turbulent flow. The $k - \epsilon$ model of two-equation model types was adapted for the sake of simple implementation, although it has been realized that this model could not give the correct results in the flow separation zone or adverse pressure gradient zone (Rodi, 2017).

4.1 Two Different Models

Two models, *interFoam evaluation model* and *weir-groyne comparison model*, will be set up in this research for addressing the issues in numerical simulation of flow in `interFoam` solver, and for analyzing the different flow behaviours between groyne and weir, respectively.

4.2 `interFoam` evaluation model: Set-up

The *interFoam evaluation model* was constructed for addressing the practical issues of the detail flow simulation in the `interFoam` solver. The *interFoam evaluation model* will show the differences of 2D simulation and 3D simulation using the weir.

The *interFoam evaluation model* included the control structure at the end of the flume to control the water level as depicted in the figure 4.1. It should be noted that there are no inlet and outlet tanks at both ends of the flume. Although no discharge adjustment is needed for getting the required water level in the flume, the adjustment of the control structure height is necessary to get the correct water level.

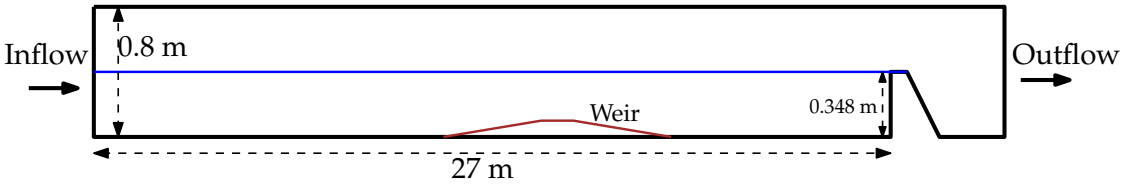

FIGURE 4.1: Flume of *interFoam evaluation model* in which the control structure is applied at the end of the flume. There are no inlet and outlet tanks like the Deltares Flume.

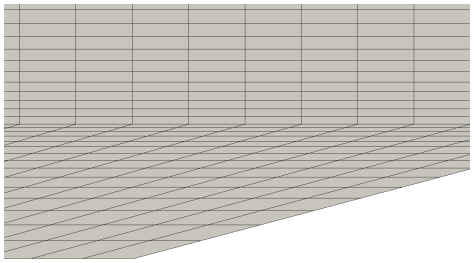

(A) Meshing by `blockMesh`.

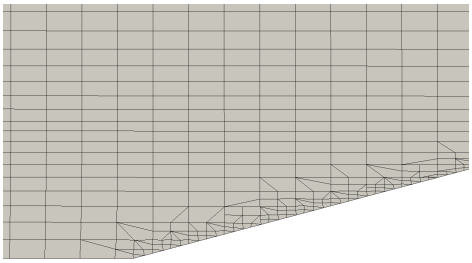

(B) Meshing by `snappyHexMesh`.

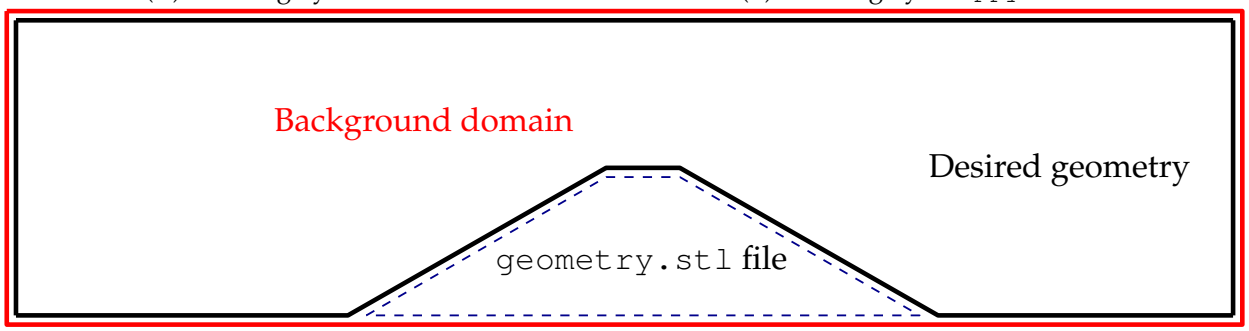

(C) Desired geometry for simulation which is shown by the solid black lines, and the groyne `geometry.stl` file to be used by the `snappyHexMesh`.

FIGURE 4.2: Meshes created by the different meshing utilities. The `blockMesh` uses the solid black geometry of 4.2c to create the mesh in figure 4.2a. The mesh in figure 4.2b is created by `snappyHexMesh` with the help of `geometry.stl` file and background domain of red solid line from the figure 4.2c.

The *interFoam evaluation model* was set up by `blockMesh` utility and `snappyHexMesh` utility for accessing whether the *structured non-orthogonal* mesh created by `blockMesh` and the *unstructured more-orthogonal* mesh done by `snappyHexMesh` can affect the numerical results or not. The *more-orthogonal* means that mesh produced by the `snappyHexMesh` has a large number of orthogonal cells compared to the number of non-orthogonal cells that located along the cutting boundary. These small number of non-orthogonal cells are by-products of `snappyHexMesh` resulting from the cell removal process.

The `snappyHexMesh` removes the groyne `geometry.stl` out of the background domain as shown in the figure 4.2c, causing the unstructured mesh along the snapping boundary depicted in the figure 4.2b. It should be noted that the *smooth* snapping boundary is obtained by using `snap` function of `snappyHexMesh`, so-called *snapping*, otherwise it will create the staircase along the slope of the groyne, so-called *castellated*. The snapping creates the smaller cells near the boundary causing the excessive amount of computation. The castellated mesh type is described in the figure 4.3a and the example meshing of the *interFoam evaluation model* flume is also shown in the figure 4.3b.

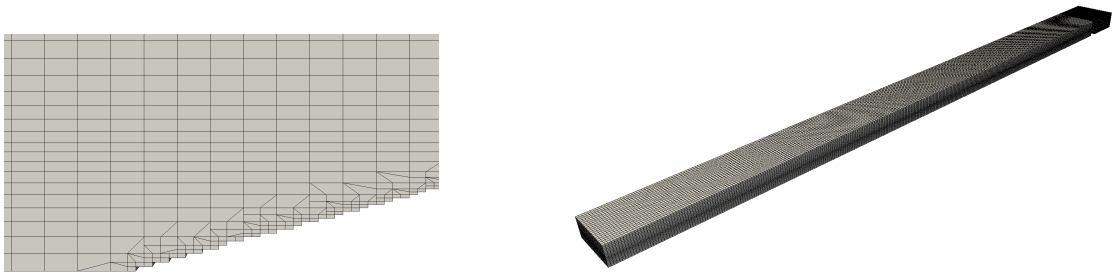

(A) Castellated mesh by `snappyHexMesh`.

(B) Example mesh of the *interFoam evaluation model* flume.

FIGURE 4.3: *interFoam evaluation model*'s flume mesh characteristics.

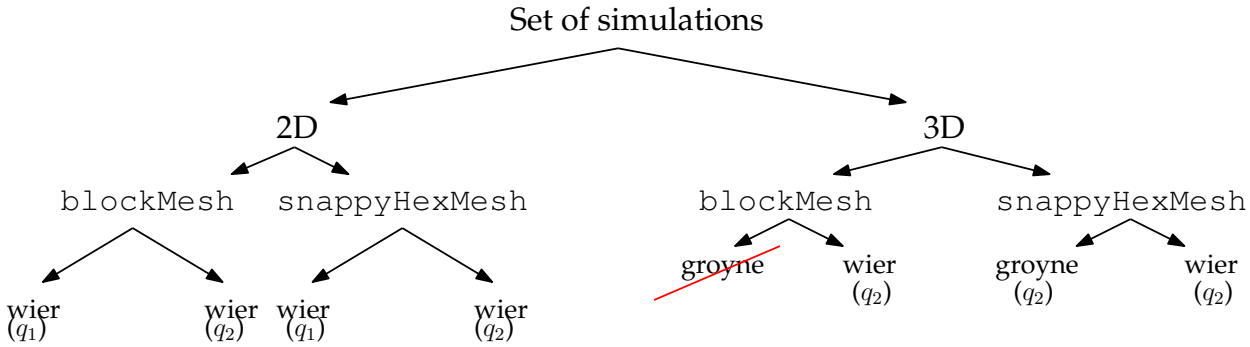

FIGURE 4.4: Set of simulations for the *interFoam evaluation model*. Only the weir is installed in the 2D simulations whereas both of groyne and weir are used in the 3D simulations.

The *interFoam evaluation model* was created in 2D and 3D settings for understanding the dimensionality effects on the simulation results. The dimensions of the *interFoam evaluation model* flume are shown in the figure 4.1 and it width is 0.5 m for 2D simulations. The specific discharge for inlet is $q_1 = 0.1018\ \mathrm{m}^2/\mathrm{s}$ and the water level is approximately 0.493 m.

For setting up the 3D flume, its width has to be widened from 0.5 m to 2.0 m to reduce the flow velocity i.e. the specific discharge became $q_2 = 0.02545\ \mathrm{m}^2/\mathrm{s}$ but keeping the same water level, because the velocity of q_1 is so high that the mesh has to be very fine enough in all three dimensions, leading the huge use of computer memory. This is not the case for 2D simulation because it does not have the computational cells in the z-direction. In order to compare 3D simulation results with the 2D results, an additional set of 2D simulations were carried out using q_2. The set of simulations are briefly described in the figure 4.4.

The *interFoam evaluation model* is at first simulated by including the weir and then the groyne in the second step. The simulations including the groyne have to necessarily be 3D simulations, otherwise it does not make sense for 3D geometry in 2D flow simulation. By using the `blockMesh` meshing utility, however, the 3D simulation for the flow over the groyne cannot be accomplished since it gives rise to severely non-orthogonal grids shown in the figure 4.5 leading to the numerical instability. Nevertheless, the results of groyne simulation will not be presented in the report since it was intended only for investigation if the 3D groyne simulation can be simulated stably or not.

The definition of boundary conditions for the *interFoam evaluation model* are described in the table 4.1 and their patches are also visualized in the figure 4.6. Unlike the boundary condition of the flume walls named *bank* patch in *weir-groyne comparison model*, the *interFoam evaluation model* found only the use of `free-slip` condition applicable since the `noSlip` condition leads

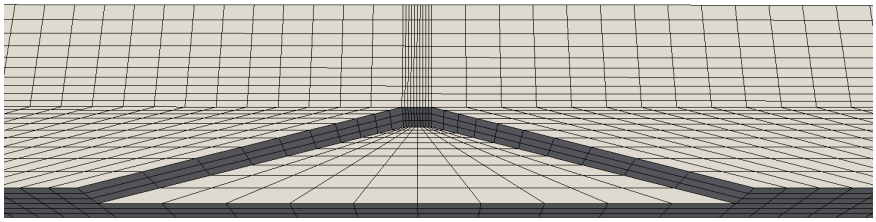

FIGURE 4.5: Severely non-orthogonal mesh generated by the `blockMesh` utility for the flow over the groyne. Therefore the 3D simulation of the flow over the groyne in structured mesh cannot be accomplished due to its severe non-orthogonality.

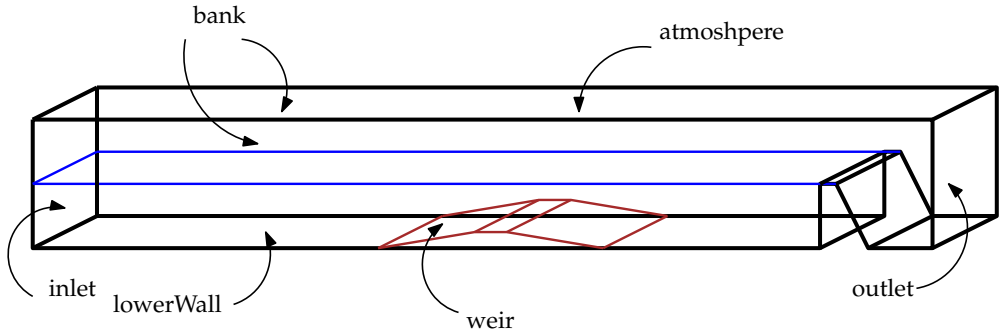

FIGURE 4.6: Patches for defining boundary conditions in the *interFoam evaluation model*. The corresponding boundary conditions for the patches can be seen in the table 4.1.

to numerical instability. The reason for instable computation seems the lack of suitable finer mesh size in the z-direction or across the flume.

4.3 weir-groyne comparison model: Set-up

The *weir-groyne comparison model* is intended to analyze the differences between the flow around the submerged groyne and the flow over the weir. The numerical flume was constructed with reference to the laboratory flume of Stolker, (2005), which was used for the study of flow over the weir at the Deltares. The dimensions of the flume are $27.6(L) \times 0.5(B) \times 0.7(H)$ in meter. The schematic drawing of the flume is depicted in the figure 4.7:

Although the control structure was used in the laboratory flume to regulate the water level, the numerical flume of *weir-groyne comparison model* did not include that control structure shown in the figure 4.8. The advantage of not using the structure is that the air entrainment flow can be avoided downstream of the control weir, leading to the usage of large size of the mesh. Instead of using that structure, the *weir-groyne comparison model* used only inflow and outflow tanks at the upstream and downstream respectively, and used the trial-and-error discharge adjustment method for water level regulation. The detailed description of this *weir-groyne comparison model* set-up and its drawbacks are reported in the appendix D.

TABLE 4.1: Boundary conditions applied in the *interFoam evaluation model*. It should be noticed that the condition at the bank will be changed depending on 3D or 2D simulation.

patch	U	p_{rgh}	k	ϵ	ν_t	α or γ
inlet	vHFRIV [1]	zG	fixedValue	fixedValue	calculated	vHFR [10]
outlet	zG [2]	zG	iO [6]	iO	calculated	zG
lowerWall	noSlip	fFP [4]	kRWF [7]	eWF [8]	nkWF [9]	zG
weir	noSlip	fFP	kRWF	eWF	nkWF	zG
bank	slip	fFP	zG or kRWF	zG or eWF	zG or nkWF	zG
atmosphere	pIOV [3]	tP [5]	iO	iO	calculated	iO

[1] variableHeightFlowRateInletVelocity
[2] zeroGradient
[3] pressureInletOutletVelocity
[4] fixedFluxPressure
[5] totalPressure
[6] inletOutlet
[7] kqRWallFunction
[8] epsilonWallFunction
[9] nutkWallFunction
[10] variableHeightFlowRate

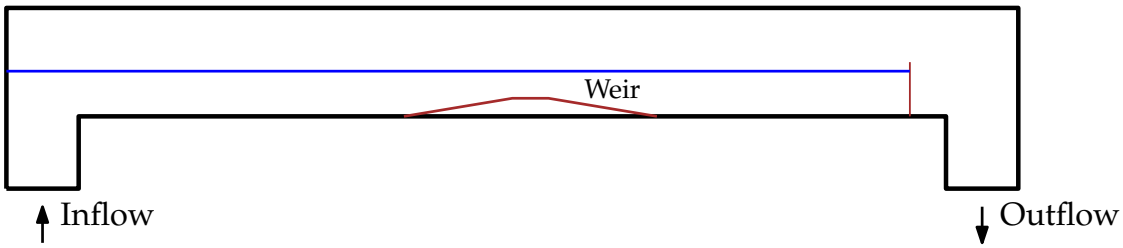

FIGURE 4.7: Deltares flume which was used for the study of flow over the weir by (Stolker, 2005).

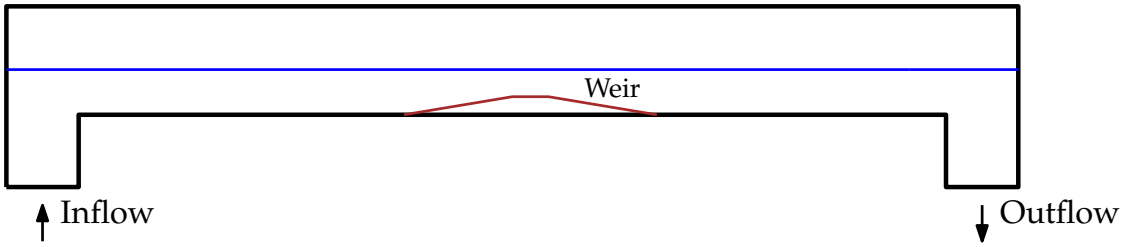

FIGURE 4.8: *weir-groyne comparison model* flume where the control structure was not applied at the downstream. The water level was regulated by trial-and-error adjustment of the inlet and outlet discharges.

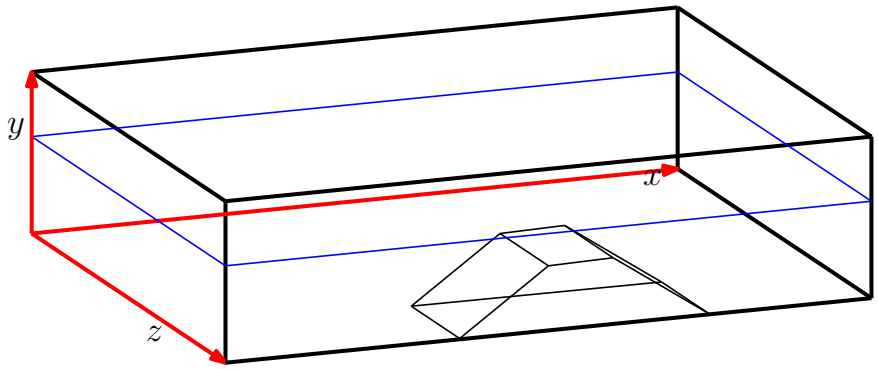

FIGURE 4.9: Coordinate system of the flume. The red-arrow lines indicate the reference coordinate. It should be noted that saying the larger values of z-coordinate refer to the locations nearby the groyne.

The reference coordinate system is defined as the red arrow lines drawn in the figure 4.9. It should be realized that the groyne exists near the larger z-coordinate because it helps the reader understand the analysis of the simulation results which will be explained in the coming chapter.

The current research used two types of groynes and one type of weir in two different sizes of flumes. These two types of the groynes are different only in the aspect of leeward slope of the structure which are 1:4 leeward slope and 1:8 leeward slope respectively, but share the same front slope of 1:4.

The complete list of the simulations are shown in the table 4.3. A set of simulations consists of the 9 simulations comprising the flow simulations over the groyne and the weir with different flume settings and structural dimensions. The flow properties, however, are kept the same for all cases, using the unit discharge (q) for different sizes of the flumes. Besides, the preliminary simulation without the weir and the groyne was also carried out to adjust the water level.

TABLE 4.2: A set of groyne and weir simulations. The `groyne5S` case studies the flow over the three groynes while the rest includes a single structure.

No.	Flume			Dimensions			Flow	
	L (m)	B (m)	H(m)	L_g (m)	S_1	S_2	Q (m^3/s)	d (m)
`groyne0`	27.0	2.0	0.7	0.5	1:4	1:8	0.0824	4.209
`groyne1`	27.0	2.0	0.7	0.7	1:4	1:8	0.0824	4.209
`groyne5`	27.0	2.0	0.7	0.5	1:4	1:4	0.0824	4.209
`groyne5S`	35.0	2.0	0.7	0.5	1:4	1:4	0.0824	4.209
`groyne6`	27.0	2.0	0.7	1.0	1:4	1:4	0.3296	4.08
`groyne7`	27.0	8.0	0.7	4.0	1:4	1:4	0.3296	4.08
`groyne8`	27.0	8.0	0.7	3.0	1:4	1:4	0.3296	4.08
`groyne9`	27.0	8.0	0.7	6.0	1:4	1:4	0.3296	4.08
`groyne10`	27.0	2.0	0.7	1.5	1:4	1:4	0.0824	4.209
`groyne11`	27.0	8.0	0.7	2.0	1:4	1:4	0.3296	4.08
`weir5`	27.0	2.0	0.7	2.0	1:4	1:4	0.0824	4.209
`weirL`	27.0	8.0	0.7	8.0	1:4	1:4	0.3296	4.08

The test cases `groyne0`, `groyne1`, `groyne5`, `groyne5S`, `groyne6`, `groyne10`, and `wier5` are simulated using the narrow width of the flume while the cases `groyne7`, `groyne8`, `groyne9` and `wierL` are simulations for the wider flume. This set of simulations can provide the reasonable pictures of the flow behaviour around the flume and the weir in small-scale and large-scale

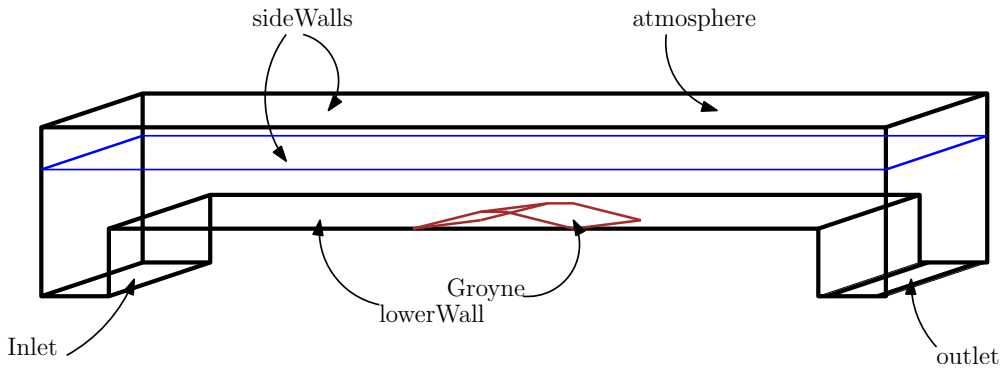

FIGURE 4.10: Patches of the flume *weir-groyne comparison model* where boundary conditions were assigned. The corresponding boundary conditions for the patches can be seen in the table 4.3.

TABLE 4.3: Boundary conditions applied in the *weir-groyne comparison model*.

patch	U	p_{rgh}	k	ϵ	ν_t	α or γ
inlet	fRIV [1]	zG	fV [6]	fV	calculated	fV
outlet	fRIV [2]	zG	iO [6]	iO	calculated	zG
lowerWall	noSlip	fFP [4]	kRWF [7]	eWF [8]	nkWF [9]	zG
groyne	noSlip	fFP	kRWF	eWF	nkWF	zG
bank	noSlip	fFP	kRWF	eWF	nkWF	zG
atmosphere	pIOV [3]	tP [5]	iO	iO	calculated	iO

[1] flowRateInletVelocity
[2] zeroGradient
[3] pressureInletOutletVelocity
[4] fixedFluxPressure
[5] totalPressure
[6] fixedValue
[7] inletOutlet
[8] kqRWallFunction
[9] epsilonWallFunction
[10] nutkWallFunction

dimensions.

The table 4.3 summarizes the brief description of boundary conditions which were applied on the patches shown in the figure 4.10. The abbreviations used are also explained in the table footnotes.

Chapter 5

Results of *interFoam Evaluation Model*

5.1 Regulation of water level

A method of defining water level at the downstream end of a flume is an important prerequisite for hydraulic modelling. The use of control structure in *interFoam evaluation model* can guarantee to have the correct water level at all time after the spin-up time as shown in the figure 5.1. The interface diffusion does not occur in the flume in this case. The unsteadiness of flow which is explained in the appendix D, was not observed like in the the discharge adjustment method (*weir-groyne comparison model*). The *weir-groyne comparison model* took much longer time to reach the required water level. Besides, that method gives rise to the interface diffusion near the end of the flume.

5.2 Mesh type effects

The dependence of flow behaviour on the mesh types, *structured non-orthogonal mesh* and *unstructured more-orthogonal mesh*, is addressed using the simulation results of only *interFoam evaluation model*. Later, for the sake of brevity, the former type of mesh will be referred as `blockMesh` and the latter one will be called `snappyHexMesh`. The analysis has twofolds which are (1) 2D simulations and (2) 3D simulations.

5.2.1 2D simulations

In 2D simulations, the weir is included in the middle of the flume. Using the specific discharge q_1, the flow separation was observed upstream of the weir in the `snappyHexMesh` case while the separation existed only downstream in the `blockMesh` case as depicted in the figures 5.2a and 5.2b, respectively. Theoretically and from the laboratory result of Deltares (Stolker, 2005) the eddy or flow separation should be downstream of the weir instead of upstream. The enlarged version of velocity vectors of eddies in the figures 5.2a and 5.2b are also visualized in the figures 5.3a and 5.3b.

Moreover, the deformed velocity profiles shown in the figures 5.4a and 5.4b firmly indicate the existence of flow separation at the upstream and downstream for the `snappyHexMesh` and `blockMesh` cases, respectively. In the figure 5.4b the dotted colored lines represent the experimental velocity profiles from Deltares report (Stolker, 2005). The measured velocity profiles depict flow separation downstream of the weir. The measured and simulated profiles in the figure 5.4b do not match exactly because the non-orthogonality of mesh will introduce the numerical artifacts in the simulations. Nevertheless, these two results show the flow separation phenomenon generally and that the *structured non-orthogonal mesh* is able to reproduce this flow phenomenon while the *unstructured more-orthogonal mesh* is not able to do it for this particular hydraulic structure.

FIGURE 5.1: Initial Simulation of flume without weir but including the control structure. No interface diffusion was observed along the flume.

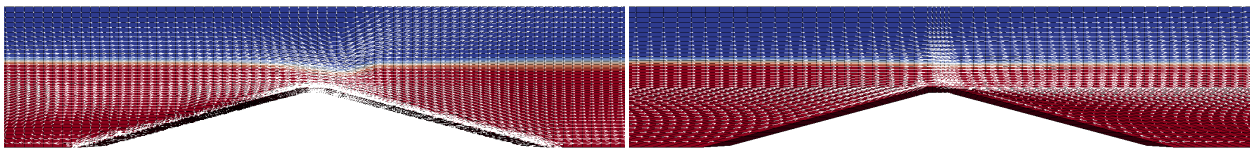

(A) Eddy upstream of the weir in 2D simulation `snappyHexMesh` case.

(B) Eddy downstream of the weir in 2D simulation `blockMesh` case.

FIGURE 5.2: Velocity vectors showing the eddy in 2D simulations. The red part represents the water and the blue part does for the air phase.

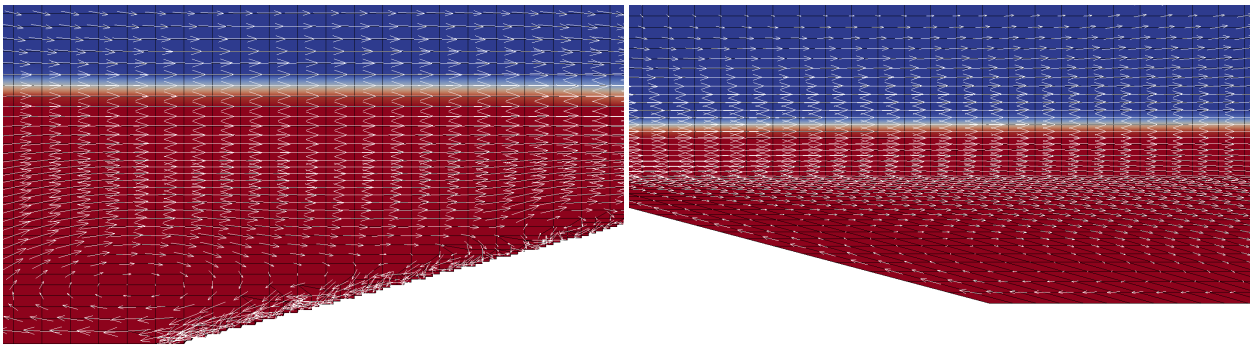

(A) Eddy in the `snappyHexMesh` case.

(B) Eddy in the `blockMesh` case.

FIGURE 5.3: Enlarged version of the figures 5.2a and 5.2b.

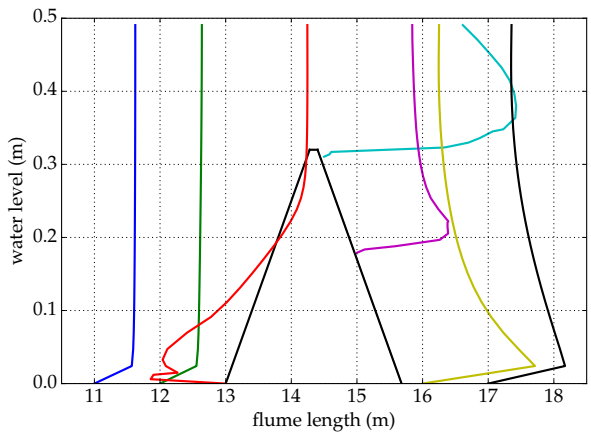

(A) Velocity profiles upstream of the weir inferring flow separation in `snappyHexMesh` case.

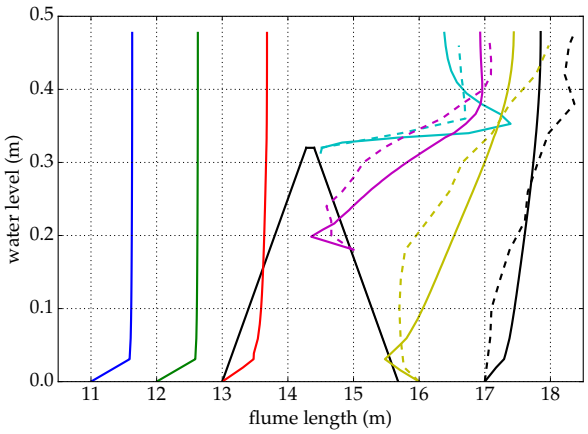

(B) Velocity profiles downstream of the weir inferring flow separation in `blockMesh` case. The dotted colored lines represent the measured velocity profiles.

FIGURE 5.4: Velocity profiles showing the eddy in 2D simulations using the specific discharge q_1. The magnitude of the velocity profiles is *not* to scale.

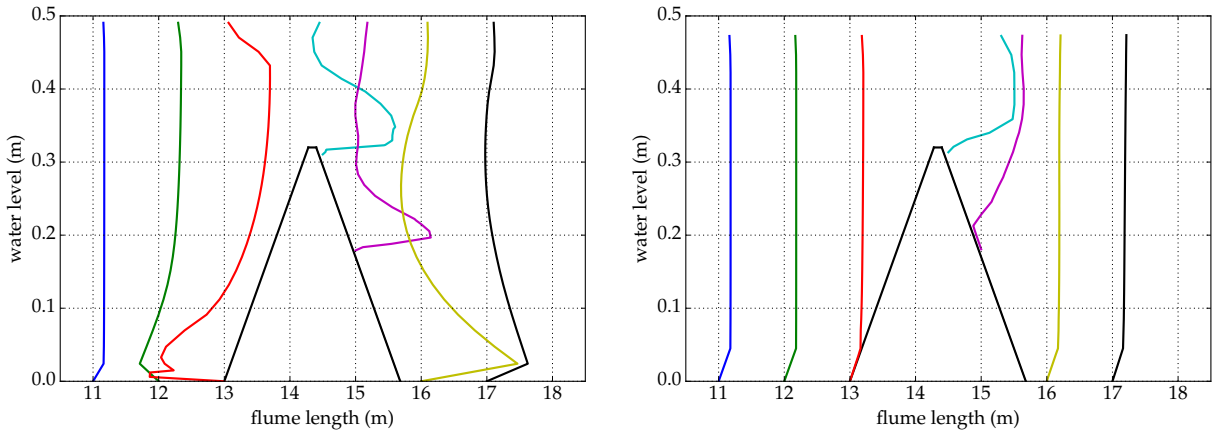

(A) Velocity profiles near the weir inferring flow separation in `snappyHexMesh` case.

(B) Velocity profiles showing the flow separation in the `blockMesh` case.

FIGURE 5.5: Velocity profiles in 2D simulations using the specific discharge q_2. The magnitude of the velocity profiles is *not* to scale.

The 2D simulations were run again with the small specific discharge q_2. In the `snappyHexMesh` case the velocity profiles also indicated that the flow separation occurred upstream and downstream of the weir as described in the figure 5.5a. However in the `blockMesh` case there was trivial flow separation as portrayed in the figure 5.5b.

5.2.2 3D simulations

The 3D simulations of flow over the weir were carried out in 2.0 m wide flume with the specific discharge q_2 using two types of the mesh. The velocity profiles of the `snappyHexMesh` and `blockMesh` are depicted in the figures 5.6a and 5.6b.

The velocity profiles of the figure 5.6b are nearly identical to those of the figure 5.5a. It means that both of 2D and 3D simulations using `blockMesh` are able to reproduce the same results in this case. However the `snappyHexMesh` mesh gives rise to different velocity profiles for 2D and 3D simulations. Since the figure 5.5a is very distinct from other three figures 5.5b, 5.6a and 5.6b, it can be concluded that the 2D simulation of `snappyHexMesh` is not reliable one for this study.

5.3 Analysis

The `blockMesh` mesh can reproduce apparently the correct flow behaviour in 2D and 3D simulations although the non-orthogonality of the mesh was known to introduce numerical diffusion. Near the boundary edges, the flow is aligned with the mesh orientation, so the flow misalignment artifact cannot occur.

The `snappyHexMesh` failed to simulate the correct flow behaviours in 2D simulations for both of discharges q_1 and q_2 i.e. the failure of simulations are independent of the flow velocity. However this type of mesh was able to reproduce the flow correctly in 3D simulation for q_2. Therefore it can be concluded that the unstructured mesh of `snappyHexMesh` plays an important role in only 2D configuration.

The reason for the failure of 2D simulation using the `snappyHexMesh` mesh is the existence of extra computational cells in the cross-direction of flume. Moreover, these cells are located only around where the weir exists. In other words, the cells appear as a result of cutting weir

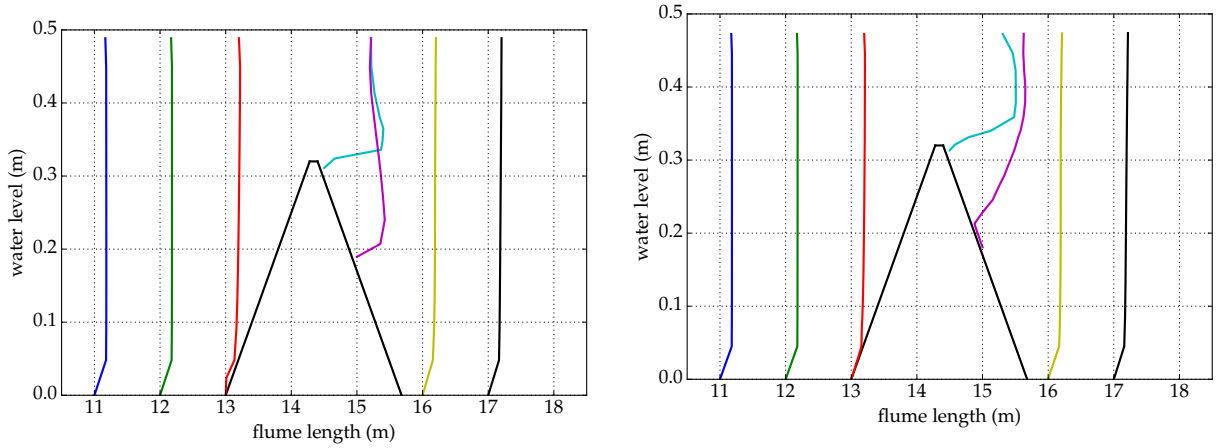

(A) Velocity profiles in the `snappyHexMesh` case.

(B) Velociy profiles in the `blockMesh` case where the trivial flow separation can be seen.

FIGURE 5.6: Velocity vectors in 3D simulations using the specific discharge q_2. The magnitude of the velocity profiles is *not* to scale.

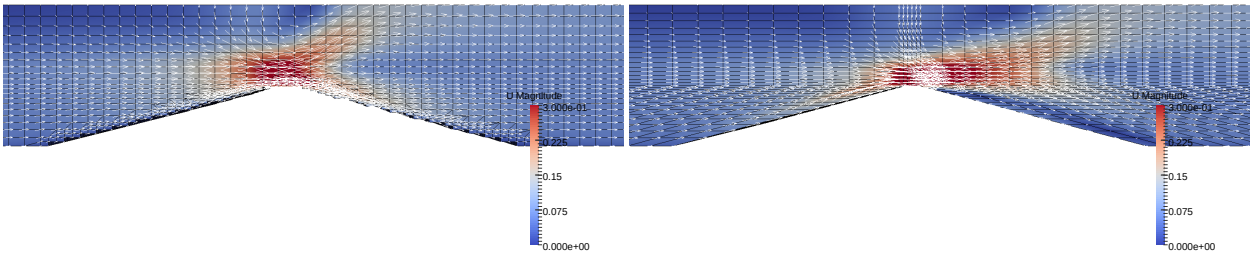

(A) Velocity vectors and magnitude for `snappyHexMesh` 3D simulation. Downward flow is obvious downstream of the weir.

(B) Velocity vectors and magnitude for `blockMesh` 3D simulation. The high velocity tends to straight downstream of the weir.

FIGURE 5.7: Velocity vectors in 3D simulations using the specific discharge q_2.

geometry `.stl` file out of the background 2D mesh. Finally it causes inhomogeneity of cells in the cross-direction of flume, leading to the unsystematic computations and meaningless results.

The differences in velocity vectors of 3D simulations for `snappyHexMesh` and `blockMesh` cases can be seen in the figures 5.7a and 5.7b. In the figure 5.7b, the velocity vectors show that the flow tends to go straight downstream of the weir in the case of `blockMesh` mesh. However, in the `snappyHexMesh` mesh simulations, the downward flow is obvious after the top of the weir as described in the figure 5.7a. This causes the differences in velocity profiles downstream of the weir. The mesh has a large influence on the flow direction.

Although the `snappyHexMesh` worked out correctly in 3D configurations, there is one drawback which is mesh size limitation. For instance, as shown in the figure 4.1, there are two structures, weir and control structure, need to be inserted in the 3D model which have to to be simulated accurately. If one would like to use the high flow velocity, he should expect higher velocity near the structure. This leads to the finer mesh cells and huge consumption of computational power for 3D simulations.

Chapter 6

Results of *Weir-Groyne Comparison Model*

This chapter presents the results of simulations of flow over the groyne and the weir using the *weir-groyne comparison model*. The differences of flow behaviours between the weir and the groyne are also explained in this chapter. This chapter disclaims the validation of the simulation results against the experimental measurements.

6.1 Streamlines

The streamlines are the curves which are tangent to the velocity vectors of the flow in the fluid domain (Kundu and Cohen, 2008). These lines are able to describe the instantaneous picture of the whole flow direction. The main objective of this section is to identify the differences in streamlines of the flow over the weir and the groyne.

The post-processing tool `Paraview` can provide the functionality of slicing the geometries in x, y and z directions, and visualizing the streamlines in each slice. It is also possible to extract the streamlines in each slice for the multiple layers of other different directions.

The analysis of the streamline patterns starts with the groyne cases in both of wide and narrow flumes. The flow area should be divided into two parts based on the length of the groyne as shown in the figure 6.1. This first part is the part I where the flows are disturbed by the groyne, and the second one is the part II where the flow area is contracted by the presence of the groyne. In the part I, the flow lines can climb up the front face of the groyne and become more complicated streamlines after the groyne. The flow velocity is low in the part I, especially the leeward side of the groyne due to the shelter zone. However in the part I, one spot of high flow velocity can be observed on top of the groyne. Regarding the part II, the high flow velocity occurs there due to the flow contraction phenomenon, and the streamlines are not mixed up unlike those in the part I. The mixing process can occur between these two parts, because the velocity gradient can still develop there and the mixing layer can occur consequently.

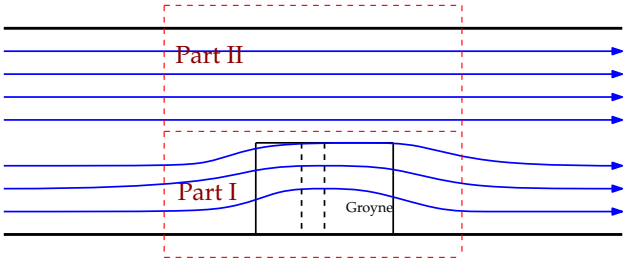

FIGURE 6.1: Division of the flow area into two parts. The part I is the area disturbed by the groyne, and the part II is one where the flow can move freely without the obstacles.

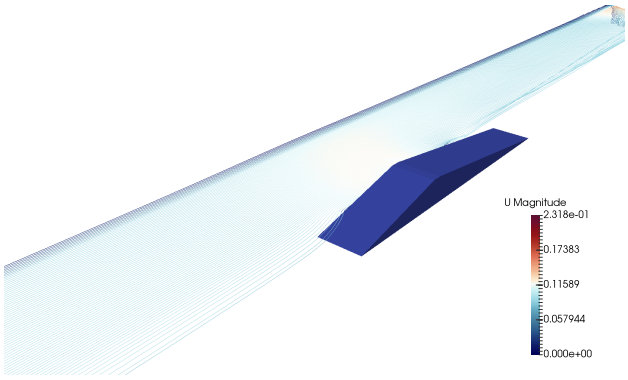

(A) Streamlines at $y = 0.1$ m.

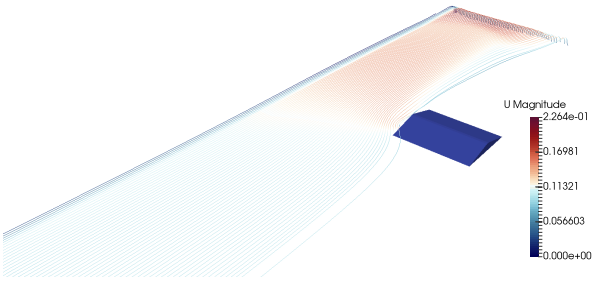

(B) Streamlines at $y = 0.1$ m.

FIGURE 6.2: Streamlines around the `groyne0` and `groyne8` at $t = 6200$ s. At the bottom $y = 0.1$ m, the streamlines flow around the groyne.

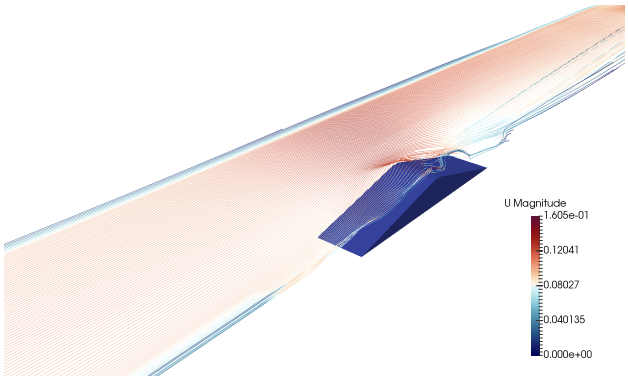

(A) Complex streamlines in the narrow flume.

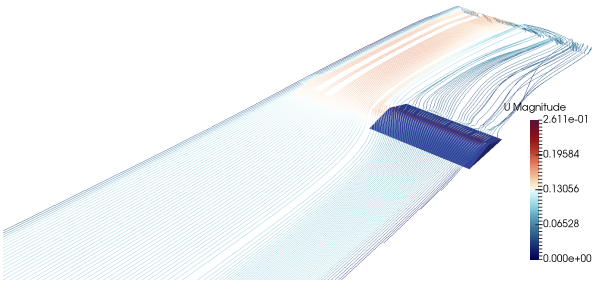

(B) Streamlines in the wide flume.

FIGURE 6.3: Streamlines around the `groyne5` and `groyne7` at $t = 6200$.

Near the bed of the flume the streamlines are passing around the structure and in other layers the streamlines can occupy the whole area i.e. only a small part of the conveyance is blocked. It shows that the flow lines in the large portion of the total water depth can overcome the structure while the flow near the bottom layer will bend around it. This is very distinct feature from the flow over the weir in which all of the water amount has to go over the structure, causing more energy loss which will be explained later.

One difference between the narrow flume and the wide flume was observed in terms of dimensionality of flow in the flume. In the narrow flume tests, the streamlines become chaotic or complex after passing the groyne which means that the flow occurs more turbulent condition. The streamlines passing over the groyne are still parallel in the wide flume test cases. The narrower flume enhances the 3-dimensionality of flow lines or eddies due to the near wall effect while the wide flume accommodates the parallel streamlines before and after both of the weir and the groyne.

The streamlines over the short groyne and the long groyne in the wide flume test are also different as shown in the figures 6.4a and 6.4b. The short groyne prevails the behaviour of the flow deflection in the horizontal plane while for the long groyne, only the certain part can cause flow deflection and the rest part is likely to be the weir flow phenomenon.

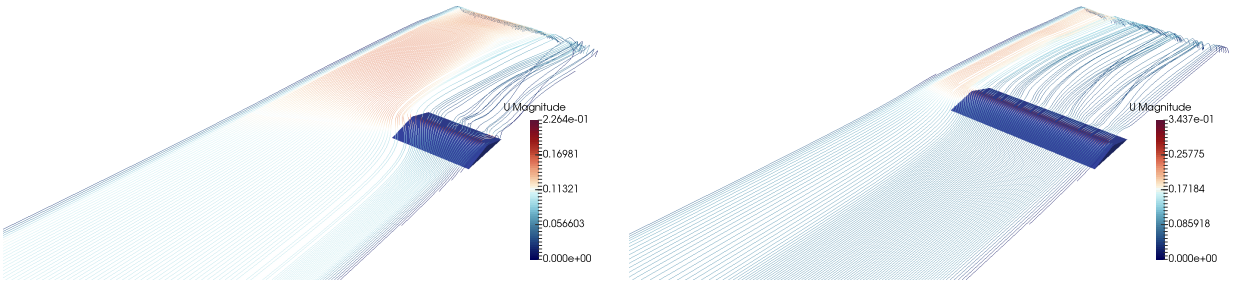

(A) Streamlines around the short groyne in wide flume (`groyne8`).

(B) Streamlines around the long groyne in wide flume `groyne9`.

FIGURE 6.4: Streamlines around the `groyne8` and `groyne9` at $t = 6200$ s.

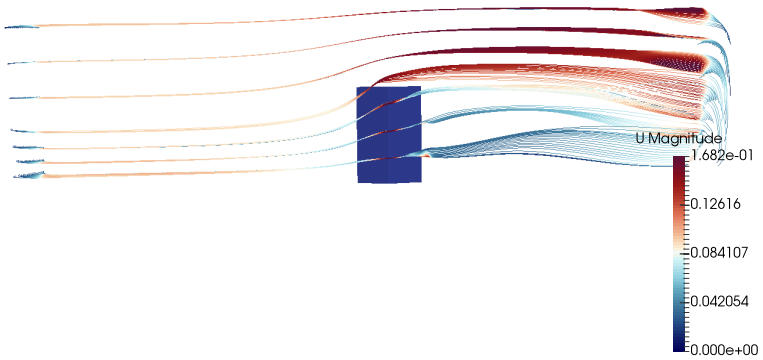

FIGURE 6.5: Plan view of the streamlines over the groyne in the test case `groyne7`. The streamlines are found to deviate from the original direction over the reach of the groyne. The streamline deviated the most on the edge between the groyne tip and the part II.

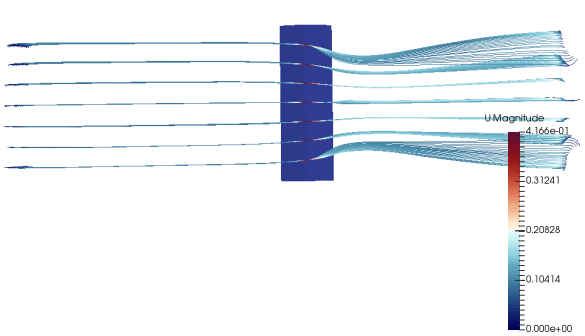

(A) Plan view of the streamlines over the weir in the wide flume (weirL). The streamlines in the y-direction slice for the seven z-direction layers describe the symmetry about the half-point of the weir length.

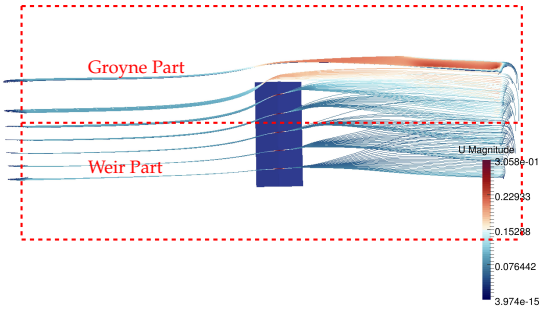

(B) Streamlines in the test groyne9 of which half of the groyne length can serve as the weir up the symmetry line while the rest part is similar to the groyne.

FIGURE 6.6: Streamlines around weirL and groyne9 at $t = 6200$ s.

6.1.1 Plan view of the streamlines

The streamlines in the y-direction slice for the different z-layers are visualized from the bird-eye view. The streamlines over the long weir in the wide flume are symmetry about the center line of the length of the weir, as depicted in the figure 6.6a. This is not the case for the short weir in the small flume of $B = 0.5$ m, because as mentioned earlier, the small flume can cause the complicated flow structures and enhance the 3-dimensionality of flow.

Having looked at the streamlines for the groyne case in the bird-eye view shown in the figure 6.5, the streamlines are found deviating from the original direction over the reach of the groyne. The most deviation of the streamline occurs on the edge between the groye tip and the part II. This is similar to the "topographic steering" phenomenon, which defines the flow direction changes due to the bed topography.

The obvious difference between the weir case and the groyne case is that the center streamline is the most straight in the former case while it is the most deflected line in the latter case. In the weir case, the symmetry enforces the center line to be the straight, but in the groyne test, the combination of the lack of geometric symmetry and the existence of the part II, which is the groyne-free zone, encourages the deflection even more than it should be.

Having compared the streamlines of the groyne9 test in the figure with the lines of the weirL, half of the groyne length seems similar to the weir operation up to the symmetry line while around the rest of the groyne length the flow bends around it like the groynes normally cause.

6.2 Velocity profiles

The velocity profiles downstream of the weir and the groyne at $x = 15.6$ m in the z-direction of the flume are depicted in the figures 6.7a and 6.7b, respectively. In the weir case, the velocity profiles show little variation because the geometry is homogeneous across the flume. However, for the groyne that blocks only a certain part of the flume, the velocity profiles are varied, leading to the

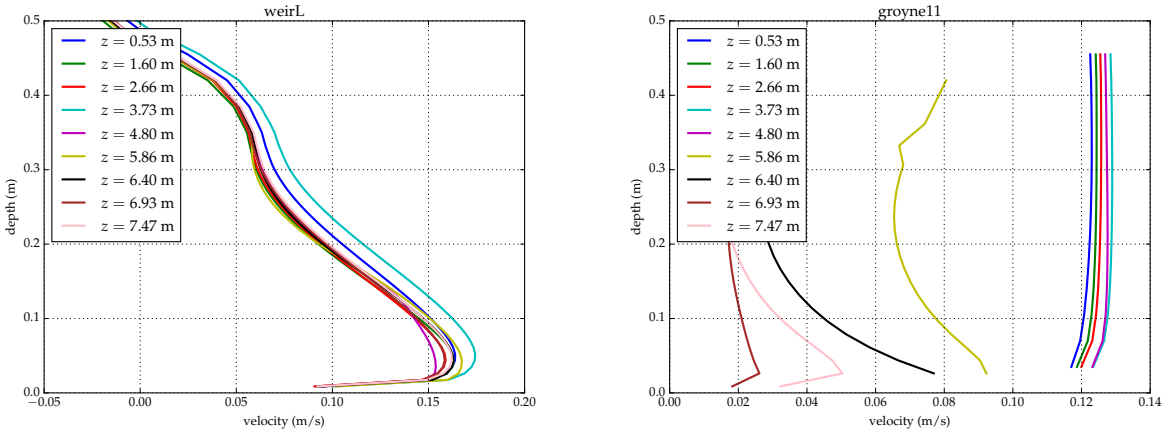

(A) Velocity profiles downstream of `weirL` case at $x = 15.6$ m.

(B) Velocity profiles downstream of `groyne11` case at $x = 15.6$ m.

FIGURE 6.7: Velocity profiles vary downstream of the groyne due to groyne-free region whilst the profiles do not vary in the weir case.

complex flow feature. Such a difference also causes the velocity gradient in the z-direction of horizontal plane. It should be noted that the velocity profiles are not validated with the experimental measurements.

6.3 Energy loss, ΔH

The energy loss is defined as the $\Delta H = H_1 - H_3$ where H_1 and H_3 are the energy heads at the upstream and downstream of the structure respectively. The energy head, H_i, is defined as again $H_i = h_i + \frac{u_i^2}{2g}$ for $i = 1, 2, 3$, where h_i is the water level above the groyne head and u_i is the flow velocity. The energy loss is mainly caused by the flow expansion and turbulent motion of the flow.

The figure 6.8a shows that variation of energy loss along the width of the flume. The huge energy loss occurs in the weir cases because the weir blocked the whole cross-sectional area, causing the large water level drop across between upstream and downstream. For the groyne cases, in the part I has the more energy loss compared to the loss amount in the part II since the part I has the blockage. Nevertheless, the energy loss caused by the groyne are far lower than in the weir cases. This is the investigation of the ΔH in the near field.

The relationship between the blockage ratio and the energy loss can be seen in the figure 6.8b where the blockage ratio is defined as the ratio of the groyne length to the channel width. This relationship is constructed by using the energy levels in the far field from the groyne. The average of slight variation of the ΔH over the width of the channel was taken for the sake of the a single value of ΔH. The large blockage ratio can cause the greater energy loss, no matter what the exact dimensions of the groyne and the flume width are. This finding is more relevant to the groyne case because one can expect the energy loss by merely knowing the ratio of the channel area and groyne length.

Looking at the results of 8 m wide flume simulations will give the clear picture for the energy head loss variation, and the relationship between blockage ratio, $\frac{L_g}{B}$, and energy loss per groyne length, $\frac{\Delta H}{L_g}$, shown in the figures 6.9a and 6.9b respectively. There is a transition region in energy loss for the groynes, represented by the slopes. This is mainly caused by the groyne-free zone where the flow can accelerate. The acceleration of flow keeps the energy level constant in the

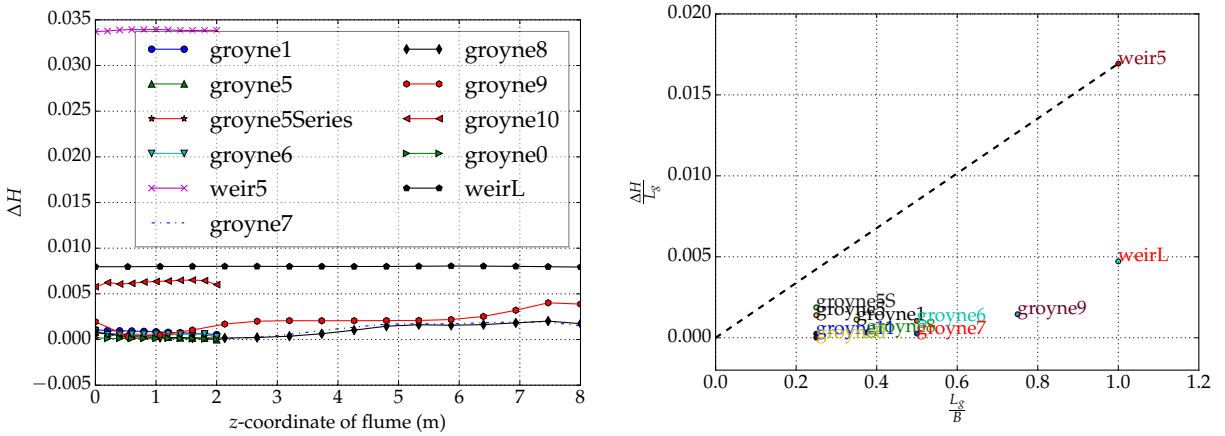

(A) Variation of the energy loss across the width of the channel.

(B) Relationship between blockage ratio ($\frac{L_g}{B}$) and energy loss per groyne length ($\frac{\Delta H}{L_g}$).

FIGURE 6.8: Energy loss of the simulation cases. In the figure 6.8a the greater energy loss occurs near the blockage area (i.e. the part I in the groyne cases, and the whole section in the weir). In the figure 6.8b, the points showing energy loss per groyne length exist under the dotted blue line, indicating that the weir is not superposition of groyne.

groyne-free zone. Downstream of the groyne in part I, however, the flow is retarded therefore the energy loss occurs. This leads to the variation of ΔH or transition zone across the flume width.

The energy loss per blockage length of the groyne, $\frac{\Delta H}{L_g}$, is lower than that of the weir because of existence of free-flow area possessed by the groyne. Moreover, $\frac{\Delta H}{L_g}$ is not linearly related to blockage ratio, $\frac{L}{B}$, for the weir and the groyne because the dots shown as groynes in the figure 6.9b are not on the straight dashed line connecting the weir point and the origin. The reason for not being linear is the contribution of groyne-free zone where the accelerated flow occurs i.e. the higher flow velocity causes the energy level to rise partly.

The variation of energy loss is contributed mainly by the velocity since according to the figure 6.10a the water level was not found varying but the energy head varied across the flume. The velocity profile in the z-direction can also be seen in the figure 6.10b. The flow is retarded behind the groyne while in the groyne-free zone the flow is accelerated. This is the main cause for variation of ΔH. It should be noted that the energy head is composed of water level and velocity head by the formula $H = h + \frac{u^2}{2g}$.

6.4 Analysis

The general flow behaviour in the narrow flume and the wide flume tests are different in terms of profound 3-dimensionality because of close existence of flume walls. Consequently the simulation results of the corresponding flumes differ regarding the streamlines.

For the groyne simulations, the flow area can be divided into two parts, which are part I and part II, which are blockage part and groyne-free zone, respectively. The flow bends around the groyne in the part II while the flow climbs up the structure in the part I. This reduces the energy loss compared to the energy loss in the weir case, because the weir blocked the whole width of the channel.

The flow structures in the weir and the short groyne are different by means of the streamlines similarity, and the presence of the part II, the groyne-free zone. The streamlines over the weir are more symmetric than the ones around the groyne because of the existence of part II in the latter

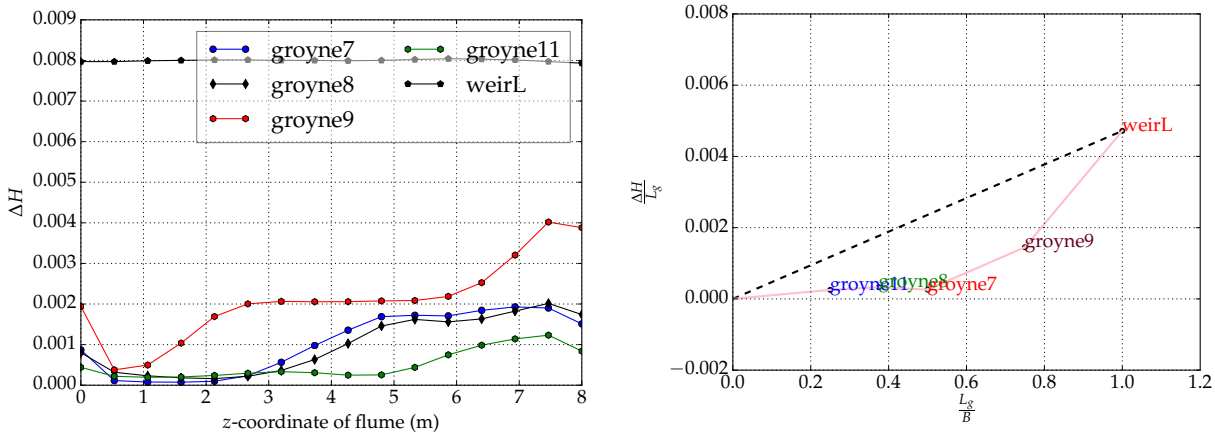

(A) Variation of the energy loss across the width of the wide flume.

(B) Relationship between blockage ratio ($\frac{L_g}{B}$) and energy loss per groyne length ($\frac{\Delta H}{L_g}$).

FIGURE 6.9: The figure 6.9a depicts the transition in ΔH for the different groynes. The figure 6.9b shows that energy loss of the groyne is lower than that of the weir.

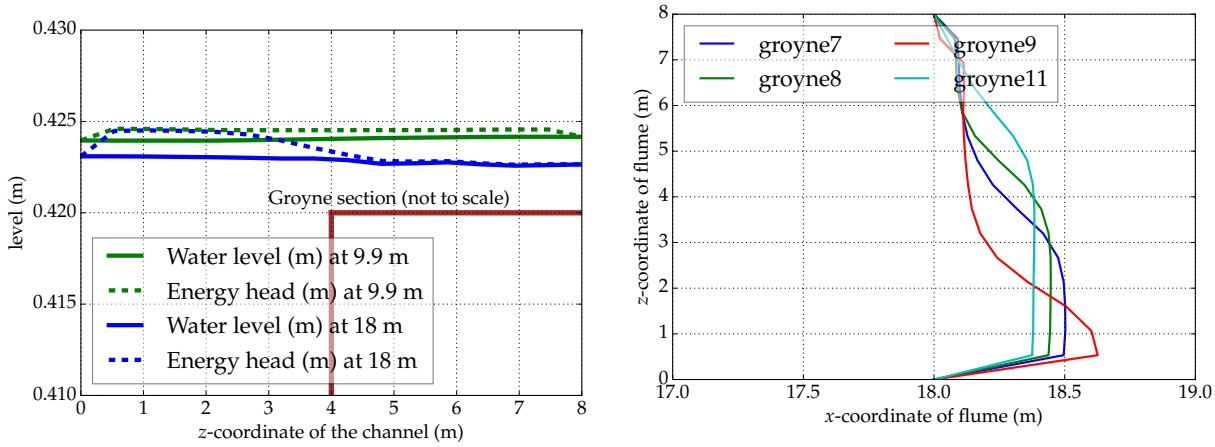

(A) Variation of energy head across the flume width in `groyne7` simulation case. This variation is caused mainly by the high flow velocity in the groyne-free zone rather than the variation of water level alone.

(B) Velocity profiles in the z-direction of flume for the plan view. The steep velocity gradient occurred to the long groyne compared to the short groyne. The velocity gradients become steeper for increasing length of groyne.

FIGURE 6.10: Variation of energy head and velocity profiles across the flume width.

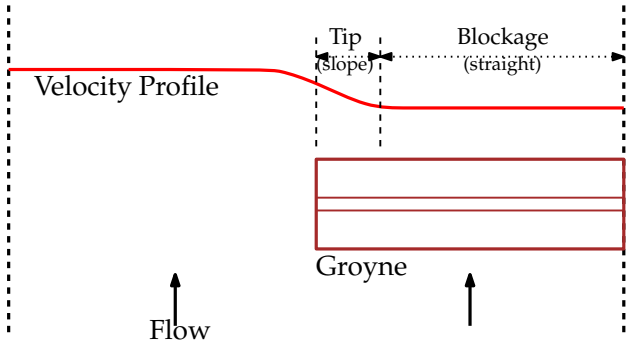

FIGURE 6.11: Division of tip and blockage of the groyne. The tip is responsible for velocity gradient in the horizontal plane while the blockage mainly causes the energy loss.

case. Moreover the streamlines over the groyne are more complex due to overflow and filling up of water downstream.

The energy loss, ΔH, is varied along the channel width, by means of that the more energy loss is expected over the reach of the groyne length while the less energy loss occurs in the rest of the channel. The larger blockage ratio, $\frac{L_g}{B}$, gives rise to the greater energy loss, ΔH, in the average sense which means that averaging the variation of ΔH by taking the upstream and downstream energy levels far from the structure.

The groyne affects the flow by two means of geometrical properties; blockage and groyne tip. The blockage part of the groyne blocks the flow as the weir does while the tip makes the flow deflect and creates velocity gradient in the horizontal plane. The latter property is not feasible in the weir structure. It is possible to divide the groyne into blockage and tip parts based on the velocity profiles (figure 6.10b) or ΔH profiles (figure 6.9b). The portion of groyne corresponding to the slope of velocity profile or ΔH profile is the tip while the rest is the blockage part. The figure 6.11 visualizes this explanation.

The short groyne portrays the tip effect preferably rather than the blockage effect since only the velocity gradient is observed whilst no straight part is found in the profile of the figure 6.10b. For the long groyne, the straight part of the profile is equal to or longer than the slope part, meaning that the blockage effect is comparable to the tip effect. Therefore the ratio of tip and blockage portions can be used to differentiate the short groyne and long groyne.

Chapter 7

Conclusions and Recommendations

7.1 Conclusions

In this research, two different models, the *interFoam evaluation model* and the *weir-groyne comparison model*, were set up using the multiphase solver `interFoam` under the `OpenFOAM` framework. The *interFoam evaluation model* was intended to address the issues of simulation of flow over the weir. The *weir-groyne comparison model* was built up for the study of flow differences between the weir and the groyne.

7.1.1 `interFoam` evaluation model

The *interFoam evaluation model* assessed the mesh type and the dimensionality effects on the numerical results. Besides it was proven that the use of a control structure at the downstream end of the flume is feasible for fixing the water level in the current study.

1. The two types of meshes, the *structured non-orthogonal* mesh created by the `blockMesh` utility and the *unstructured more-orthogonal* mesh generated by the `snappyHexMesh` utility, were applied for addressing the issues of mesh type in simulation results. The weir structure was used for observing the velocity profiles upstream and downstream. The simulations were carried out in 2D and 3D configurations. Two specific discharges were applied for these simulations.
2. Theoretically the flow separation is observed only downstream of the weir beyond a certain limit of flow velocity. In 2D simulations, the `snappyHexMesh` case could not simulate this flow behaviour correctly i.e. the flow separation was found upstream instead of downstream of the weir. In the `blockMesh` case, however, the non-orthogonal mesh was able to simulate the eddy or flow separation downstream. These observations hold in the same way for both specific discharges.
3. In 3D simulations, only the small specific discharge was used for the sake of saving computational time, because the greater discharge requires finer meshes to capture the flow process. The 3D simulation result of `snappyHexMesh` is totally different from 2D results in case of a small discharge. For the `blockMesh` case, the 3D and 2D simulations are identical.

   The reason for getting the flow separation in the wrong position in 2D simulation of `snappyHexMesh` case is the existence of additional computational cells in the z-direction or across the flume. The figure 7.1 depicts these additional cells in the cross-direction of the flume. These cells are by-products of the meshing algorithm, leading to the unnecessary incorrect computations for 2D simulations. It is not the case for 3D configurations of the `snappyHexMesh` meshes.
4. The `snappyHexMesh` method seems to work the best only in 3D simulations. It should be noted that the current research could not prove that the flow separation can be simulated in 3D `snappyHexMesh` simulations with small specific discharge. Regarding the

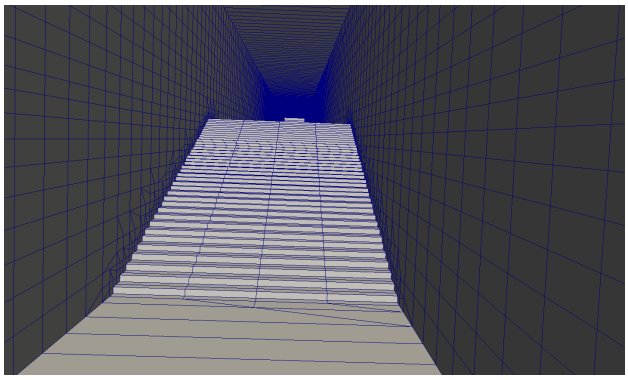

FIGURE 7.1: Additional cells which are by-products of the `snappyHexMesh` algorithm in 2D simulations causes the flow separation upstream of the weir.

`blockMesh` or non-orthogonal mesh, although it can reproduce the flow behaviour generally, the numerical diffusion can occur due to its non-orthogonality, leading to numerical artifacts-prone results.

The following research questions can be answered:

Which kinds of boundary conditions are required for the `interFoam` solver to simulate the open channel flow in the numerical hydraulic flume?

The hydraulic model, logically and mathematically, needs the discharge or velocity at the upstream boundary condition and the water level at the downstream condition for being the well-posed problem. The `interFoam` solver does not provide the built-in function for defining the water level boundary condition (Thorenz and Strybny, 2012).

Three methods are available for defining the water level boundary condition according to the literature (Jellesma, 2013; Thorenz and Strybny, 2012; Teuber et al., 2013). The first method is to use the fixed height of the patch used for assigning the water level, and the body force term to be incorporated into the governing equations as the driving force (Jellesma, 2013). The second method suggests to implement the new source codes for boundary conditions functions (Thorenz and Strybny, 2012). This method will make the `interFoam` solver pretend as the traditional hydraulic model. The last method is to simply insert the gate or additional structure for controlling the water level before the end of computational mesh (Teuber et al., 2013).

In conclusion, the `interFoam` solver cannot avoid the use of flow discharge and water level for the upstream and downstream boundary conditions, respectively.

How can the required boundary conditions be implemented in the `interFoam` solver for simulation of flow over the hydraulic structures?

In order to mimic the experimental configuration of the simulation, the discharge boundary condition is needed at the upstream boundary while the water level should be defined at the downstream end of the domain. It has been mentioned that the `interFoam` solver does not provide the built-in functionality for fixed water level boundary condition.

Therefore, the control structure needs to be added near the downstream part of the computational domain in order to regulate the water level, the so-called *physical method* for boundary condition. It should be noted, however, that the negative discharge should be used at the exact boundary edge of the domain for driving the flow out of the flume. For upstream boundary condition, there is no special trick to define the discharge or velocity.

How does the computational mesh affect the numerical simulations of the `interFoam` in the study of flow over the weir and the groyne?

Two types of meshes, the *structured non-orthogonal* mesh and the *unstructured more-orthogonal* mesh are used for 2D and 3D simulations of flow over weirs and groynes. The obvious difference was found between 2D and 3D simulations for using the *unstructured more-orthogonal* mesh, regarding the location of flow separation. This is due to the additional cells created by the `snappyHexMesh` meshing process, which appear across the flume width in 2D simulations. It should be noted that these extra cells are located only where the geometry `.stl` file applies i.e. the weir exists. This leads to the *inhomogeneity* of computational cells for the whole 2D configuration.

Analyzing the results of 3D simulations, the flow separation was not observed at all both upstream and downstream sides of the weir in the *unstructured more-orthogonal* case. However, using the *structured non-orthogonal* mesh, the flow separation occurred downstream of the weir as usual. It can be deduced that the flow direction is affected by the mesh orientation.

Therefore, the numerical results of FVM really depend on the mesh properties, which are orthogonality, flow-mesh alignment and structuredness.

7.1.2 weir-groyne comparison model

The *weir-groyne comparison model* was set up for the purpose of observing the differences between the groyne and the weir. Its settings are different from the *interFoam evaluation model*'s settings. Having simulated different geometries of the groynes and weirs in narrow and wide flumes, the observations are summarized as follows:

1. In the groyne case, there are two flow areas: (1) blockage part I and (2) groyne-free part II. The streamlines bend around the tip of the groyne in part II while the rest flows over the groyne. Due to the velocity differences between these two parts, a mixing layer occurs and momentum is exchanged consequently.
2. Although the mixing process cannot occur in the weir flow because there is no velocity gradient across the flume direction, there is a greater energy loss than in the groyne case, because the weir blocks the flow area totally.
3. Looking at the top view of flow line patterns, the streamlines over a weir are symmetric around its middle line. For the flow over a groyne, the streamlines are deflected, especially near the tip of the groyne due to asymmetry of geometry.
4. The short groyne is found to behave differently from the weir in terms of energy loss and streamline patterns. The energy loss is mainly caused by the velocity gradient in the short groyne while it is caused by the blockage in the weir. Regarding the differences in streamlines, the weir does not depict horizontal variation of velocity profiles while the groyne shows variation of profiles due to groyne-free zone. However the flow over a long groyne is a combination of weir flow and groyne flow because some part of the groyne can accommodate the weir flow.
5. The energy loss is varied along the width of the flume in the groyne case, from the near-field perspective. The variation is mainly caused by the variation of velocity head. Near the groyne part where the flow is retarded more energy loss occurs than in the free flow zone where the flow velocity is high.
6. By averaging the energy loss variation or far-field perspective, there is a relationship between blockage ratio and energy loss per groyne length. More or less energy loss can be expected for the same blockage ratio.
7. The groyne can be divided into two portions: blockage and tip that can causes different flow processes respectively. Based on the tip and blockage effects, the long and short groynes can be differentiated in such a way the short groyne expresses the tip effect rather than the blockage, and the long groyne does other way round. The tip effect is indeed represented by the slope of velocity profile and the blockage effect is shown by the straight line of profiles.

To answer the research questions:

> What are the differences in 3-dimensional flow structure between the weir and the groyne?

The flow over weir causes the flow separation in vertical direction while the flow over groyne possesses the vertical and horizontal flow separations. In the groyne case, some part of the flow deflects around the groyne tip and some flow lines overcome the rest part of the groyne. The flow over the weir, however, is partly different from the flow behaviour around groyne because the weir blocks entirely the flow area and no flow deflection is feasible at all in horizontal plane.

Moreover, velocity profiles downstream of the weir shows little variation along the z-direction of flume whereas the profiles downstream of the groyne varies a lot depending on the groyne length. Therefore, the velocity gradient happens to the flow in the groyne case and the flow around groyne is more complicated than the flow over weir, due to filling up of water downstream.

> How does the groyne and the weir differ in terms of energy head loss?

It is obvious that the head loss caused by the groyne is smaller than the loss due to the weir, because the groyne does not obstruct completely the flow area. The groyne allows flow acceleration in a certain part of the flume width, leading to the rise of energy level there. This contributes the variation of ΔH along the channel width. This is not the case for the weir simulation. Due to the aforementioned flow acceleration of the groyne and energy level rise, head loss per blockage length, $\frac{\Delta H}{L_g}$, is found not linear to the blockage ratio, $\frac{L_g}{B}$, and the weir is not the superposition of groyne.

> To which extent (for which part) does a long groyne behave as a weir?

In this research, the groyne of 6 m long is a long groyne in the 8 m wide flume. The simulation results show that the length of 5 m blockage portion of the groyne can behave as the weir because this part can block the flow totally, leading to the uniform energy head loss. The rest 1 m tip portion can cause the flow deflection as the traditional groyne does, and the energy head loss is not uniform over this short length.

7.2 Recommendations

Recommendations are provided for the *interFoam evaluation model* and the *weir-groyne comparison model*, respectively.

7.2.1 `interFoam` evaluation model

The following facts for addressing the numerical issues in flow simulation over the weir using the `interFoam` solver, are recommended:

1. In order to overcome the use of control structures for controlling the water level, the mathematical boundary conditions should be devised for water level boundary conditions as implemented by Thorenz and Strybny, (2012). It can save the extra computational cells and power. Besides, using this technique the water level can precisely be defined without preliminary simulations for adjusting the control structure height.
2. The simulation of using the larger specific discharge should be done for ensuring the 3D `snappyHexMesh` can reproduce the flow separation downstream of the structure.

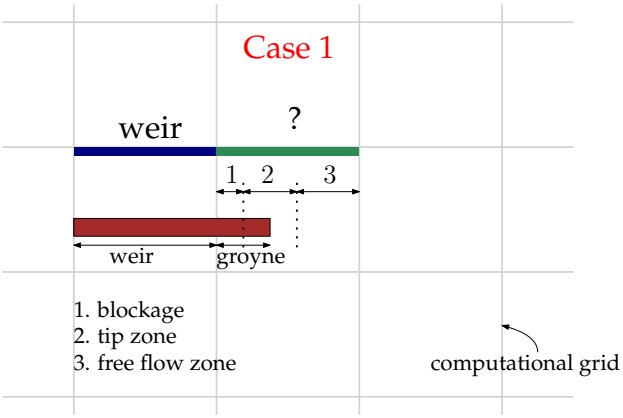

(A) Case 1: The groyne is short enough for the tip effect to be considered in only one cell. Three flow zones (1,2 and 3) need to be parameterized in the primary cell.

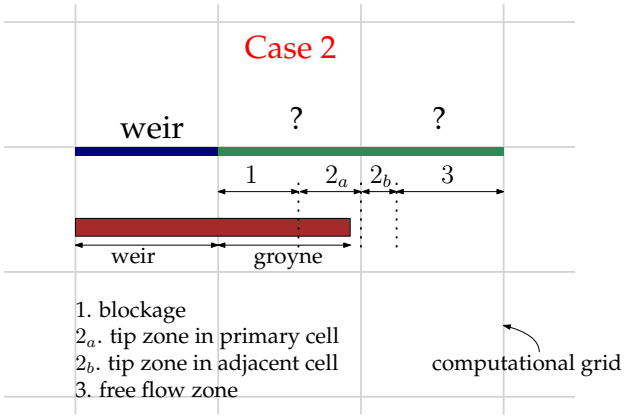

(B) Case 2: The groyne tip effect extends to the adjacent grid cell from the primary cell. Hence, groyne parameterization is needed in extra cell.

FIGURE 7.2: Sub-grid approach for modelling the short and long groynes. The *green* line indicates the analysis is needed for parameterization of groyne. The *blue* one shows the weir formulation can be used for that part of groyne because this part is similar to weir.

3. It has been verified that the structured non-orthogonal mesh always simulate the flow separation downstream of the structure, but results are prone to numerical drawbacks. Therefore in the future research the correction schemes should be implemented, but it will cause extra computational time.
4. The scientific proof should be necessary for failure of flow separation in the unstructured meshes for 2D simulations.

7.2.2 weir-groyne comparison model

Using the simulation results of *weir-groyne comparison model*, the approach of representing a groyne in hydraulic models is presented below although the exact numerical values for energy loss of groyne cannot be provided in the current research.

Based on the velocity and energy head loss profiles, it is remarked that the flow over the groyne can be divided into (1) blockage, (2) tip zone, and (3) free flow zone. The three flow zones will play an important role in the sub-grid approach of hydraulic models. The complete understanding of these flow zones is required for 2D parameterization of energy loss in the groyne.

There are two cases for using groyne structure in the sub-grid approach: case 1 and case 2 as shown in the figures 7.2a and 7.2b, respectively. In these figures, the *brown* rectangle can be divided into weir and groyne based on the dimension of computational grid cell. The structure occupying full width of the grid is similar to the weir, therefore the traditional weir formulation can be applied to this grid. The part extruded from the weir cell acts as the groyne in next grid cell. This cell necessitates the parameterization of flow around a groyne.

The extruded length of groyne makes two aforementioned different cases: case 1 and case 2. In case 1 (figure 7.2a), the groyne exists within only one cell, the so-called *primary* cell. In this single cell, three kinds of flow can be observed, namely (1) retarded flow caused by blockage, (2) the deflected flow by the tip, and (3) free flow away from the obstruction. Here, the knowledge of comparison of blockage and tip effects explained in the section 6.4 should be used to differentiate the short groyne and long groyne. If the groyne is short one, the blockage effect can be eliminated and only the energy loss done by velocity gradient or tip effect should be considered.

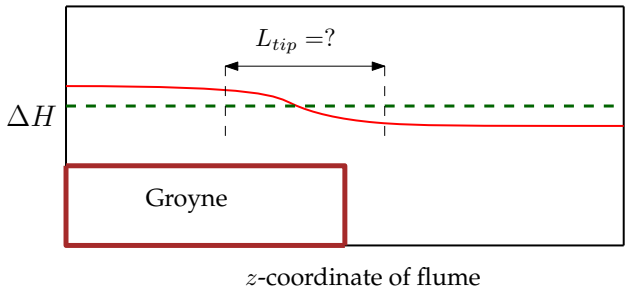

FIGURE 7.3: Parameterization of energy loss in the groyne. The red line is the actual energy loss and the green line is the resultant of averaging the energy loss. It is questionable for the length of gradient of energy loss, L_{tip}.

For the case 2 (figure 7.2b) in which the groyne occupies most part of computational cell, the tip effect can extend in the *adjacent* cell although the groyne tip ends in the *primary* cell. In this case, parameterization should take place in these two cells. In the *primary* cell, both the blockage and tip effects will be dominant, therefore the parameterization should include these two effects for this cell. However, the blockage effect is absent and only tip effect and free flow are present in the *adjacent* cell. Therefore another parameterization different from the *primary* one will be required in this cell.

A simple parameterization is the averaging of energy loss occurring to the groyne. As shown in the figure 7.3, the actual energy loss represented by the red line is not uniform over the flume width. The varying energy loss should be estimated by a single value for representation of groyne in simpler hydraulic models. The single value of energy loss shown by the green line can be obtained by averaging the red line. Parameterization of energy loss reads:

$$\Delta H_{avg} = \frac{1}{B} \int_0^B \Delta H(z) dz \tag{7.1}$$

where ΔH = averaged energy loss, B = width of flume, and z= the coordinate of flume width. The resulted ΔH_{avg} should be transformed again into the energy loss coefficient appropriately. This coefficient can be used as the energy loss coefficient of the groyne for hydraulic models.

There are two issues to be addressed in the future researches. The first issue is how to determine the necessity of adjacent cell i.e. which criteria should be applied to decide whether it is case 1 or case 2. The length of transition of ΔH , L_{tip} drawn in the figure 7.3, should be used for the criteria because elongation of ΔH transition necessitates the adjacent cell. The L_{tip} is expected to be dependent on the water level or discharge and independent of the groyne length. Therefore the future researches should focus on validation of this fact by conducting a set of various experiments.

The another issue to be addressed is to construct the relationship between ΔH, groyne geometry and flow properties. It is about to estimate the magnitude of ΔH slope in the figure 7.3 while the first issue is about to calculate L_{tip}. From this research, it has been known that the long groyne causes the greater energy loss. However it still requires a set of simulations to generalize the energy loss with respect to water depth and discharge. Finally, tackling this issue can give a better estimate of energy loss coefficient which will be used for depth-averaged hydraulic models.

Finally, the theoretical analysis for contribution of three flow zones shown in the figures 7.2a and 7.2b to the energy loss is advisable for better parameterizations of groyne in the sub-grid approach. Besides, for further numerical simulations, different turbulent modellings should be applied to realize a better understanding of the flow occurring behind the structure.

Appendix A

Flow near Groyne Fields

A.1 Flow near the emerged groyne fields

Yossef and Vriend, (2010) investigated the nature of flow around the series of groynes for both of submerged and emerged conditions. The mixing layer was observed in the groyne fields as in the previous single groyne case and the width of the mixing layer was found to increase along the downstream direction. They characterized the flow pattern near the groyne fields via three types of eddies: (1) a large-size and energetic primary eddy near the downstream part of groyne filed, (2) a small-size and weak secondary eddy driven by the primary one with opposite vorticity, and (3) a dynamic eddy shedding from the tip of upstream groyne to the downstream direction. The dynamic eddy can interact with the primary one, causing the change in size. The whole circulation pattern is forced by the mean velocity with the exchange of momentum through the mixing layer (Yossef and Vriend, 2010). They did not consider the 3D flow structures which can occur at the tip of the groynes in reality.

Regarding the exchange process between the main channel and the groyne fields, Uijttewaal et al., (2001) investigated extensively in the laboratory, noticing that the dominant structure for the exchange process is 2D structure whilst there is little interaction with 3D turbulence. It should not be confused, however, with the effect of water depth and bottom friction on the property of general 2D horizontal coherent structure, because Uijttewaal et al., (2001) pointed out the lateral mixing layer can diminish due to the bottom friction, or decrease in size governed by the water depth. The strong 3D turbulent flow pattern can be expected at the transition of river and groyne field interface where the sudden change in bathymetry is present.

Sukhodolov, (2014) implemented field-scale experiments for the study of hydrodynamics around the submerged and non-submerged groynes, including the measurement of vertical turbulent fluxes. He found that the vertical flux of momentum is the strongest at the river bed and the horizontal flux dominate near the free surface. The 3D flow patterns which were categorized as impinging jets could be captured and it was concluded that these structures afforded the great amount of turbulent fluxes of momentum near the river bed in the groyne fields (Sukhodolov, 2014).

There is very few amount of literature focusing on the detail measurements for the vertical downward flow pattern around the groyne which are very complicated to visualize in the laboratory, whilst some literatures are available for the study of Q2CS which are mainly visible and can exchange the momentum across the mixing layer. The reader is referred to the research of Talstra, (2011) and Uijttewaal and Van Schijndel, (2004) for the study of flow pattern changes caused by the groyne geometry.

A.2 Flow near the submerged groyne fields

It was found that the flow pattern near the groyne during the submerged case differs from the flow during the emerged condition in terms of eddy formation and mixing layer width (Yossef,

2005). The width of the mixing layer remains the same in downstream direction because of the downstream groyne fields that support the velocity gradient between the main stream and the slow velocity field inside the groyne field. The mixing layer can enter the main stream region to a larger extent than the emerged groyne case. The horizontal circulation pattern can be hindered by the flow over the groynes which is similar observation as in a single submerged groyne case. This is because the momentum transfer by the overflow across the groyne is supposed to be in balance against the momentum transfer through the mixing layer. Eventually there exists a periodical flow pattern of acceleration and deceleration between the area over and around the groynes. Therefore the zone between the groyne fields can be considered as the low-velocity region (Yossef and Vriend, 2010).

Sukhodolov, (2014) emphasized that during the submergence, the flow character is highly 3D because of the flow separation over the crest of the groyne or wake. Moreover he expressed the mean streamwise velocity profile as exponential function which is the characteristic of the wake-type flow model.

A.3 Flow through permeable groynes

The permeable groynes can reduce the flow separation at the tip of the groyne compared to the solid-type structure, and thus decreases the recirculation behind the groyne (Alauddin et al., 2011). The permeability can be measured in terms of the blockage percentage (Uijttewaal, 2005b) which is apparently equivalent to the definition of blockage ratio by Azinfar and Kells, (2008). Yeo et al., (2005) also claimed that the length of the flow circulation zone decreases as the increasing permeability of the groynes. Regarding the backwater effect of the groyne, the permeable groynes of over 40% permeability do not enhance this effect (Kang et al., 2011). Uijttewaal, (2005a) demonstrated that the permeable groynes can decrease the turbulent intensity, but it cannot demolish an energetic mixing layer. It should be noted that a vast amount of permeability can cause the similar flow pattern behind a single pier (von Kármán vortex), leading to very complex flow structure behind the groyne zone (Yeo et al., 2005).

It is required to pay more attention to the detail modelling the interaction between the permeable groynes and the turbulent flow. Due to the complicated nature of hydrodynamics behind the groynes, the robust turbulence modelling or numerical algorithm can be required to do so.

A.3.1 Numerical studies

As mentioned above, the highly 3D coherent turbulent flow structure around the groyne is so complicated that detailed measurement cannot be done for visualization by the 2D Particle Image Velocimetry (PIV) apparatus. Unfortunately any report of experimental measurement using the 3D PIV techniques has not been published in the research field of flow around the groynes (Koken and Constantinescu, 2008). This difficulty can be overcome by using the numerical modelling which solves the small and large length-scales of turbulent eddies. In this literature review, the prospective advantages and limitations of mathematical models for solving the hydrodynamics problem, especially dealing with the turbulent scales, around the groyne, will be assessed rather than studying the nature of the flow, because the primitive study of the nature of the flow should not come from the numerical artifact-prone solutions.

A.3.1.1 Mathematical models for flow simulation around the groyne

It has been recognized from the experimental studies of subsection 2.2.1 that there exists two main features of the flow around a single groyne and a series of groynes, which are (1) flow separation and consequent flow circulation, and (2) turbulent motions in the mixing layer and circulation zone. In fact many researchers have attempted to simulate such kinds of flow dynamics as much

as to be realistic in the fields of not only hydraulics engineering but also aerodynamics applications. Therefore the quality of numerical models indeed depend on how extent they could simulate or visualize these two features correctly.

Zaghloul, (1983) developed a finite element model which is able to simulate the circulating flows making use of the combination of Helmholtz-type vorticity equation and Poisson-type equation in which the Reynolds equations were transformed into the former type, and the continuity equation was transformed into the latter one using the stream function, respectively. Here the Reynolds equations stand for the Reynolds-averaged Navier-Stokes equations (RANS), one of the solvable methods for turbulent flow. These two equations are solved alternately for each time step to attain the fields values of vorticity and stream function until the flow pattern around the obstacle is relatively steady. The Boussinesq hypothesis was applied to circumvent the unknown terms, Reynolds stresses. This mathematical model was also solved by Zaghloul, (1982) with the use of finite difference method. Zaghloul and McCorquodale, (1973) attempted to simulate the flow around a groyne using the developed method but they failed to validate the results against the experimental results (Molls and Chaudhry, 1995).

Differently from the novel method of Zaghloul, (1982), Tingsanchali and Maheswaran, (1990) used the conventional 2D depth-averaged flow equations along with standard $k-\epsilon$ turbulence closure model instead of Boussinesq hypothesis. Due to the discrepancy between their first-run simulation results and Rajaratnam and Nwachukwu, (1983)'s experimental results i.e. the recirculation length and width are greatly underestimated in their case, they modified the turbulence model considering the streamline curvature correction derived from the flow separation, to attain the correct results. Moreover they also included one parameter into the friction coefficient, C_f, for 3D skewed boundary layer according to Phillipsburg, (1960) in order to improve the calculated bed shear stress. This approach requires the pre-researched experimental value of skewness angle in the boundary layer to account for the 3D effect.

Molls and Chaudhry, (1995) attempted to overcome the deficits of Tingsanchali and Maheswaran, (1990)'s model which is curvature correction in standard $k-\epsilon$ model, with the new numerical algorithm, Alternating-Direction-Implicit (ADI) for solving 2D governing equations in which the *effective* stresses were considered. The effective stresses included laminar viscous stresses, turbulent stresses, and stresses due to depth-averaging. They used the Boussinesq hypothesis for defining the effective stresses via the eddy viscosity, neglecting the depth-averaging stresses due to its complicatedness. The eddy viscosity was assumed constant near the groyne as well as in the entire flow field, and observed that the calculated eddy viscosity was almost equal to those provided by advanced turbulence closure models (Molls and Chaudhry, 1995).

Apart from 2D hydraulic models, Ouillon and Dartus, (1997) used the *non-hydrostatic* 3D hydrodynamic models to study the flow around a single groyne with *rigid-lid* model and *free-surface* model; the rigid-lid model assumed the water surface unable to move freely as in reality, using the so-called *rigid-lid assumption* whereas the free-surface model needs some tricks e.g. Volume-of-Fluid (VOF) method, Marker-and-Cells method, to represent the correct evolution of surface elevation (Duchêne, 2014). The non-hydrostatic model included the contribution of vertical acceleration unlike the Shallow Water equations, and it can simulate the correct pressure field near the groyne. Ouillon and Dartus, (1997) concluded the hydrostatic assumption seems suitable for large-scale flow models whereas the incorrect pressure distribution may result in near the groyne.

Since the application of the $k-\epsilon$ model is limited for the circulating flow near the wall (Dewan, 2010) although it has been widely used in general usage of hydraulics i.e. its intrinsic isotropic property failed to capture the anisotropic turbulence near the wall, the non-linear $k-\epsilon$ model was invented. This nonlinear closure model was applied by Kimura and Hosoda, (2003) to simulate the 3D flow patterns around the bluff body. An alternative way to standard $k-\epsilon$ model is the $k-\omega$ closure model which is able to deal with the adverse pressure gradient (Rodi, 2017). In fact there are a variety of closure techniques for Reynolds stresses, for instance many versions of algebraic

models, one-equation models, and two-equation models, that only the *mean* flow property e.g *mean* velocity profile, can be retrieved due to the property of RANS equations (Wilcox, 1995).

Until now, the aforementioned numerical models are under the scope of RANS which averaged the fluctuated signals via Reynolds decomposition, and then ensemble-averaging method. This averaging results in a new set of equations consisting of the unknown terms, called Reynolds stresses. Due to the unbalance in system of equations and the unknown variables, the closure modelling became necessary to determine the value of Reynolds stresses about which are already described above. In fact another two numerical approaches are available to solve the turbulent flow; namely Large Eddy Simulation (LES) and Direct Numerical Simulation (DNS), and they are more advanced than the RANS. The DNS approach solves all sizes of turbulent scales on very fine mesh which require enormously computational power, without any turbulent closure modelling scheme. This is called *resolving* the turbulent scales while the RANS *models* these scales. Therefore using the RANS method does not need a lot of computational power as much as the DNS needs. The approach lying in between these two methods is LES in which the equations are spatially filtered, and resolves the large-size turbulent scales but not the small scales. The Subgrid-Scale (SGS) model or other closure models need to be used for handling the unresolved scales via the subgrid-scale stress tensor (Berselli et al., 2005).

The *backscatter* models are also available for taking into account the interaction of the resolved and unresolved turbulent properties (Talstra, 2011). The backscatter model inherited from the concept of *inverse* energy cascade in which the transfer of energy goes from smaller motion to large motions, contrary to the normal energy cascade where the large-scale motions feed energy to the small-scale ones. One of the backscatter models is the DANSLES developed by Talstra, (2011) for capturing the generation mechanism of 2D structures by unresolved 3D turbulent flow. The DANSLES was inspired by one existing model known as DA-LES (Depth-Averaged Large Eddy Simulation), and therefore the developer named his model *Depth Averaged Navier-Stokes with Large Eddy Stimulation* (DANSLES). Although the model could give rise to the satisfactory results for the experiments (straight channel flow, shallow lateral expansion and shallow mixing layer), its primary limitation is only for the case of constant water depth.

As the computational power is getting increasingly strong during these days, the LES approach became popular for its capturing the large-scale turbulent flow patterns, the vortex shedding or complex vortex system and anisotropy of turbulence (Rodi, 2017; Koken and Constantinescu, 2008). For the 2D models, the Horizontal LES (HLES) can be applicable for the simulation of large eddy structure around the groyne (Yossef, 2005). Some hybrid methods between LES and RANS are also invented for reducing the simulation time of LES and overcoming the difficulty of RANS on massively separated flows (Spalart, 2009). The novel method for solving fluid dynamics problems, the Lattice Boltzmann method, coupled with the LES model, was applied by Xin et al., (2010) for studying the flow around a groyne.

Appendix B

Common practices for modelling the groynes in the large-scale problems

Due to the big gap in length scales of flow in the main stream and around the groyne, the 3D local hydrodynamic processes are eliminated in the large 2D models by using the *sub-grid approach*. The sub-grid approach is generally used for the case the hydraulic structures in the river are relatively small compared to the size of the computational mesh (Deltares, 2014). In this sub-grid approach the governing momentum equations need to modified in such a way to compensate the eliminated flow behaviour by inserting some extra terms.

In 1D modelling case, the Manning coefficient or the Chézy coefficient is simply used for the loss of total energy including the turbulence induced loss. Michael Scurlock et al., (2015) renovated the formulation of the coefficient using the near-prototype experiment for different shapes of weir hydraulic structures. This approach does not require the intensive 3D modelling for acquisition of turbulent dissipation of energy. Therefore for the huge study area where one cannot afford a 3D model, the friction coefficient in 1D model is still in use. However it still requires to devise such a coefficient for the groyne structure.

Also for the 2D modelling, in the sub-grid approach there are two formulations as described above for modelling the groynes which are (1) the weir formulation by which the flow over the groyne is assumed as the flow over the weir, and (2) the drag resistance approach by which the groyne is assumed as a large obstacle in the channel (Ali, 2013). Both of these two approaches are apparently useful only for the submerged conditions (Ali, 2013; Leeuwen, 2006) because the formulations are based on the continuous flow lines over the structure; in the emerged case the flow lines do not appear on the top of the groyne but only deflect around it, hence the formulations seem not valid for that case.

Apart from the sub-grid approach, the new hybrid Shallow Water/3D flow solver was introduced by the Flow Science® Inc. in which the 3D meshes are used around the local hydraulic structure where the vertical pressure gradient and velocity are intense, while the Shallow Water equations are solved for the large-scale flows.

In short, there are two ways to represent the groyne in the large-scale models via the friction coefficient in the governing equations, which are (1) using the weir formulas by assuming that the groynes are akin to the weirs, and (2) using the drag resistance formulas by assuming them as if they are a part of the bottom roughness (Kruijt, 2013).

B.0.1 Modelling groyne using the weir formulation

When the length of the groyne is full over the width of the river and submerged, the flow over the groyne can be assumed as the weir flow (Ali, 2013). Many researches have devised the discharge relationship between upstream and downstream using the discharge coefficient for perfect and imperfect flow conditions (Leeuwen, 2006). These relationships are based on the Bernoulli equation and momentum conservation principle which are applied before and after the structure

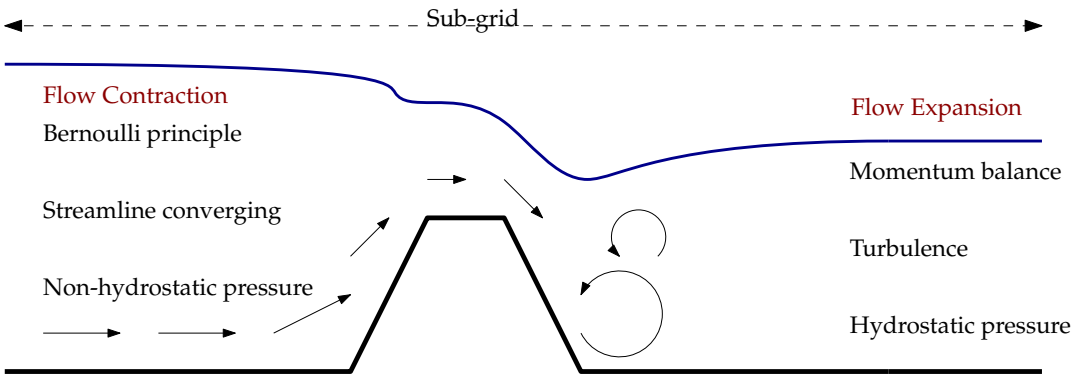

FIGURE B.1: The sub-grid approach where the Bernoulli principle is applied before the groyne since the energy is conserved but momentum is lost by the drag force of the groyne, and the momentum balance is used behind it because the energy loss is expected due to the turbulence (Zijlema, 2017). The *blue* line represents for the water level.

respectively, and again felt by the friction coefficient and contraction coefficient based on the empirical data. The figure B.1 depicts the application of these two principles over the groyne or weir.

In the figure B.2, the Bernoulli principle and the momentum balance equations read as follows respectively:

$$H = h_1 + \frac{\beta_1 u_1^2}{2g} = h_2 + \frac{\beta_2 u_2^2}{2g} \tag{B.1}$$

and

$$\frac{1}{2}\rho g(d_2 + h_g)^2 + \rho\alpha_2 u_2^2 d_2 = \frac{1}{2}\rho g d_3^2 + \rho\alpha_3 u_3^2 d_3 \tag{B.2}$$

where H = head level above the weir crest line, h = water depth above the crest, u = velocity, ρ = density, g = gravitational acceleration, and α, β = correction coefficients which are very close to 1 for the assumption of that the vertical velocity profile remains the same in the streamwise direction (Kruijt, 2013). The continuity equation for the three sections are written as:

$$q = u_1 d_1 = u_2 d_2 = u_3 d_3 \tag{B.3}$$

Solving the system of equations B.1 and B.2 with the continuity equation B.3 can estimate the energy head loss, $\Delta H = H_1 - H_3$, and discharge coefficient via finding the upstream water depths by providing the downstream water depth and discharge (Ali, 2013). The formula for determining the discharge coefficient reads (Ali, 2013):

$$q = C_w\sqrt{2g\Delta H} \tag{B.4}$$

Alternatively, in the sub-grid approach the weir formula is used to determine the energy loss term, for example the following relationship can provide the discharge coefficient, C_w (Kruijt, 2013):

$$q = C_w \frac{2}{3}\sqrt{\frac{2}{3}g}H_1^{\frac{3}{2}} \tag{B.5}$$

where q is the unit discharge, g is the gravitational acceleration, and H_1 is the upstream energy head. Other researchers also provided different formulas for other shapes of weirs empirically. Having measured the flow properties in the laboratory, the value of coefficient can be determined and added to the governing equations in the numerical solver packages.

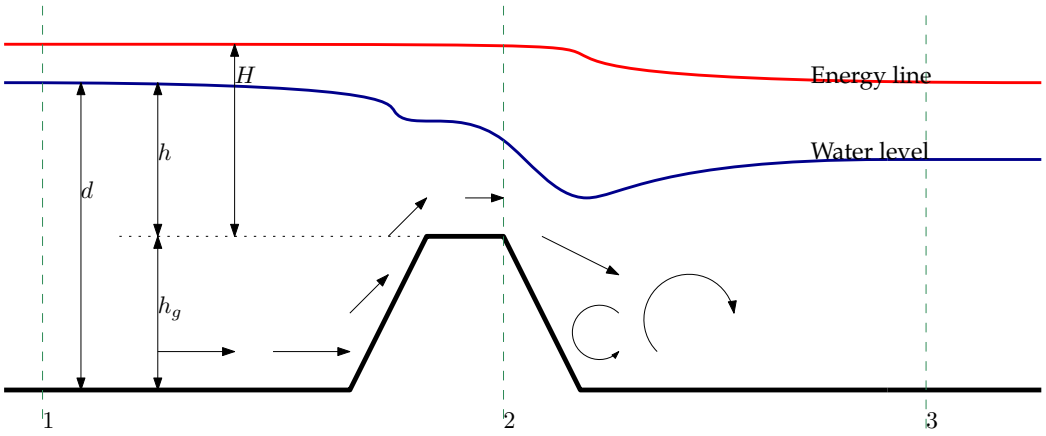

FIGURE B.2: Schematization of flow over a weir for determination of the discharge. The *red* and *blue* denote the energy line and water level respectively. Noted that the parameters d, h and H also hold for the section 2 and 3 which are cut by the *green* lines (Kruijt, 2013).

The special attention should be paid when one uses the weir formulations even for the submerged groynes because the previously proposed formulas give rise to different coefficients (Kruijt, 2013). It also should be kept in mind that when using the weir formulations, one has to assume that the water surface slope in the groyne fields is equivalent to that in the main stream. Although the weir configuration is different from the groyne due to the fact that the former one is constructed stretching the full width of the river while the latter one was built partly, in the certain conditions the weir formulation can be used for determining the energy loss coefficient (Kruijt, 2013).

Here one remark should be regarded concerning the usage of sub-grid approach as this word appears in two aspects of numerical methods. The first aspect means that the hydraulic structure can be mimicked by modifying the bed topography, the so called "structural approach", where the structure will appear upon the river bed. Due to the lack of very fine grid cells over the structure and model domain, it is wise to apply the *sub-grid approach* which the energy-preserving and momentum-preserving numerical schemes are used before and after the structure respectively, to overcome the complicated hydrodynamic processes near the structure. The second aspect indicates the addition of new term to the governing equations, a method which parameterizes the energy loss by the structure, without doing anything on the bed topography, also called the *sub-grid approach*. Therefore this method will be named the "non-structural approach". In this aspect, the coefficient of energy loss or drag-resistance should be realized from the experimental observations for a specific type of structure.

For the perspective of numerical discretizations, when used the structural approach the conservative schemes should be applied as suggested by the figure B.1. In other words, the energy-preserving scheme should be used before the structure because it is necessary to obtain the Rankine-Hugoniot jump condition (Zijlema, 2017), and the momentum-preserving scheme has to be applied after the structure where the energy is not conserved anymore due to turbulent dissipation. Some of software packages have the ability to change the appropriate numerical schemes automatically for river applications with the hydraulic structures (e.g. Delft3D). This is also one of the methods to eliminate the detail hydrodynamics processes occurring inside the control volume (Deltares, 2014).

In the non-structural approach, to consider the losses induced by the groyne in the computational software packages, for instance Delft3D, the additional force term is added to the governing equations i.e. momentum equations. This term is similar to friction term constructed by the the contraction or discharge coefficient (Deltares, 2014). The order of friction term formulation can be

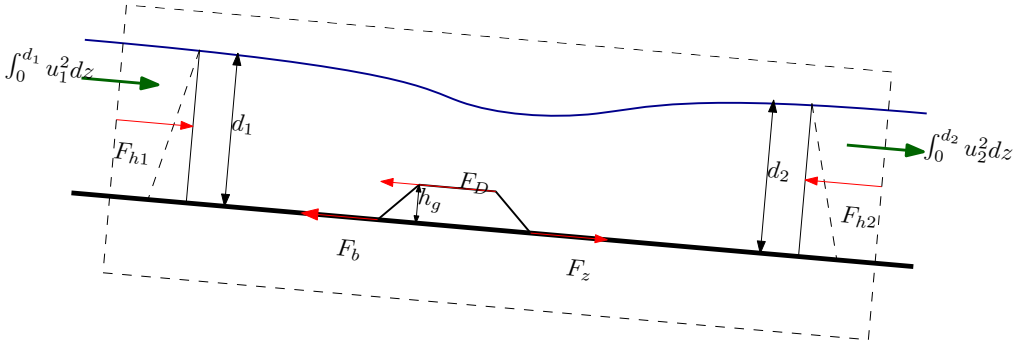

FIGURE B.3: Forces in the control volume. The change of momentum inside the control volume $\int_0^{h_1} u_1^2 dz - \int_0^{h_2} u_2^2 dz$ is in balance with the hydrostatic pressures F_{h1} and F_{h2}, gravity force F_z, drag force by the structure F_D, and bottom resistance F_b (Kruijt, 2013).

quadratic or linear as below respectively:

$$M_\xi = -\frac{c_{loss-u}}{\Delta x} u\sqrt{u^2+v^2} \tag{B.6}$$

$$M_\eta = -\frac{c_{loss-v}}{\Delta y} v\sqrt{u^2+v^2} \tag{B.7}$$

and

$$M_\xi = -\frac{c_{loss-u} u}{\Delta x} \tag{B.8}$$

$$M_\eta = -\frac{c_{loss-v} v}{\Delta y} \tag{B.9}$$

for ξ and η coordinate system, where c_{loss} is the energy loss coefficient, u, v denote the velocity components, and Δx and Δy denote the mesh size. The value of c_{loss} needs to be specified by the user at input. It is therefore important to estimate the accurate value of c_{loss} for the groyne by including the possible physical mechanisms of different ways of energy dissipation.

B.0.2 Modelling groyne using the drag-resistance approach

As already mentioned in the subsection B.0.1, there are two aspects for using the name of sub-grid approach, namely (1) structural approach, and (2) non-structural approach. In the non-structural approach the coefficient of additional loss (due to the groyne) can be determined by using (1) the weir formulation, and (2) the drag-resistance approach, which is explained in this subsection.

The drag resistance approach is derived from the momentum balance in the control volume of the water. Inside this control volume, there is a force exerted by the groyne structure upon the water mass, called the *drag force*, leading to the drag resistance for the motion. Contrary to the weir formulation case, in this case the control volume of the momentum balance is stretched between upstream and downstream of the structure (Leeuwen, 2006; Kruijt, 2013) as depicted in the figure B.3. In the drag-resistance approach, the groyne is assumed to contribute for the bed resistance, i.e. it is seen as the form drag. The drag force formula B.10 can be used to determine the drag coefficient C_d:

$$F_d = C_d A_s \rho \frac{u^2}{2} \tag{B.10}$$

where $F_d =$ drag force, $C_d =$ drag coefficient, and $A_s =$ cross-sectional area.

Having applied the momentum balance B.11 to find out the drag force F_d with the use of figure B.3, we can find out the drag coefficient by using the equation B.10.

$$\rho \int_0^{h_1} u_1^2 dz - \rho \int_0^{h_2} u_2^2 dz = F_{h1} - F_{h2} + F_z - F_b - F_D \tag{B.11}$$

where u_1, u_2 = streamwise velocities, h_1, h_2 = water depths, F_{h1}, F_{h2} = hydrostatic pressure forces, F_z = gravity force, F_b = bottom resistance, and F_D = drag force by the structure. In fact, the equation B.10 can also be written as below:

$$F_D = \frac{1}{2}\rho C_d h_g u_1^2 \tag{B.12}$$

where h_g = height of the groyne.

To translate the form drag as the friction term, Yossef, (2005) introduced a new formulation for the total drag resistance summing up (1) the bed resistance, and (2) the resistance due to the groynes, based on the following balance equation:

$$ghi = \underbrace{\frac{g}{C_{base}^2} u_{gr}^2}_{\text{bed resistance}} + \underbrace{\frac{1}{2} C_d \left(\frac{h_g}{S}\right) u_{gr}^2}_{\text{groynes resistance}} \tag{B.13}$$

for a unit area in the groyne fields away from the mixing layer which means not considering the momentum exchange between main stream and groyne field. In equation B.13, u_{gr} is the velocity in the groyne fields, g is the gravitational acceleration, h is the local water depth, C_{base} is the base Chézy coefficient in the main channel defined by $C_{base} = 18 \log \frac{12h}{k_s}$ where k_s is the bed roughness height, h_g is the groyne height, S is the spacing between two groynes, and C_d is the representative drag coefficient of the groynes taking into account the resistance of the groynes. The effective Chézy roughness coefficient ($C_{effective}$) for the resistance of the groynes can be determined using the equation B.13 as below:

$$C_{effective} = \sqrt{\frac{1}{\frac{1}{C_{base}^2} + \frac{1}{2g} C_d \left(\frac{h_g}{S}\right)}} \tag{B.14}$$

since the relationship $C = \frac{u}{\sqrt{hi}}$ exists for velocity, depth, water surface slope and Chézy coefficient. It should be noted that using the equation B.14 implies that the water surface slope in the groyne fields is equal to that of the main channel. Having determined the value of C_d by equation B.13, the $C_{effective}$ value can be realized with the measurement of other parameters.

Other researchers (Van Broekhoven, 2007; Azinfar, 2010) also reported the different descriptions for the form drag resistance of the groyne using the numerical and experimental methods and were found that their results are different from each other (Kruijt, 2013). However Kruijt, (2013) observed that the most important parameter to these equations is the ratio of the water depth to the groyne height, which is similar to the blockage ratio introduced by Raju and Singh, (1975). Having used the wind tunnel facility to study the blockage effect on the flow around a 2D plate, Raju and Singh, (1975) proposed the following formula for the drag resistance taking into account the blockage effect:

$$C_d = C_{d0} \left(1 - \frac{h_g}{D}\right)^{-2.25} \tag{B.15}$$

where C_{d0} is the drag coefficient of a plate without blockage effect, or base drag coefficient, h_g is the groyne height, and D is the height of the wind tunnel. The equation B.15 shows the dependence of the drag coefficient on the blockage ratio, $\frac{h_g}{D}$, which is equivalent to the water depth to groyne height ratio.

The functional relationship between the flow parameters and groyne geometries, and the drag coefficient can be found with the help of dimensional analysis. The functional form of the drag coefficient can be written as below using the dimensional analysis for the different settings of groynes (Azinfar, 2010):

$$\text{Single submerged groyne} : C_d = f(Re_1, Fr_1, A_r, \frac{h_g}{L}, \frac{h_1}{h_g}, \Delta, \alpha) \tag{B.16}$$

$$\text{Single emerged groyne} : C_d = f(Re_1, Fr_1, \frac{L}{B}, \frac{h_1}{L}, \Delta, \alpha) \tag{B.17}$$

where Re_1, Fr_1 = Reynolds number and Froude number at the upstream respectively, A_r = blockage ratio for the submerged groyne defined by $A_r = \frac{A_s}{h_1 B}$, B = width of the channel, A_s = projected area of the groyne which is $A_s = h_g L$, L = length of the groyne, $\frac{h_g}{L}$ = aspect ratio of the submerged groyne, $\frac{h_1}{h_g}$ = submergence ratio, $\frac{L}{B}$ = blockage ratio, and $\frac{h_1}{L}$ = depth to length ratio, Δ = the shape factor of the groyne, and α = the flow angle between the groyne and the channel bank. The dimensional parameters, Re and Fr, affect on the drag force of the groyne insignificantly while the blockage ratio is of paramount importance for determining the drag resistance.

In fact Ali, (2013) defined three sources of energy losses contributed to the total loss of energy in the flow; (1) form drag of the obstacles, (2) skin friction and grain of the bed, and (3) the side wall friction. The determination of the from drag of a particular structure is the most relevant part for this section. The drag coefficient which causes the form drag component in turn, is to be found out by the series of experiments for different types of geometries, otherwise used as a calibration parameter in the numerical models. In the sub-grid approach, the usage of form drag eliminates the detail study of turbulent flow structures interaction and turbulent dissipation of energy. Actually the scientific knowledge of the form drag can be attributed by the turbulence modelling.

Appendix C

1D Analysis

The objective of this 1D analysis is to identify the relationship between the drag coefficient and the water level.

From the chapter 2, it was known that the simple one-dimensional momentum balance in the river reach consisting of the groynes can be described by the equation B.13 according to Yossef, (2005), in which the control volume is limited to the groyne fields far away from the turbulent mixing layer. In this 1D analysis, the similar form of balance is written as below for the control volume including the groyne fields and also the main channel, to recognize the relationship between the hydraulic conditions and the drag coefficient:

$$ghi = \frac{g}{C_{base}^2}u^2 + \frac{C_D}{2}\frac{A_g}{A_f}u^2 \tag{C.1}$$

where u is the averaged velocity for the whole channel, A_g is the cross-sectional area of the groyne plane perpendicular to the direction of the flow, and A_f is the surface area of the river bed per groyne field, given by the product of the groyne field spacing and river width. The equation C.1 can be written also as below:

$$ghi = \frac{g}{C_{base}^2}\left(\frac{q}{h}\right)^2 + \frac{C_D}{2}\frac{hL_g}{A_f}\left(\frac{q}{h}\right)^2 \tag{C.2}$$

where L_g is the length of the groyne, and q is the unit discharge.

The figure C.1 depicts the effect of the groyne resistance on the water depth for the constant unit discharge. The graph is plotted by the non-linear equation:

$$gih^3 - \frac{C_D}{2}L_g\frac{q^2}{A_f}h - \frac{g}{C_{base}^2}q^2 = 0 \tag{C.3}$$

that can be solved by the numerical root-finding method, `fsolve` Python package. The geometry of the groyne possessing the larger roughness value or drag coefficient can cause the higher water depth in the river.

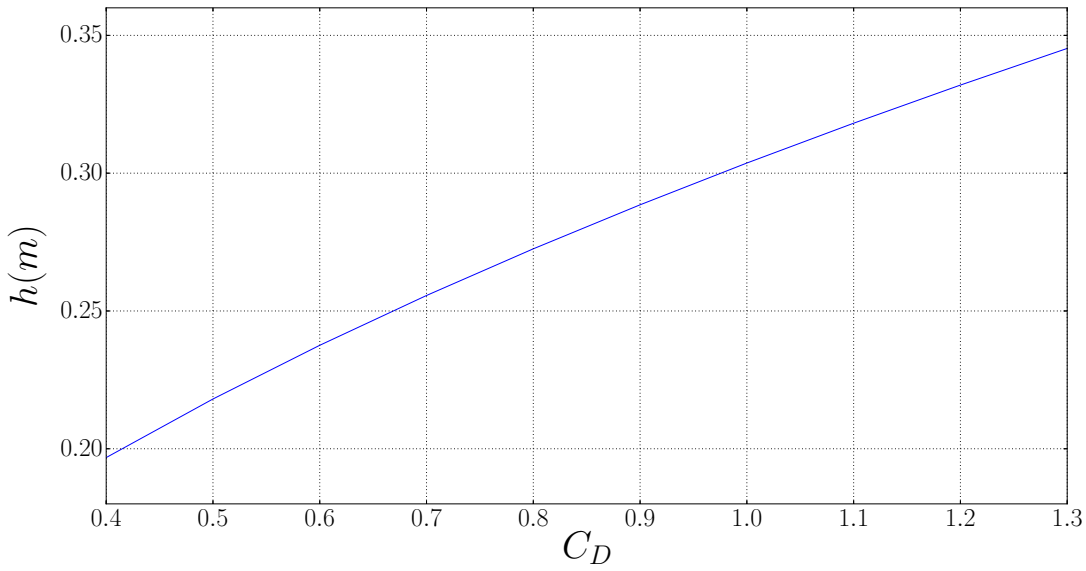

FIGURE C.1: Effect of the groyne resistance, C_D, on the water depth, h. The shape of the groyne possessing the large roughness can provide the higher water depth.

Appendix D

Setting up the numerical flume

There are three methods to set up the numerical flume in the `OpenFOAM` using the `interFoam` multiphase solver:

1. **Using the mathematical boundary conditions**: this is the traditional that the mathematically derived boundary conditions are defined at the upstream and downstream in the computational domain without any physical aid on the computational domain. For example, in the shallow water applications or (hydrostatic) hydraulic simulations, the velocity or discharge is set at the upstream and the water level is applied at the downstream, based on the characteristic lines or Riemann invariants. In the computational fluid dynamics applications, however, the water level cannot be represented by the pressure field simply, therefore it requires the knowledge of connection between the pressure and the water level in order to define the required water level at the downstream. Moreover, in the multiphase simulations like `interFoam`, the definition of water level by means of pressure is more complex due to the existence of water and air phases and unfortunately it cannot be implemented easily for not having well documented. The use of `groovyBC` functionality in the `swak4FOAM` to define the boundary conditions in the inlet and outlet, especially the water level boundary condition in the outlet because it is essential to regulate the water level in the flume. However this method is not straightforward.
2. **Using the Inlet/Outlet tanks**: In order to circumvent the complexity of using mathematical boundary conditions in the flume, the physical aids which are the inlet and outlet water tanks in this case, can be applied to regulate the flow conditions. In fact, although the mathematical boundary conditions are still in need in this method, they are of very simplicity, and therefore can be applied to control the water level without many mathematical difficulty. The inlet tank is installed at the upstream of computational domain while the outlet tank is annexed at the end of the domain, which is very similar appearance to experimental flumes. The upward- and downward-directed velocity boundary conditions are defined at the bottom faces (patches in `OpenFOAM` terminology) of the inlet and outlet tanks respectively, that represent the realistic inflow and outflow discharges. Therefore the water level can be regulated by means of outflow discharge i.e. the time of starting the negative velocity can determine the water level at this location. It simply states that the later the negative discharge starts to work, the higher the water level results in the flume. However the drawback of this method is that one requires some trial-and-error simulations to obtain the required water depth and the corresponding discharge, because it is quite hard to foresee the correct timing of triggering the negative discharge.
3. **Using the weir at the downstream**: This is the simplest and very practical approach to control the water level at the downstream. In this approach the tanks are not essential anymore, but due to the past experience the outlet tank should be installed for the sake of preventing numerical oscillations. The existence of the weir at the downstream can cause the reflective waves towards the flume area, so the location of interested study area should be chosen carefully and sometimes the flume need to be extended to be free from the downstream

effects. Some of the simulations show that using the weir at the downstream is not appropriate for low discharge because the air and water interface is too sharp at where the outflow occurs from the tip of the weir, causing the expensive computation time.

D.1 Artifacts in the setting-up of the numerical flume

The two artifacts were observed during the setting up of numerical flume without having any hydraulic structure. It should be noted that using the other construction methods have their own failures although not stated here explicitly. The following two findings may correspond to the physical or numerical artifacts.

1. The small wave height of the translatory waves can occur in the flume immediately after the inlet discharge is large enough, and these waves will not diminish within the reasonable simulation time. These waves can cause unsteady velocity profiles. Due to this behaviour, the resulting flume cannot be used for further analysis of the research. This artifact can be mitigated by modifying the size of the inlet tanks. In fact by using the dimensional analysis and several simulations, it can be deduced the relationship between this translatory wave and hydraulic and geometrical parameters. Roughly speaking the wave celerity, c, (not to be confused with the formal definition of wave celerity (e.g. $c = \sqrt{gh}$) in wave theory, actually more appropriate to name 'unsteadiness of velocity profile') is the function of the inlet unit discharge, q, length of inlet tank, L_t, the length of the flume, L and undisturbed water depth, h, as follows:

$$c \propto \frac{qh}{L_t L}$$

   It states that using the longer dimension of the inlet tank can reduce the artificial perturbations or the translatory wave celerity. The fast rate of inlet discharge can cause this unnecessary wave, and therefore one should control the discharge rate to enter gradually. It is remarkable finding that the water depth at the end of the flume also causes the unsteadiness of the velocity profile. This means that the water volume acts as the reflective boundary condition at the flume end.

2. The diffusion of air-water interface occurs around the end of the flume. The reason might be that the numerical error because the discharge balance between inlet and outlet tanks is made sure to be zero. Otherwise the water level might be approaching to be in equilibrium in the longer simulation, because during the research due to the time limitation, the simulation time is until 8000 s ~ 2.22 hr.

Appendix E

Modified VOF equation

This appendix derives the modified VOF equation which mitigates the over-diffusive interface phenomenon resulted from the numerical discretization on the initial VOF equation 3.13. This derivation is mainly extracted from the paper of Damian, (2012).

The original VOF equation 3.13 came out from the decision of using the single-field representation to describe the interface, among the two representative methods for interface tracking. Derivation of the modified VOF equation here makes use of the two-fluid Eulerian model for two phases (Berberović et al., 2009). Hence, the equations for each fluid denoted by a and b in the system can be written as:

$$\frac{\partial \gamma}{\partial t} + \nabla \cdot (\boldsymbol{u}_a \gamma) = 0 \tag{E.1}$$

$$\frac{\partial (1-\gamma)}{\partial t} + \nabla \cdot (\boldsymbol{u}_b (1-\gamma)) = 0 \tag{E.2}$$

Rewritting the transport equation of γ, equation 3.13 here:

$$\frac{\partial \gamma}{\partial t} + \nabla \cdot (\boldsymbol{u} \gamma) = 0 \tag{E.3}$$

and $\boldsymbol{u}$ in the above equation can be replaced by the equation 3.16 resulting in the following equation:

$$\frac{\partial \gamma}{\partial t} + \nabla \cdot ((\gamma \boldsymbol{u}_a + (1-\gamma)\boldsymbol{u}_b)\gamma) = 0 \tag{E.4}$$

By the definition of relative velocity $\boldsymbol{u}_r = \boldsymbol{u}_a - \boldsymbol{u}_b$, the equation E.4 can be rearranged as follows with the use of $\boldsymbol{u}_b = \boldsymbol{u}_a - \boldsymbol{u}_r$:

$$\frac{\partial \gamma}{\partial t} + \nabla \cdot ((\gamma \boldsymbol{u}_a + (1-\gamma)(\boldsymbol{u}_a - \boldsymbol{u}_r))\gamma) = 0 \tag{E.5}$$

The next steps are:

$$\begin{aligned} \frac{\partial \gamma}{\partial t} + \nabla \cdot ((\gamma \boldsymbol{u}_a + \boldsymbol{u}_a - \boldsymbol{u}_r - \gamma \boldsymbol{u}_a + \gamma \boldsymbol{u}_r)\gamma) &= 0 \\ \frac{\partial \gamma}{\partial t} + \nabla \cdot ((\boldsymbol{u}_a - (1-\gamma)\boldsymbol{u}_r)\gamma) &= 0 \end{aligned}$$

Taking the divergence inside the whole bracket in the second term:

$$\underbrace{\frac{\partial \gamma}{\partial t} + \nabla \cdot (\boldsymbol{u}_a \gamma)}_{=0 \text{ by } E.1} - \nabla \cdot ((1-\gamma)\gamma \boldsymbol{u}_r) = 0$$

leading to the following equation:

$$\nabla \cdot ((1-\gamma)\gamma \boldsymbol{u}_r) = 0 \tag{E.6}$$

Therefore the equation E.6 can be added to the original VOF equation 3.13 without changing the magnitude of the whole equation. The final equation reads:

$$\frac{\partial \gamma}{\partial t} + \nabla \cdot (\boldsymbol{u}\gamma) + \nabla \cdot ((1-\gamma)\gamma \boldsymbol{u}_r) = 0 \tag{E.7}$$

Bibliography

Alauddin, Mohammed, Takashi Tashiro, and Tetsuro Tsujimoto (2011). "Design of groynes modified with both alignment and permeability for lowland river problems". In: *Journal of Japan Society of Civil Engineers, Ser. A2 (Applied Mechanics (AM))* 67.2, I_645–I_652.

Ali, S (2013). "Flow over Weir-like Obstacles". In:

Azinfar, H and JA Kells (2008). "Backwater prediction due to the blockage caused by a single, submerged spur dike in an open channel". In: *Journal of Hydraulic Engineering* 134.8, pp. 1153–1157.

Azinfar, Hossein (2010). "Flow resistance and associated backwater effect due to spur dikes in open channels". PhD thesis.

Berberović, Edin et al. (2009). "Drop impact onto a liquid layer of finite thickness: Dynamics of the cavity evolution". In: *Physical Review E* 79.3, p. 036306.

Berselli, Luigi Carlo, Traian Iliescu, and William J Layton (2005). *Mathematics of large eddy simulation of turbulent flows*. Springer Science & Business Media.

Bom, Sam (2017). "Scour holes in heterogeneous subsoil: A numerical study on hydrodynamical processes in the development of the scour holes". In:

Bracewell, Ronald Newbold (1986). *The Fourier transform and its applications*. Vol. 31999. McGraw-Hill New York.

Brackbill, JU, Douglas B Kothe, and Charles Zemach (1992). "A continuum method for modeling surface tension". In: *Journal of computational physics* 100.2, pp. 335–354.

Carmer, CF von, AC Rummel, and GH Jirka (2004). "Influence of secondary motion in large-scale coherent vortical structures on the mass transport in a shallow turbulent wake flow". In: *Shallow Flows: Research Presented at the International Symposium on Shallow Flows, Delft, Netherlands, 2003*. Taylor & Francis, p. 103.

Casulli, Vincenzo and Guus S Stelling (1998). "Numerical simulation of 3D quasi-hydrostatic, free-surface flows". In: *Journal of Hydraulic Engineering* 124.7, pp. 678–686.

Cheng, Zhen, Tian-Jian Hsu, and Joseph Calantoni (2017). "SedFoam: A multi-dimensional Eulerian two-phase model for sediment transport and its application to momentary bed failure". In: *Coastal Engineering* 119, pp. 32–50.

Damian, S Márquez (2012). *Description and utilization of interfoam multiphase solver*.

Deltares, Delft (2014). "3D/2D modelling suite for integral water solutions". In: *Delft, the Netherlands*.

Dewan, Anupam (2010). *Tackling turbulent flows in engineering*. Springer Science & Business Media.

Duchêne, Vincent (2014). "On the rigid-lid approximation for two shallow layers of immiscible fluids with small density contrast". In: *Journal of Nonlinear Science* 24.4, pp. 579–632.

Ducrocq, Thomas et al. (2017). "Flow and drag force around a free surface piercing cylinder for environmental applications". In: *Environmental Fluid Mechanics*, pp. 1–17.

Duguay, JM, RWJ Lacey, and J Gaucher (2017). "A case study of a pool and weir fishway modeled with OpenFOAM and FLOW-3D". In: *Ecological Engineering* 103, pp. 31–42.

Francis, JRD, AB Pattanaik, and SH Wearne (1968). "TECHNICAL NOTE. OBSERVATIONS OF FLOW PATTERNS AROUND SOME SIMPLIFIED GROYNE STRUCTURES IN CHANNELS." In: *Proceedings of the Institution of Civil Engineers* 41.4, pp. 829–837.

Greenshields, Christopher J (2015). "Openfoam User Guide". In: *OpenFOAM Foundation Ltd, version* 3.1.

Hans Petter Langtangen, Kent-Andre Mardal (2016). *Introduction to Numerical Methods for Variational Problems*.

Higham, JE et al. (2017). "Using modal decompositions to explain the sudden expansion of the mixing layer in the wake of a groyne in a shallow flow". In: *Advances in Water Resources*.

Higuera, Pablo, Javier L Lara, and Inigo J Losada (2013). "Simulating coastal engineering processes with OpenFOAM®". In: *Coastal Engineering* 71, pp. 119–134.

— (2014). "Three-dimensional interaction of waves and porous coastal structures using OpenFOAM®. Part I: Formulation and validation". In: *Coastal Engineering* 83, pp. 243–258.

Hirt, Cyril W and Billy D Nichols (1981). "Volume of fluid (VOF) method for the dynamics of free boundaries". In: *Journal of computational physics* 39.1, pp. 201–225.

Jellesma, Manfred (2013). "Form drag of subaqueous dune configurations". MA thesis. University of Twente.

Kadota, A, K Suzuki, and WSJ Uijttewaal (2006). "The shallow flow around a single groyne under submerged and emerged conditions". In: *River Flow*. Vol. 1, pp. 673–682.

Kang, Joongu et al. (2011). "Experimental investigation on the local scour characteristics around groynes using a hydraulic model". In: *Water and Environment Journal* 25.2, pp. 181–191.

Kimura, Ichiro and Takashi Hosoda (2003). "A non-linear k–ε model with realizability for prediction of flows around bluff bodies". In: *International Journal for Numerical Methods in Fluids* 42.8, pp. 813–837.

Koken, Mete and George Constantinescu (2008). "An investigation of the flow and scour mechanisms around isolated spur dikes in a shallow open channel: 1. Conditions corresponding to the initiation of the erosion and deposition process". In: *Water Resources Research* 44.8.

Kruijt, Maurits (2013). "Resistance of submerged groynes". MA thesis. Delft University of Technology.

Kuhnle, Roger A, Yafei Jia, and Carlos V Alonso (2008). "Measured and simulated flow near a submerged spur dike". In: *Journal of Hydraulic Engineering* 134.7, pp. 916–924.

Kundu, PK and IM Cohen (2008). "Fluid mechanics. 2004". In: *Elsevier Academic Press, San Diego). Two-and three-dimensional self-sustained flow oscillations* 307, pp. 471–476.

Leeuwen, KC van (2006). "Modeling of submerged groynes in 1D hydraulic computations". MA thesis. University of Twente.

Maliska, Clovis R (1994). *Transferência de calor e mecânica dos fluidos computacional: fundamentos e coordenadas generalizadas*. Livros Técnicos e Científicos.

Michael Scurlock, S, Christopher I Thornton, and Steven R Abt (2015). "One-Dimensional Modeling Techniques for Three-Dimensional Grade Control Structures". In: *Journal of Hydraulic Engineering* 141.5, p. 05015001.

Molls, Thomas and M Hanif Chaudhry (1995). "Depth-averaged open-channel flow model". In: *Journal of hydraulic engineering* 121.6, pp. 453–465.

Moraes, Antonio de Oliveira Samel et al. (2013). "Analysis of the non-orthogonality correction of finite volume discretization on unstructured meshes". In: *22nd International Congress of Mechanical Engi-neering. Ribeir˜ to Preto, SP*, pp. 3518–3530.

Moriche, Manuel, Oscar Flores, and Manuel Garcia-Villalba (2017). "On the aerodynamic forces on heaving and pitching airfoils at low Reynolds number". In: *Journal of Fluid Mechanics* 828, pp. 395–423.

Ouillon, Sylvain and Denis Dartus (1997). "Three-dimensional computation of flow around groyne". In: *Journal of hydraulic Engineering* 123.11, pp. 962–970.

Paik, Joongcheol, Fabian Bombardelli, and Nam Joo Lee (2014). "Numerical Simulation of Turbulent Free Surface Flow Around a Circular Cylinder". In: *ICHE 2014. Proceedings of the 11th International Conference on Hydroscience & Engineering*. Karlsruhe, pp. 991–1000.

Pattanaik, Akshayabandhu (1966). "The effects of groynes on river flow". PhD thesis. University of Manchester Institute of Science and Technology.

Phillipsburg, NJ (1960). "On the Three-Dimensional Turbulent Boundary Layer Generated by Secondary Flow1". In: *Journal of Basic Engineering*, p. 233.

Rajaratnam, Nallamuthu and Benjamin A Nwachukwu (1983). "Flow near groin-like structures". In: *Journal of Hydraulic Engineering* 109.3, pp. 463–480.

Raju, KG Ranga and Vijaya Singh (1975). "Blockage effects on drag of sharp-edged bodies". In: *Journal of Wind Engineering and Industrial Aerodynamics* 1, pp. 301–309.

Rhoads, J (2014). "Effects of grid quality on solution accuracy". In: *OpenFOAM workshop 2014*.

Rodi, Wolfgang (2017). "Turbulence Modeling and Simulation in Hydraulics: A Historical Review". In: *Journal of Hydraulic Engineering* 143.5, p. 03117001.

Roulund, Andreas et al. (2005). "Numerical and experimental investigation of flow and scour around a circular pile". In: *Journal of Fluid Mechanics* 534, pp. 351–401.

Rusche, Henrik (2003). "Computational fluid dynamics of dispersed two-phase flows at high phase fractions". PhD thesis. Imperial College London (University of London).

Sattar, Ahmed MA, Hrvoje Jasak, and Vanja Škurić (2017). "Three dimensional modeling of free surface flow and sediment transport with bed deformation using automatic mesh motion". In: *Environmental modelling & software* 97, pp. 303–317.

Schulze, Lydia and Carsten Thorenz (2014). "The Multiphase Capabilities of the CFD Toolbox OpenFOAM for Hydraulic Engineering Applications". In:

Shen, Hayley H et al. (2002). *Environmental fluid mechanics: theories and applications*. ASCE Publications.

Spalart, Philippe R (2009). "Detached-eddy simulation". In: *Annual review of fluid mechanics* 41, pp. 181–202.

Stelling, GS and M Zijlema (2009). "Numerical modeling of wave propagation, breaking and run-up on a beach". In: *Advanced Computational Methods in Science and Engineering*. Springer, pp. 373–401.

Stolker, Chris (2005). *Stroombeelden bij recht aangestroomde kribben*.

Sukhodolov, Alexander N (2014). "Hydrodynamics of groyne fields in a straight river reach: insight from field experiments". In: *Journal of Hydraulic Research* 52.1, pp. 105–120.

Sun, Rui and Heng Xiao (2016). "SediFoam: A general-purpose, open-source CFD–DEM solver for particle-laden flow with emphasis on sediment transport". In: *Computers & Geosciences* 89, pp. 207–219.

Talstra, Harmen (2011). "Large-scale turbulence structures in shallow separating flows". In: *Optima Grafische Comminicatie, Rotterdam*.

Talstra, Harmen, Wim SJ Uijttewaal, and Guus S Stelling (2006). "Emergence of large-scale coherent structures in a shallow separating flow". In: *Proc. Int. Conf. Fluvial Hydraulics (River Flow), Taylor and Francis, UK*, pp. 261–269.

Te Chow, Ven (1959). *Open channel hydraulics*. McGraw-Hill Book Company, Inc; New York.

Teuber, Katharina et al. (2013). "High-Resolution Numerical Analysis of Flow Over a Ground Sill Using OpenFOAM". In:

Thorenz, Carsten and Jann Strybny (2012). "On the numerical modelling of filling-emptying systems for locks". In: *Reinhard-Philip Hinkelmann, Yui Liong, Dragan Savic, Mohammad Nasermoaddeli, Karl-Friedrich Daemrich, Peter Fröhle und Daniela Jacob (Hg.): Proceedings, 10th International Conference on Hydroinformatics HIC 2012. International Conference on Hydroinformatics. Hamburg*.

Tingsanchali, Tawatchai and Selvaratnam Maheswaran (1990). "2-D depth-averaged flow computation near groyne". In: *Journal of Hydraulic Engineering* 116.1, pp. 71–86.

Tryggvason, Grétar (2011). *Lecture slides: Classical turbulence modelling*.

Uijttewaal, Wim S (2005a). "Effects of groyne layout on the flow in groyne fields: Laboratory experiments". In: *Journal of Hydraulic Engineering* 131.9, pp. 782–791.

Uijttewaal, Wim SJ (2005b). "The flow in groyne fields". In: *Water Quality Hazards and Dispersion of Pollutants*. Springer, pp. 231–246.

Uijttewaal, WSJ and J Tukker (1998). "Development of quasi two-dimensional structures in a shallow free-surface mixing layer". In: *Experiments in Fluids* 24.3, pp. 192–200.

Uijttewaal, WSJ and SAH Van Schijndel (2004). "The complex flow in groyne fields: numerical modeling compared with experiments". In: *Proceedings of 2nd International Conference on Fluvial Hydraulics (River Flow 2004)*. Vol. 2, pp. 1331–1338.

Uijttewaal, WSJ, D v Lehmann, and A van Mazijk (2001). "Exchange processes between a river and its groyne fields: Model experiments". In: *Journal of Hydraulic Engineering* 127.11, pp. 928–936.

Van Broekhoven, RWA (2007). "Het effect van kribverlaging op de afvoercapaciteit van de Waal ten tijde van hoogwater". In:

Van Prooijen, BC (2004). *Shallow mixing layers*. Delft University Press Delft, Netherlands.

Wilcox, David C (1995). "Turbulence Modelling for CFD". In: *Journal of Fluid Mechanics* 289, pp. 406–407.

Wilcox, David C et al. (1998). *Turbulence modeling for CFD*. Vol. 2. DCW industries La Canada, CA.

Xin, Yu et al. (2010). "A lattice Boltzmann model coupled with a Large Eddy Simulation model for flows around a groyne". In: *International Journal of Sediment Research* 25.3, pp. 271–282.

Yeo, Hong Koo, Joon Gu Kang, and Sung Jung Kim (2005). "An experimental study on tip velocity and downstream recirculation zone of single groynes of permeability change". In: *KSCE Journal of Civil Engineering* 9.1, pp. 29–38.

Yeo, HongKoo and JoonGu Kang (2009). "Flow analysis around a submerged groyne". In: *Advances in water resources and hydraulic engineering*, pp. 1762–1766.

Yossef, Mohamed Fathy Mohamed (2005). *Morphodynamics of rivers with groynes*. Delft University Press Delft, Netherlands.

Yossef, Mohamed FM and Huib J de Vriend (2010). "Flow details near river groynes: experimental investigation". In: *Journal of Hydraulic Engineering* 137.5, pp. 504–516.

Zaghloul, N and JA McCorquodale (1973). "A numerical model for flow past a spur-dike". In:

Zaghloul, Nabil A (1982). "The Application of FEM and FDM to Flow Separation Pattern; A Comparison Study". In: *Finite Elements in Water Resources*. Springer, pp. 207–216.

— (1983). "A finite element method for flow separation". In: *Computer methods in applied mechanics and engineering* 41.2, pp. 159–174.

Zagonjolli, Migena, Frank Platzek, and Jan van Kester (2017). *Modelling the flow over a groyne and weir in WAQUA*.

Zijlema, Marcel (2017). *2DH shallow water equations, numerical solution of the 2DH shallow water equations*.

Zijlema, Marcel and Guus S Stelling (2005). "Further experiences with computing non-hydrostatic free-surface flows involving water waves". In: *International journal for numerical methods in fluids* 48.2, pp. 169–197.